1 STOCK LOCATION	2 DATE RECEIVED			12 SCREEN				17 ACCESSION NUMBER			
	YR	MO	DAY	☐ OBTAIN BETTER COPY	☐ REJECT			*N74-14891*			
	74	03	16	☐ OBTAIN AUTHORITY	☐ OUT OF PRINT SOD						
					☐ ERRATA						

3 RECEIPT TYPE & FORMAT				13A ANNOUNCEMENT		13B FAS	☒ GRA	18 PAGES	19 SHEETS	20 LOW LIMIT	21 ☐
	☐ MAGNETIC TAPE			VOL	ISSUE	☐ YES	☐ WGA			PC / MF	SUB-SCRIP-TION
☐ LOAN	☒ PC	☐ 35 MM	☐ CARDS	74	08	☐ NO		195			
☐ LAST COPY	☐ MF	☐ 16 MM	☐ OTHER (BOX 16)				☐ UNLAWN				

4 STOCK RECEIVED FOR SALE		5 LOAN ETC.	14 REPRODUCTION INSTRUCTIONS		MAKE MICROFICHE		22 PRICES		#.75 12.00		
PC	MF	DUE OUT	BLOWBACK →		☐ YES ☒ NO		☐ U UNIT		☒ P PC →	☐ WI	
	6	RET	PRINT ↓	NO | 1 UP | 2 UP	15 PRESTOCK		☐ E PC + MN BOX 16		☐ M MN →	☒ DEMAND	

6 TRANSACTION					NO	1	4	7	PC DUE IN		23 CATEGORY	24 DISTR CODE	25 INITIALS ACC	11 NOT FULLY
NEW ITEM	☐	DUPE	SUPER-SEDES	☒ PRIOR NUMBER	1 UP	2	5	8	PC PRINT				DB A	LEGIBLE ☐ COLOR ☐

7	2 UP	3	6	9	PC SOURCE TO ORDER		26 FILL FROM		27 PUBLIC RELEAS-ABILITY
NASA-CR-121184	MIX	SAME SIZE	ORDER STOCK FROM ⊙↓	MF PRINT CODE	*M*		PAPER COPY ETC. *SS*	☐ MICRO-NEGA-TIVE *XN*	*C*

8 REPORT NUMBERS (XREF)	☐ →

16 REMARKS

NASA

Volume II

9 RELATED DOCUMENT	☐ →

10 CONTRACTING OFFICE-BILLING CODE

NASA — 100

28 FORM, PRICE, ETC.	29 ANN CODE
12 11	

1 ARCHIVES

3/16

DOCUMENT TRAVELER

N74-14891

OPTIMIZATION IN THE DESIGN OF A 12
GIGAHERTZ LOW COST GROUND RECEIVING
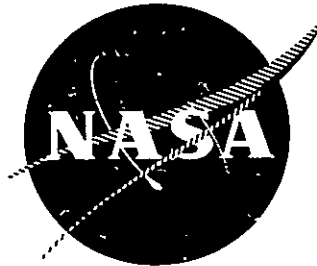SYSTEM FOR BROADCAST SATELLITES, VOLUME
VOLUME II

K. Ohkubo, et al

Stanford University
Stanford, California

October 1972

OPTIMIZATION IN THE DESIGN OF A 12 GIGAHERTZ LOW COST
GROUND RECEIVING SYSTEM FOR BROADCAST SATELLITES

Volume II

Antenna System and Interference

by

K. Ohkubo, C. C. Han, J. Albernaz, J. M. Janky, and B. B. Lusignan

Center for Radar Astronomy
Stanford University
Stanford, California

prepared for

NATIONAL AERONAUTICS AND SPACE ADMINISTRATION

Final Report

OPTIMIZATION IN THE DESIGN OF A 12 GIGAHERTZ LOW COST
GROUND RECEIVING SYSTEM FOR BROADCAST SATELLITES

Volume II

Antenna System and Interference

by

K. Ohkubo, C. C. Han, J. Albernaz, J. M. Janky, and B. B. Lusignan

Center for Radar Astronomy
Stanford University
Stanford, California 94305

prepared for

NATIONAL AERONAUTICS AND SPACE ADMINISTRATION

October 15, 1972

NASA Lewis Research Center
Cleveland, Ohio
Dr. E. F. Miller, NASA Technical Monitor

TABLE OF CONTENTS

PRECEDING PAGE BLANK NOT FILMED

iii

TABLE OF CONTENTS (CONT'D)

TABLE OF CONTENTS (CONT'D)

TABLE OF CONTENTS (CONT'D)

LIST OF FIGURES

LIST OF FIGURES (CONT'D)

LIST OF FIGURES (CONT'D)

LIST OF FIGURES (CONT'D)

LIST OF FIGURES (CONT'D)

LIST OF TABLES

ABSTRACT

This report analyzes the antenna characteristics of a low cost

mass-producible ground station to be used in broadcast satellite systems.

It is found that a prime focus antenna is sufficient for a low-cost but

not a low noise system. For the antenna feed, waveguide systems are

the best choice for the 12 GHz band, while printed-element systems are

recommended for the 2.6 GHz band. Zoned reflectors are analyzed and

appear to be attractive from the standpoint of cost. However, these

reflectors suffer a gain reduction of about one dB and a possible increase

in sidelobe levels. The off-axis gain of a non-auto-tracking station

can be optimized by establishing a special illumination function at the

reflector aperture. A step-feed tracking system is proposed to provide

automatic procedures for searching for peak signal from a geostationary

satellite. This system uses integrated circuitry and therefore results

in cost saving under mass production. It is estimated that a complete

step-track system would cost only \$512 for a production quantity of

1000 units per year.

Protection ratios of FM television and telephone systems have been

analyzed and standard small antenna sidelobe pattern models have been

established to provide a guideline for properly choosing the satellite

spacings. It is found that these antenna pattern models yield about 35%

better orbit frequency space utilization than that of CCIR models, which

were never meant to apply to small antennas. Sidelobe suppression in only one pattern plane using a two-absorber array technique is experimentally evaluated and found effective in reducing the first sidelobe.

A design of mass-producible 12 GHz antenna feed subsystem to be used in either a prime focus or a Cassegrain antenna system is also presented. It consists of a multimode feed horn, a capacitive-type pin polarizer, a nonuniform waveguide high-pass filter and a field-shaped waveguide-to-coaxial-line coupling probe. Theories which led to minimizing the length and broadening the bandwidth of these components are presented. A unique design of a non-uniform waveguide high-pass filter with the steepest cut-off characteristics ever reported is presented. The success of the design of this filter is vital for the 12 GHz band low cost system using IF signal as low as 120 MHz. This feed system would cost only $7.40 for a production quantity of 1000 units per year.

Costs of reflectors, antenna feeds and step-track systems are estimated for various production quantities. This information was used to optimize the cost of broadcast satellite ground terminals. The cost of a step-feed tracking system is found insensitive to antenna size.

CHAPTER I

INTRODUCTION

1.1 BACKGROUND

The introduction and development of satellite communication services
in the last decade has heralded a totally new concept of long distance
telecommunication. The INTELSAT global system is a prime example of
providing telecommunications access quickly to a transoceanic region.
Apart from being expensive the traditional approach to providing commu-
ication services over remote distances is also limited in application.
Microwave relay towers cannot be installed over the oceans, and sub-
marine cables of sufficient.capacity for transmitting both television
and telephone signals are extremely costly. Today, satellite communi-
cation may be said to have passed through an experimental period lasting
about five years, followed by an initial utilization period which now
has resulted in full operational status.

While the global communication satellite has already proven itself
in its present form, the regional point-to-point communication satellite
systems and the direct-broadcast satellite systems have aroused great
expectations. The inevitable rise of so-called domestic communication
satellites has already begun, with the Molniya system successfully
operating in USSR, and another system to be implemented in Canada.
Domestic satellite systems for the United States have been proposed and
are under review. As to the direct broadcast satellite systems, in 1967,
Stanford University conducted an intensive study[1] of methods to provide

educational television programs for India, Brazil and Indonesia from broadcast satellites. That study recommended that a great number of low-cost earth terminals be installed in schools, villages, homes, etc.. Since then several design studies for low-cost ground stations have been initiated and supported by the National Aeronautics and Space Administration (NASA). For example, in 1970, General Electric Corporation completed designs[2] of low-cost mass-producible receivers (excluding antenna systems) for the 2.25 GHz and 12 GHz bands, and in 1971 Stanford University completed design[3] of a small 2.6 GHz ground station which is also mass-producible. NASA's ATS-F satellite will be launched in May 1973 and will be employed to explore the technical and economic feasibility of regular television transmissions of educational and health information to low-cost ground receivers in remote areas of the United States. At the present time, despite the development of technology and consequent cost reductions, earth stations for the INTELSAT system still remain costly-on the order of $3-4 million. Economic studies[1,3,4,5] indicate that for national networking, point-to-point and point-to-points services, and for many other services in remote areas, satellites are highly competitive with other communications technologies, but only if smaller (less than 20 ft.) ground station antennas can be used.

The success of the INTELSAT system is attributed to the development of synchronous satellites which enables the coverage of about one-third of the earth with one satellite and of about 90% of the earth with three equidistant satellites. As more satellites reside on the synchronous equatorial orbit for broadcasting and for regional point-to-point communication, and more earth terminals are used for reception,

- 2 -

the potential for mutual interference increases. Small earth stations can be interfered with by adjacent satellites more easily than large stations. This ultimately may limit the number of satellites that can be used in synchronous orbit. Therefore, careful planning is definitely needed to coordinate them into a system free from interference. This stimulates us to investigate interference among satellite systems, and to develop low-cost techniques to reduce interference., Earth station antenna characteristics are the major factors[6] in determining orbit-frequency conservation and therefore need to be thoroughly studied.

After surveying the radiation pattern characteristics of some large antennas such as Goldstone Station (California) and Andover Station (Maine), in 1966 the International Radio Consultative Committee (CCIR) suggested a reference antenna sidelobe pattern for antennas of diameter greater than 100 wavelengths. This reference pattern is given as Gain = 32-25 log θ (dB), with respect to isotropic. This standard has been widely used to calculate interference between satellite systems when precise information concerning the antenna pattern of an earth station is not available. For instance, all bidders of the U.S. domestic satellite system adopted the CCIR guideline. Although CCIR derived its earth station reference antenna pattern through "empirical" data, all the ground stations under investigation were designed to have maximum on-axis gain instead of low sidelobe levels. In general, these stations have large blockage due to bulky tracking feeds and feed support structures, which inevitably result in high sidelobes. Some of these stations even have uniform illumination which intrinsically produces high sidelobes. Thus, the CCIR reference sidelobe pattern has long been considered too

conservative an estimate. A blanket adoption of the CCIR guidelines will

result in using large antenas, which would place satellites in a dis-

advantageous position economically in competing with alternative forms

of communications. Therefore, it is necessary to re-establish an earth

station reference antenna pattern, especially with regard to small earth

station antennas. This not only requires us to bring the standard

sidelobe suppression techniques into consideration, but also to develop

new low-cost sidelobe suppression techniques, such as suppression of

sidelobes only in the direction of the synchronous equatorial orbit,

where other satellites are located.

There are several basic antennas which have high directivity and low

noise characteristics as required in satellite communications. The

paraboloid reflector antenna is presently an economically optimized

approach. A true parabolic reflector is in general an expensive unit

and represents a major cost factor in an antenna system. On the other

hand a receiving aerial for satellite broadcasting does not have to be

installed on the extreme top of a building. It is sufficient to install

the reflector on the wall of a home, or on other brickwork, with an

unobstructed line of sight to the satellite. For these purposes, it is

thought that the parabolic reflector might be stepped in the manner

of Fresnel lenses to produce a smaller depth, planar base and rigid

mechanical structure. It is also expected that these characteristics

of a zoned reflector could result in a cost saving using stamping

manufacturing techniques. Furthermore the parabolic zones can be

approximated by a straight zone which allows the reflector to be made

from flat metal sheets. Thus, the RF performance of zoned reflectors

needs to be analyzed (since this information is not available in the literature) before an assessment can be made of these reflectors.

With the already congested frequency allocations the rapid increase in space traffic volume will inevitably force the use of higher frequency bands to minimize interference between satellite systems, and between satellite and terrestrial systems. Aiming at this trend, in 1971, the International Radio Consultative Committee (CCIR) allocated[7] a 12 GHz band (11.7-12.5 GHz) in addition to the orginally planned 700 MHz band (620-790 MHz) and 2.6 GHz band (2.5-2.59 GHz) for satellite broadcasting service. The allocation of the 12 GHz band is widely considered[8] to offer a potential for greater communication capacity and to be subject to less interference in future broadcast satellite systems. However, both economic and technological aspects of the 12 GHz system have not been fully and adequately explored, at least in the form in which it will be used. Therefore, it is necessary to determine the cost of various components and the optimum system choices for different applications. In parallel to system economic analysis, hardware development must be undertaken to design the unavailable critical components. For example, if an intermediate frequency of 120 MHz is chosen for a 12 GHz receiver, an RF filter (either band-pass or high-pass) with extremely steep cut-off (a separation of less than 1% between pass band and stop band) to suppress image noise is definitely required; these are not available at the present time.

Another advantage of the 12 GHz band is its ability to produce high gain (narrow-beams) with relatively small aerial size. Cost could no doubt be reduced for large quantity production. However, as the antenna

beam becomes narrower, tracking capability is required to follow the satellite in its station keeping track. It cannot be expected that a low cost system using a conventional automatic tracking scheme such as mono-pulse or conical scanning can be designed. Thus, tracking poses a major problem in the 12 GHz band, althrough modern technology has developed to the extent that drift of a satellite in synchronous orbit can be kept to within ± 0.1 degree.

1.2 OBJECTIVE AND SCOPE OF RESEARCH

This research was undertaken (1) to analyze antenna characteristics of low cost mass-producible ground stations; (2) to determine the effect of small antennas on utilization of the orbit frequency space; (3) to evaluate the performances of zoned reflectors; (4) to design, fabricate, and test a low cost, mass-producible antenna feed subsystem; and finally, (5) to, analyze the cost of a ground station, taking into account a pro-posed automatic tracking system.

The general characteristics of an antenna system are analyzed in Chapter 2. From there we specify the proper illumination function to maximize the off-axis gain of a prime-focus type antenna, which is nec-essary for a low-cost, non-auto-tracking station. Comparisons between the 2.6 GHz band and the 12 GHz band are made wherever it is necessary to do so. Antenna categories and feed components serving our purpose are selected.

In Chapter 3 it is described how antenna pattern models, especially small antennas, are set up for standard ground antennas and for antennas with reduced sideblobes developed by Stanford Univeristy researchers.

The wanted-to-unwanted signal power ratios versus satellite spacings are

calculated using different pattern models and assuming a homogeneous

satellite system, and the results are compared with that using CCIR

models. Protection ratios of television and telephone systems are also

included. Results* of subjective assessment tests of ·co-channel inter-

ference on an amplitude modulated television system is included in

Appendix A. This test determined the viewer's awareness of interference

that exists when an FM television system is operated at the same fre-

quencies as an AM-VSB television station. Experiments of evaluating the

use of an absorber array to suppress sidelobes only in the direction of

the synchronous equatorial plane are also conducted.

In Chapter 4 designs of zoned reflectors are presented and their

performance evaluated in terms of gain reduction, bandwidth limitation,

sidelobe levels, etc.. A working model of an antenna feed suitable for

mass production at 12 GHz is designed in Chapter 5; this consists of a

multimode feed horn, a waveguide capacitive-type pin polarizer, and an

exponential-raised-to-cosine Taper high-pass filter. Design criteria

to minimize the length of these components and broaden their bandwidth

are developed. Special techniques of designing high-pass filters using

dispersive non-uniform waveguide are also devised. In order to clearly

and effectively present the design criteria Chapter 5 is organized so

that its two lengthy derivations are included as appendicies; Appendix B

shows mode conversion factors versus the sizes of the step discontinuity

for a TM_{11} mode in a circular waveguide; Appendix C derives the reflec-

tion coefficient in a non-uniform waveguide (this is rather standard but

---

*This test was conducted by R. H. Miller of Stanford University
in April 1972.

it is included for the convenience of the reader).

Finally, in Chapter 6, costs of antenna systems are investigated. Reflector costs are estimated through quotes and discussion with manufacturers. Cost estimates on various feed systems are also made. Cost of a tracking system is made based on a proposed step-track scheme, and its effect on the total cost of an antenna is incidated. The cost of a ground terminal (including both receiver and antenna) has been optimized in reference 8. The results are included here for the sake of completeness.

CHAPTER 2

ANTENNA SYSTEM ANALYSIS

2.1 INTRODUCTION

The antenna system represents a major subsystem in a satellite ground terminal. The configuration of the antenna system (as well as that of other ground station subsystems) is determined by both technical and economic aspects.

The development of a new system must be planned so as to relate properly to the development of new technology. Technically the antenna system for direct reception is conditioned by:

A. R.F. carrier frequency and bandwidth

B. I.F. signal frequency

C. interference and required message quality

D. distribution method direct reception or community reception

In direct reception, each user is directly linked to the satellite, so that a receive ground station is required for each user. This definitely ensures a large enough market to enable equipment cost to be minimized. From an economic viewpoint, equipment should be:

A. simple, easy to transport and install

B. mass-producible (e. g. die casting)

C. designed to use existing low cost components

D. designed with all the circuits integrated

E. free from tuning or adjustment after assembling

F. fixed position (although a limited track is possible)

The technical and economic factors are mutually influencing.

Because a relatively high gain is required and low cost is a major concern the parabolic reflector type antenna was selected among many candidates. It is simpler than array and lens antennas of comparable performance.

2.2 ANTENNA GAIN AND EFFICIENCY

The gain of a parabolic antenna is a function of its diameter and its efficiency. Taking into consideration feed losses between the feed aperture and the receiver input port (point of reference), the effective gain in decibels can be written as:

$$G = 10 \log \frac{\eta \pi^2 D^2}{\lambda^2} - L \quad (\text{in dB}) \qquad (2.1)$$

where

L = feed loss

D = diameter of the reflector

λ = wavelength

η = overall antenna efficiency

As will be discussed in a later section, effective gain is best defined as the effective off-axis gain for total target area encompassed. Subsequent text briefly describes the factors influencing gain. The normal definitions for loss factors and the means of computing them as widely used in the industry apply, and detailed theory is omitted.

The antenna efficiency (η) is defined as

$$\eta = \frac{\text{Total Power Received}}{\text{Total Incident Power}} \times 100\%$$

- 10 -

The several factors which together determine the overall efficiency of a parabolic antenna are widely recognized as the items listed below:

(A) Forward Spillover Loss: energy not intercepted by the reflector and attributed only to the feed pattern

(B) Aperture Loss: departure from uniform illumination over the reflector aperture

(C) Cross-Polarization Loss: the fraction of energy polarized in a plane perpendicular to the desired polarization (for linear polarization) or energy with a sense of rotation opposing the desired sense (for circular polarization).

(D) Phase Error Loss: phase front curvature across the antenna aperture and defocusing.

(E) Blockage Loss: shadowing in the illumination field due to the feed horn and its support structure.

(F) Surface Loss: reflector rms surface errors due to manufacturing and alignment tolerances, gravity, wind velocity, and normal thermal gradient distortions.

In a conventional prime-focus reflecting type antenna system, a compromise must be made between spillover and aperture efficiency. For optimized aperture efficiency, the edge of the reflector intercepts the beam from the feed at a level only a few dB down from the beam peak. In this case only a small illumination taper is present across the aperture

of the reflector, resulting in nearly uniform illumination and, hence,

a high aperture efficiency. However, much of the energy in the main

beam misses the reflector, resulting in high spillover loss. This not ·

only reduces the energy available to the reflector but also increases

the antenna noise temperature, particularly at low elevation angles.

In the case of minimum spillover loss, the edge of the reflector inter-

cepts the main beam at a level many dB down from the beam peak (e. g.

near the first null). In this case, the spillover loss is relatively

low, with little main beam energy missing the reflector. However, a

large illumination taper is present across the main reflector aperture,

resulting in a very low aperture efficiency and a consequent reduction

in gain.

With conventional feed and reflector geometry, a compromise is thus

inevitable in the selection of a reflector edge illumination level that

will achieve a reasonable balance between spillover and aperture

efficiencies. A level of -8 to -10 dB is usually established as the

comprimise setting. Again as will be discussed in detail later, we

expect the maximum gain over the whole target area instead of only on

the antenna boresight axis. In this case the reflector edge illumination

level of -8 to -10 dB does not maximize the off-axis gain.

The primary pattern of the feed should have low sidelobe levels so

that the spillover, if it does occur, will not reduce the gain too signi-

ficantly. In any feed system, design characteristics and manufacturing

techniques cause some of the energy in the principal polarization to be

converted to the orthogonal sense. Circular polarization purity is a

function also of the phase and amplitude balance realized by the

The graphs corresponding to three values of h are plotted in Fig. (2-1).

Comparing the gain at $\theta = \theta_o$ it is clear that the pattern producing the

highest gain on the axis ($\theta = 0$) does not yield the maximum gain at

$\theta = \theta_o$. It can be seen that the gain at $\theta = \theta_o$ is a function of both

the peak gain and the width of the beam. Let $P(\theta)$ be the normalized

power pattern in dB. Then it is easy to prove that

$$\frac{P(\theta)}{P(\theta_o)} = \left(\frac{\theta}{\theta_o}\right)^2 \qquad (2.3)$$

The half power beam width θ_{HP} can be found by setting $P(\theta) = -3$ dB

in

$$\theta_{HP} = 3.47 \, \theta_o / \sqrt{P(\theta_o)} . \qquad (2.4)$$

Now the on-axis gain ($\theta = 0$) of a circular aperture is given by Eq. (2.1)

$$G(0) = 10 \log_{10} \eta \left(\frac{\pi D}{\lambda}\right)^2 \text{ in dB} \qquad (2.5)$$

where η is the efficiency of the aperture and is a function of the

aperture field distribution. The gain at $\theta = \theta_o$ is then given by

$$G(\theta) = G(0) + P(\theta_o) \qquad (2.6)$$

From Silver[11] we also know that

$$\theta_{HP} = \frac{K\lambda}{D} \text{ in degrees} \qquad (2.7)$$

where K is also a function of aperture field distribution. By sub-

stituting (2.5), (2.6), (2.7) we obtain

$$G(\theta_o) = 10 \log_{10} \eta \left(\frac{K}{3.47\theta_o}\right)^2 + 10 \log_{10} (-P(\theta_0) + P(\theta_o)$$

$$\qquad (2.8)$$

polarization networks and depends on the symmetry between the E- and H-plane radiation patterns of the feed.

2.3 OFF-AXIS GAIN OPTIMIZATION

For an automatic tracking ground station, the design emphasis leans toward obtaining the highest possible directivity referenced to a point source target. To achieve this end, large antenna diameters have been widely used. However, for the low cost, unmanned earth terminals, the wisdom of using high gain apertures needs to be re-examined.

Various factors, such as pointing inaccuracy, satellite movements, wind effects, etc., will cause the antenna beam peak and the satellite to drift relative to one another. These factors together produce a total equivalent solid angle of 0.54^{o^9} ($\pm 0.27^o$ from beam axis) in which the satellite will drift during normal short-term operation for a moderate size of ground station. When a non-automatic tracking station is used, the antenna gain should be optimized over the effective satellite drift angle ($\pm 0.27^o$ in this case). For it is equally probable that the satellite will be at extremes of this off-axis angle as at the center. Therefore ground station antenna without tracking capability should consider the off-axis performance as well as on-axis performance.

In theory there is no limit to the peak (on-axis) gain of a pencil beam. Surprisingly, there is a limit to the maximum gain that can be realized[10] at an off-axis angle θ_o . To prove this let us assume that the normalized power pattern of a circularly symmetric beam is represented by the Gaussian function

$$P(\theta) = e^{-h\theta^2} \qquad (2.2)$$

- 13 -

The first term is a constant. The value of $P(\theta_o)$ which maximizes $G(\theta_o)$ can be found by writing

$$\frac{dG(\theta_o)}{dP(\theta_o)} = 0 \qquad (2.9)$$

which leads to $P(\theta_o) = -4.34$. The θ_{HP} which yields maximum gain at θ_o is

$$\theta_{HP} = 1.665 \; \theta_o \text{ in degrees} \qquad (2.10)$$

The maximum gain at $\theta = \theta_o$ is then given by

$$G(\theta_o) = G(0) - 4.34$$

$$= 10 \log_{10} \; \eta \left(\frac{\pi D}{\lambda}\right)^2 - 4.34 \text{ in dB} \qquad (2.11)$$

Thus, the off-axis gain can be maximized by varying both the diameter and illumination of the reflector. If the diameter is fixed, then there is an illumination taper at the edge of the reflector which will optimize the off-axis gain.
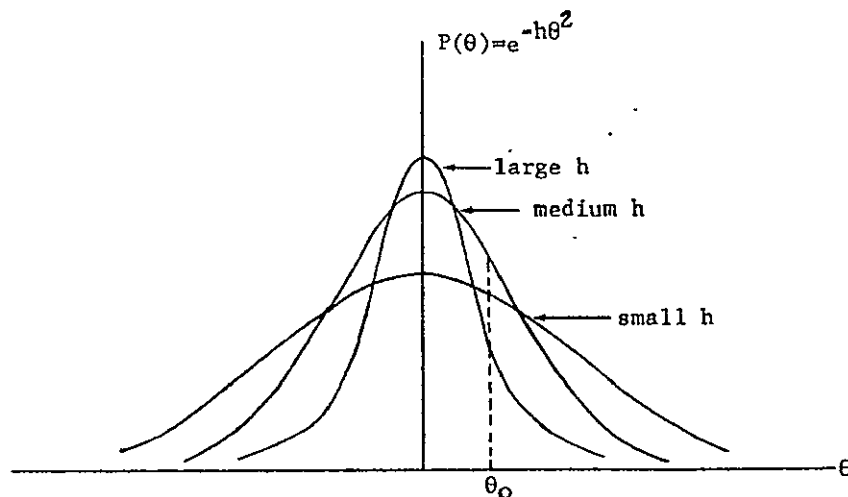
Fig. (2-1)--Illustration of off-axis gain variations.

From the stand-point of antenna efficiency we know that the ratio

of the focal length to the diameter of a reflector (f/D), in conjunction

with the feed pattern, determines the maximum efficiency available from

an aperture illuminated by a prime-focus feed. In making a tradeoff

between efficiency and f/D , only spillover and illumination factors

are considered. The remaining effects (i.e., blockage, phase errors,

cross-polarization) change insignificantly with f/D and are not considered.

The on-axis gain of a reflector is determined by optimizing the product

of aperture efficiency and spillover efficiency. For illustration the

on-axis gain of an eight-foot antenna has been computed for several

values of f/D using different circular multimode waveguide (an over-

sized waveguide propagating both TE_{11} and TM_{11} modes) patterns and

the results are shown in Fig. (2-2). In this case an edge illumination

of approximate - 10 dB produces the highest gain, which is consistent

with the conventional design criteria. For example, a reflector with

a feed size of 1.25 λ in diameter has the highest gain for a $f/D = 0.48$

(edge subtended angle is 55°), which intercepts the feed pattern at

- 10 dB point. However, for a non-autotracking station the off-axis

gain is more important than the on-axis gain. Taking the same computer

outputs and plotting gain values for a target off-axis by $\pm 0.3^{\circ}$ produces

the off-axis gain curves of Fig. (2-3). It is found that the value of

f/D which produces the highest gain in this case is not the same as in

the on-axis situation. For example, $f/D = 0.43$ instead of 0.48 gives

the highest gain at off-axis angle of 0.3° for the 1.25λ feed, which

corresponds to a 13 dB edge illumination taper. Although a large taper

will reduce the on-axis gain, it will broaden the radiation pattern

and as a result increase the off-axis gain.

- 16 -
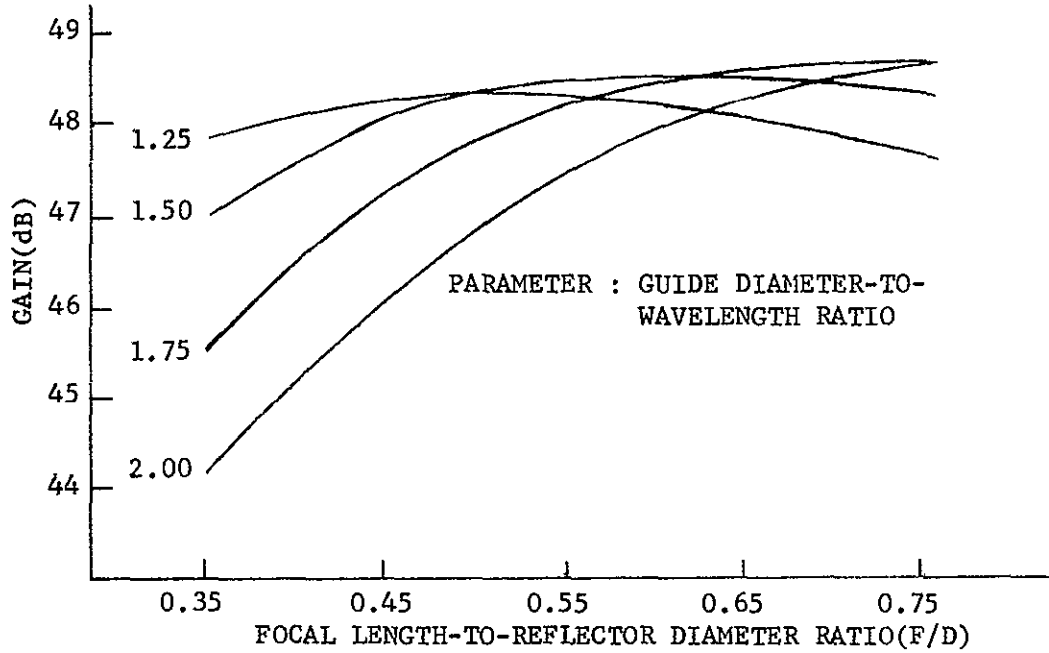
Fig. (2-2)--On-axis gain of an 8-foot reflector with multi-mode feed.
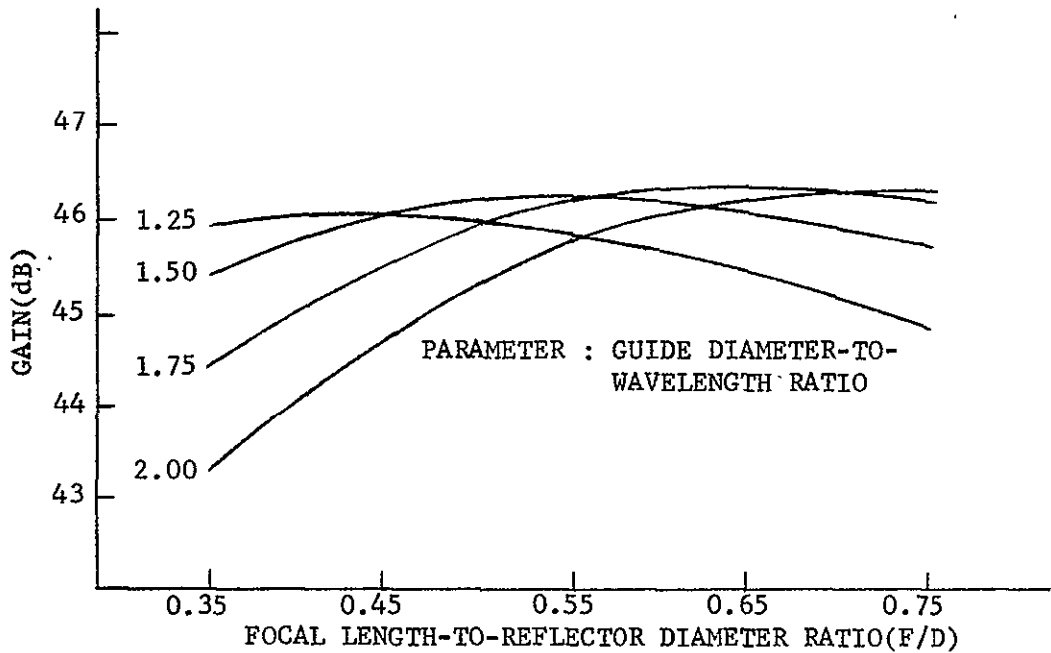
Fig. (2-3)--Off-axis (± 0.3°) gain of an 8-foot reflector with multimode feed.

2.4 NOISE TEMPERATURE

The noise temperature of an antenna system over the receive band
significantly affects the quality of a received signal, and should be
kept as low as possible. The sources of noise in the band of interest
are the earth, the atmosphere (principally water vapor and oxygen), feed
losses, and the receiver. The effect of the first two items depends
upon the distribution of energy among the several efficiency factors
previously discussed; this effect is quantified in terms of the antenna
noise temperature. The antenna noise temperature, combined with feed
loss and receiver noise temperature, is defined as the system noise
temperature.

2.4.1 Antenna Noise Temperature

The amount of noise added to the received signal prior to amplifi-
cation is directly related to antenna system losses and the equivalent
sink temperature of each loss. All factors contributing noise to the
system can be divided into three groups:

A. the energy radiated from the feed and scattered around the
    reflector

B. forward beam energy projected along and immediately around
    the antenna axis by the main lobe and principal sidelobes

C. dissipated energy within feed elements at $290^{\circ}K$

The noise temperature of the antenna (T_A) is the total of all inputs from
these noise sources and, referred to the feed horn mouth, is given by:

$$T_A(\theta) = \sum_n P_n T_n(\theta) \qquad (2.12)$$

- 18 -

where θ is the elevation angle of the antenna, P_n is the proportion of power scattered or absorbed by each loss factor, and $T(\theta)$ is the average noise temperature of the region which absorbs P_n . Since the power lost by all loss factors must equal the total radiated power, we have

$$\sum_{n} P_n = 1 \qquad (2.13)$$

The average noise temperature over the sky and earth regions of interest is found by integrating over the solid angle of coverage and normalizing with respect to the radiated pattern. Thus,

$$T_n(\theta) = \frac{\int_0^{2\pi} \int_0^{\pi} \psi_n(\theta',\phi')T(\theta',\phi')\sin\theta' d\theta d\phi'}{\int_0^{2\pi} \int_0^{\pi} \psi n(\theta',\phi')\sin\theta' d\theta' d\phi'} \qquad (2.14)$$

where

θ',ϕ' are polar coordinates with $\theta' = 0$ along with the antenna axis

$\psi(\theta',\phi')$ is the radiation pattern of the scattered power

$T(\theta',\phi')$ is the noise temperature distribution of the sky and earth which will be discussed in the following section.

As a basis for computing the sky temperature and the ground temperature the work of Hogg[12] and of Chen and Peake[13] respectively have been widely accepted. In his determination of sky temperature, Hogg assumed a simplified approximation of the International Standard Atmosphere as defined by International Union of Geodesy and Geophysics (IUGG). He then determined the loss through this model atmosphere from a site at sea level, from which the noise temperature was determined. The resulting

curves of the sky noise temperature for 2.6 GHz and 12 GHz are plotted

in Fig. (2-4) for average weather. Below the horizon, the temperature

of the earth becomes evident and the noise level becomes relatively

high. Figure (2-5) shows the ground temperature as a function of antenna

elevation angle for a terrain with average water content and surface

texture.

2.4.2 System Noise Temperature

The antenna temperature discussed in the previous paragraph includes

neither noise sources that exist between the feed and the receiver nor

the receiver. The thermal noise temperature of the antenna system, Ts,

referred to receiver input is given by

$$Ts = \frac{TA}{L} + \left(\frac{L-1}{L}\right) To + T_R \qquad (2.15)$$

where

T_o = ambient temperature (generally $290^\circ K$)

L = insertion loss of feed system (power ratio)

T_R = receiver noise temperature

The receiver noise temperature is related to its noise figure (NF_r) by

the following relation

$$NF_r = 10 \log_{10}\left[\frac{T_R}{290} + 1\right] \qquad (2.16)$$
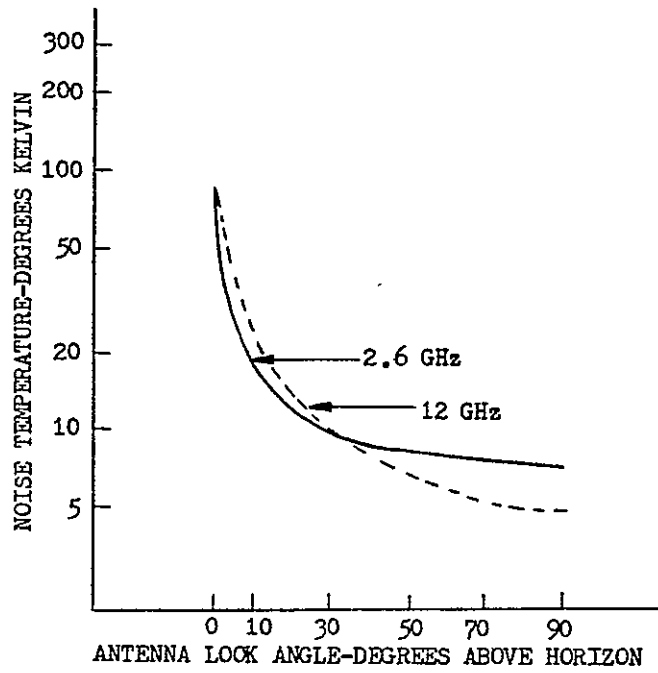
Fig. (2-4)--Sky noise temperature.
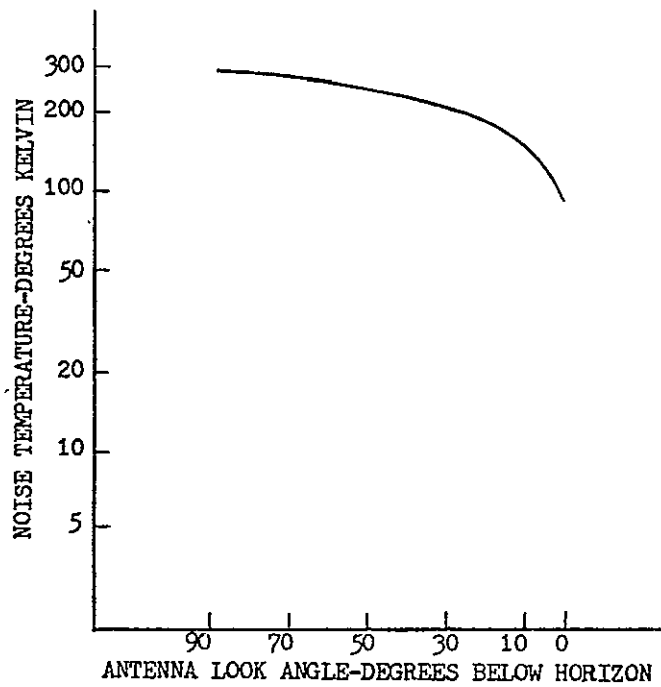
Fig. (2-5)--Ground noise temperature.

Figure (2-6) illustrates the range of noise figures possible using various

devices in the 2.6 and 12 GHz bands.
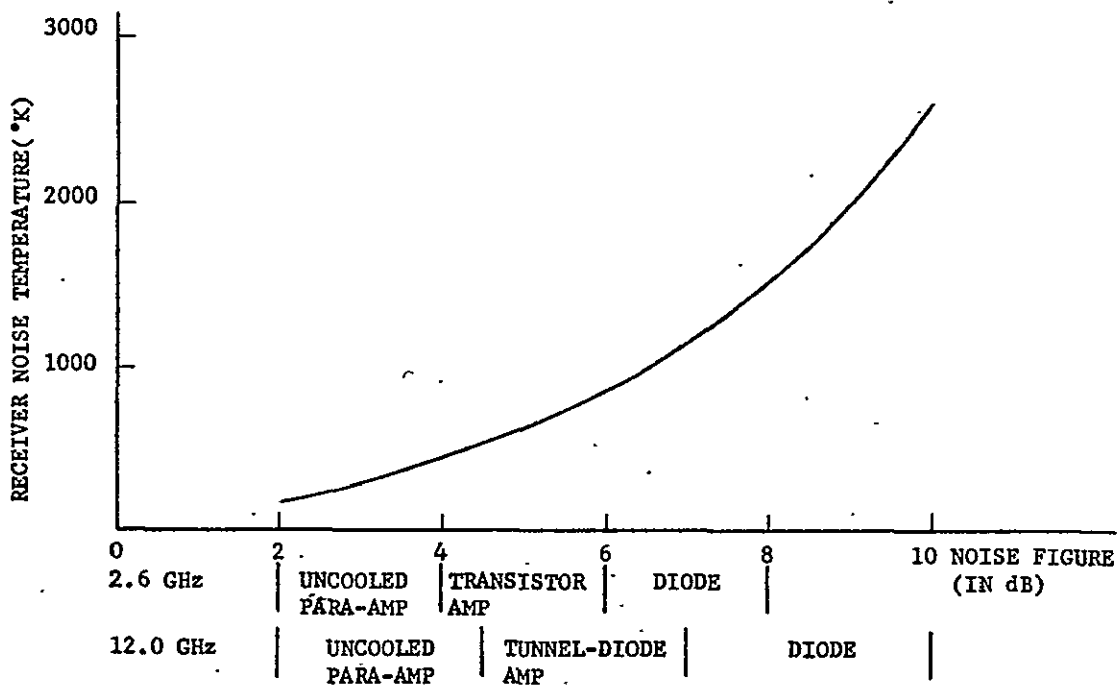
Fig. (2-6)--Receiver noise temperature vs noise figure.

2.4.3 Figure-Of-Merit (G/T_s)

The figure-of-merit describes the sensitivity of a ground receiving

station and is defined as the ratio of receiving antenna gain G to system

noise temperature T_s:

$$G/T_s \text{ (in dB)} = G(dB) - 10 \log_{10} T_s(^\circ K)$$

The importance of figure-of-merit may be seen from its relation to

satellite effective isotropic radiated power (EIRP) as given in the

following equation

$$EIRP = C/Ts + Lp + Lm - (G/Ts) \qquad (2.18)$$

where

C/T_s = carrier-to-system noise temperature ratio

Lp = path loss

Lm = total system loss (including design margin)

It is apparent that the required G/Ts of a receiving system can be reduced
by increasing satellite EIRP. This offers a cost trade-off between
satellite EIRP and ground station G/Ts. Further, G/Ts also offers a
trade-off in the selection of the size of antenna and the type of pre-
amplifier.

2.5 ANTENNA CATEGORIES

There are several basic antennas which have high directivity and
low noise characteristics as required in satellite communication. The
paraboloidal reflector antenna is presently an economically optimized
approach. Phased arrays are more attractive when the signals in two
or more directions are separated by at least ten beamwidths and when
the signals in those widely separated directions require scan rates ex-
ceeding those which are mechanically feasible by moving a single reflector.
In the case of satellite communications, the reflector antenna system is
superior to the phased array on the basis of design simplicity, lower
loss and greater bandwidth potential.

Only the prime focus (one reflector) and the Cassegrain system
(two reflectors) are considered to be potential candidate for use in a
low cost satellite communication system. The Gregorian antenna (sub-
reflector confocal with the main reflector), horn reflector antenna
and offset parabola are ruled out because of difficult mechanical problems,

such as alignment and the immense structural size involved.

The Cassegrain system is more costly than a conventinal parabolic antenna, due mainly to the additional reflector (a hyperboloid sub-reflector) required. However, on the basis of efficiency, the Cassegrain arrangement has a slight advantage even for small antennas, because the two reflectors can be shaped[14] so that the subreflector intercepts most of the feed horn energy, while the main reflector is illuminated uniformly resulting in good combination of spillover and aperture efficiency. For illustration, a seven-foot prime-focus antenna and a seven-foot Cassegrain antenna (subreflector diameter of one foot) are examined in some detail in Fig. (2-7). There is also a slight reduction of noise temperature in the Cassegrain geometry because the spillover energy is smaller and illunimates mainly the the "cold" sky instead of the "hot" earth, as does a prime-focus geometry. The trade-offs between these antennas are tabulated in Table 2-1.

Table 2-1

COMPARISIONS OF CASSEGRAIN SYSTEM AND PRIME FOCUS SYSTEM

Cassegrain Antenna (shaped Reflector)	Prime Focus Antenna
Efficiency 67%	Efficiency 53%
+ Simple Design	+ Simple Design
+ Compact	+ Compact
+ Flexibility in Feed Design	+ Restrictive Feed Design
+ Low Noise	- High Noise
+ Easy Service	- Difficult Service
- Expensive	+ Less Cost
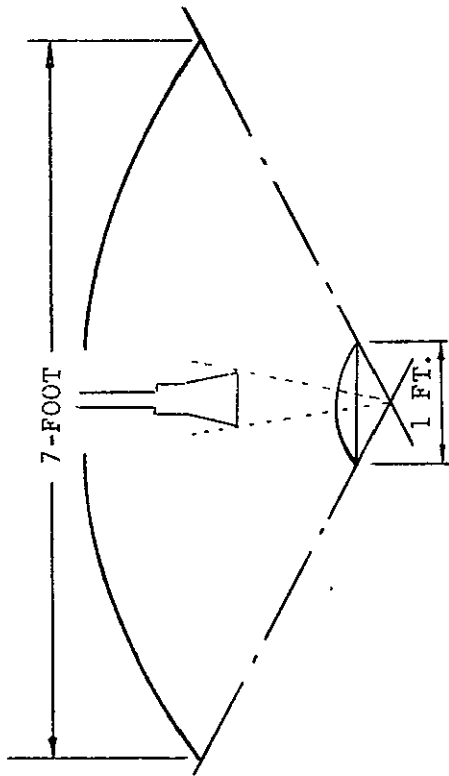
CASEGRAIN SYSTEM
(MULTIMODE FEED)

LOSSES(EST.) IN dB :

SPILLOVER	-0.25
DIFFRACTION	-0.50
BLOCKAGE	-0.45
SURFACE	-0.20
CROSS POLAR.	-0.15
PHASE	-0.05
APERTURE	-0.05
LINE	-0.02
VSWR	-0.07
TOTAL	-1.74
EFFICIENCY	67 %
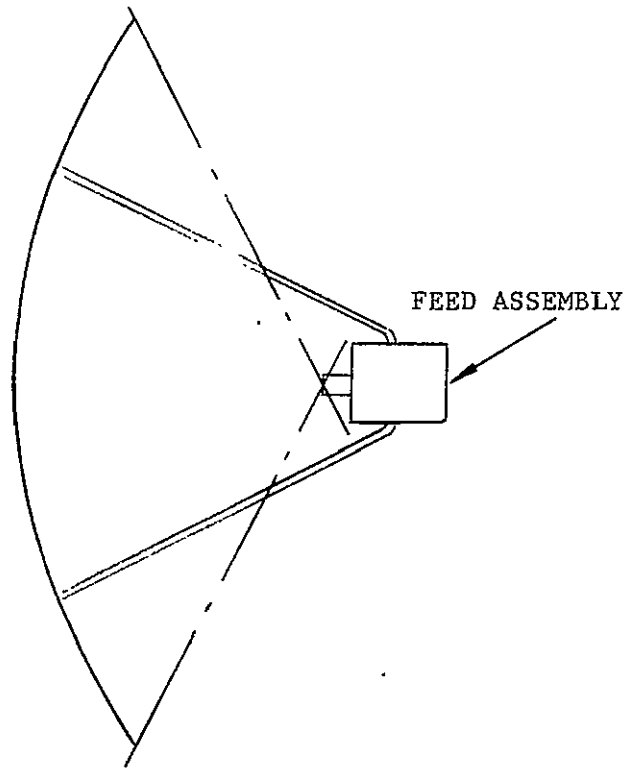
PRIME-FOCUS SYSTEM
(WAVEGUIDE FEED)

LOSSES(EST.) IN dB :

SPILLOVER	-0.50
APERTURE	-0.70
CROSS POLAR.	-0.25
SURFACE	-0.20
BLOCKAGE	-0.35
PHASE	-0.10
LINE	-0.07
VSWR	-0.12
TOTAL	-2.29
EFFICIENCY	53 %

Fig. (2-7)--Comparison of Cassegrain and prime-focus system.

2.6 ANTENNA FEED

The antenna system under consideration requires no automatic tracking capability and all the frequencies are constrained within a bandwidth no greater than 10 percent. Under these circumstances the selection of feed type and construction is governed by the following factors:

A. Type of Antenna System

In a Cassegrain system the feed illuminating the subreflector usually has much narrower beamwidth (due to small subreflector subtended angle) than that employed in a prime-focus system. The subreflector in general intercepts the feed pattern at a total angle ranging from 20 to 40 degrees. A conical horn is therefore most desirable in a Cassegrain system, since its beamwidth can be made small by increasing the aperture thus offering great design flexibility.

B. Operating Frequency

The operating frequency affects the insertion loss and physical dimensions of a feed. It also affects fabrication methods and determines manufacturing tolerance. For direct reception from satellites only the 2.6 GHz (S-Band) system and the 12 GHz (X-Band) system are recommended. An open-end waveguide (or horn) type feed offers minimum insertion loss for the X-Band system but appears bulky for the S-Band system. The use of printed-element type feed will reduce the size and yield low loss for the S-Band system but result in high loss for the X-Band system.

C. Polarization Diversity Requirement

Owing to the rotation of the plane of polarization by a variable

amount in the ionosphere, linearly polarized transmissions have

not been recommended for use at 2.6 GHz. The use of circular

polarization will avoid any loss of signal from this rotation

effect. However, this rotation effect is very small - at

most a fraction of a degree - at 12 GHz and the use of linear

polarization may be preferred.

The use of one polarization for some transmissions (or reception)

and the complementary polarization (opposite rotation if circular,

or in a plane at right-angles if linear) for other transmissions

(or reception) operating in the same frequency channel will

aid in the protection of services from mutual interference.

The simplest case is the one in which only one sense (vertical

or horizontal) of linear polarization or one sense (right hand

or left hand) of circular polarization is required. A number

of feeds exist which intrinsically operate for only one polari-

zation sense and therefore need not have hybrid networks.

Examples include open-end waveguide (or horn) and dipole feeds

for a linear polarization system, and helicons and two-arm

spiral feeds for a circular polarization system. If a system

operates for more than one sense of polarization, polarizers,

hybrid networks or multi element feeds have to be installed.

In such cases complexity, insertion loss and hence system cost

will be increased.

D. Power Handling

　　• In general a feed system consisting of waveguide components can

　　be operated at higher power levels than one consisting of strip

　　line (or microstrip) components. Therefore waveguide feeds are

　　often used in transmitting ground stations, while most of the

　　printed element feeds can only be found in receiving stations.

E. Cost Consideration
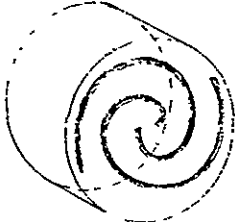
　　The cost of a feed for high quantity production can be held

　　low if construction is easy and it is mass producible. For

　　instance, die-casting methods can be used to produce waveguide

　　type feeds.

As the above factors become defined, the designer is left with less

latitude in the selection of a feed. The suitable feed compatible with

the constraints just discussed can be grouped into four categories:

waveguide open-end or simple horn, multimode guide or multimode horn,

helicone, and cavity backed printed spiral (archimedean Spiral), as

compared in Table 2-2.

The simple conical horn (or waveguide open-end) is inexpensive and

simple, and its performance is readily predicted. For the proposed

antenna configurations (prime focus or Cassegrain) it can direct more

than 85 percent of its radiated energy toward the reflector, and there-

fore provides a reasonably efficient system. Since this horn has the

highest possible gain for a given aperture, it can be used more effectively

in a smaller system than any other.

Table 2-2

COMPARISON OF ANTENNA FEED

	ARRANGEMENT	CHARACTERISTICS
SIMPLE CONICAL HORN		+ SIMPLE - PREDICTABLE - NON-SYSTEM PATTERN - PRIMARY SIDELOBES
MULTIMODE HORN(STEP DISCON. TYPE)		+ SIMPLE - IDEAL PATTERN - LIMITED BANDWIDTH - LARGER APERTURE
HELICONE		+ SIMPLE + AXIALLY SUPPORTED - CIRCULAR POLARIZATION ONLY - LESS DIRECTIVITY - POSSIBLE BEAM SQUINT
CAVITY BACKED ARCHIME-DEAN SPIRAL		+ SIMPLE(PRINTED ELEMENT) + LIGHT WEIGHT - CIRCULAR POLARIZATION ONLY - LOSSY AT HIGH FREQ. (12 GHz.) - LESS DIRECTIVITY

Multimode techniques that require mode generators and mode filters in the throat of a simple conical horn (or waveguide) have been used by several feed manufacturers[15,16] with reasonably good success. Achievement of 10 percent bandwidth is common. This horn is selected for use in the experimental model as will be discussed in Chapter 5. It features equal E - and H - plane pattern and therefore has low cross polarization loss and a unique phase center in both E - and H-planes. Step discontinuities are used as mode controllers. Fabrication appears quite inexpensive.

The helicone[17] is a combination of an axial mode helix and a conical horn. The helix is fed simply by a coaxial line and is intrinsically a circular polarization antenna. Because it can generate a circularly polarized wave without relying on such feeding networks as a balun, hybrid or polarizer, it is very attractive for use as a low cost feed. The helix can be mounted on a hollow aluminum tube, which in turn provides a secure support for the feed when it is used in a prime focus system. Although its pattern can be controlled to some degree by varying mouth diameter, horn length, helix length etc., it generally has too little directivity for use in a Cassegrain system.

The cavity-backed two-wire Archimedean spiral[18,19,20] configuration is also a circularly polarized radiator. Its two arms are fed 180 degrees out of phase by a device such as a Robert's balun,[21] and it has a circumference of at least one wavelength. The arms of the spirals are usually fabricated by photoetching the geometric configuration on copper-clad laminate. The use of an added cavity allows the Archimedean spiral to radiate in only one sense of circular polarization; the cavity

in general has a depth slightly less than a quarter wavelength. This

feed is compact and can be flush mounted. However, it only can be used

in a prime focus system because of its less directive pattern.

2.7 IMAGE REJECTION FILTER

An image rejection filter is often used to reduce the noise figure

of a receiver. The required characteristics of this filter depend on (1)

the IF frequency and RF bandwidth (which determine the separation between

the image signal (stop band) and the real signal (pass band)), and (2)

the required signal-to-noise ratio of the system, (which determines the

amount of isolation required on the image signal). For a low cost

station, the IF frequency is chosen in the VHF band. In the 2.6 GHz

band the image signal and real signal are sufficiently separated that it

is possible to utilize the proper waveguide size to attenuate the image

signal to some degree, provided that waveguide components are used. This

is only the simplest case. In general, suppression of the image depends

on an RF filter of either a bandpass or high pass type. The selection

of filter type is made on the basis of the following factors:

A. maximum skirt slope and minimum passband dissipation for the
   specified stop-band rejection.

B. construction tolerance

C. minimum tuning requirements

D. physical dimensions

E. low cost

The high pass filter in essence is a piece of cut-off waveguide.

The bandpass filter can be categorized according to its response charac-

teristics, such as maximally flat, Tchebycheff, or elliptical-function

type.[22] The latter type has the lowest theoretical loss for a particular

rejection value, but because of its equivalent circuit it is difficult

to be realized in waveguide. A Tchebycheff filter has been chosen here

because it has greater out-of-band rejection and lower pass-band dissi-

pation loss for a given number of resonant elements and pass-band width.

Conventional designs of band-pass filters use the shunt-inductance

coupled circuit; this raises design difficulties at the 12 GHz band

using waveguide components. For example, a system with IF equal to 120

MHz and an RF bandwidth of only 30 MHz at 12 GHz needs a three-element

inductive type bandpass filter in which the center element has a normal-

ized susceptance of -24. Such a high susceptance, when realized by a

center hole iris, requires an iris hole so small that it is hard to hold

the required tolerance. Furthermore, such a filter is five times more

lossy in the pass band than a high pass waveguide filter, and inevitably

requires some kind of tuning mechanism. In this case a high pass filter

is a better candidate, for it is superior to the bandpass filter in

every aspect except its longer length. Bandpass filters using other

kinds of transmission line (such as strip line) are more lossy and will

not have other significant advantages over the waveguide type.

2.8 TRACKING REQUIREMENTS

When working with synchronous satellites, an earth station antenna

is required to perform only minor pointing corrections to track the

satellite. In a prime focus system a method of manually initiating

this continuous fine tracking is to displace the direction of the main

lobe by tilting the feed about the vertex while the reflector is kept

in a fixed position.

As the feed is moved off axis by a rotation about the vertex of the reflector, the beam will move off axis on the side opposite the feed and in direct proportion to the feed displacement. It was shown by Silver[23] that, as the beam moves off axis, the gain decreases and the beam width increases. The variation of gain with feed tilt for reflectors of different shapes with a relatively directive feed is plotted in Fig. (2-8). It can be seen that the larger the value of F/D, the less the gain loss. For a parabolic reflector with F/D = 0.5 a five beamwidth feed tilt corresponds only 0.3 dB gain loss.
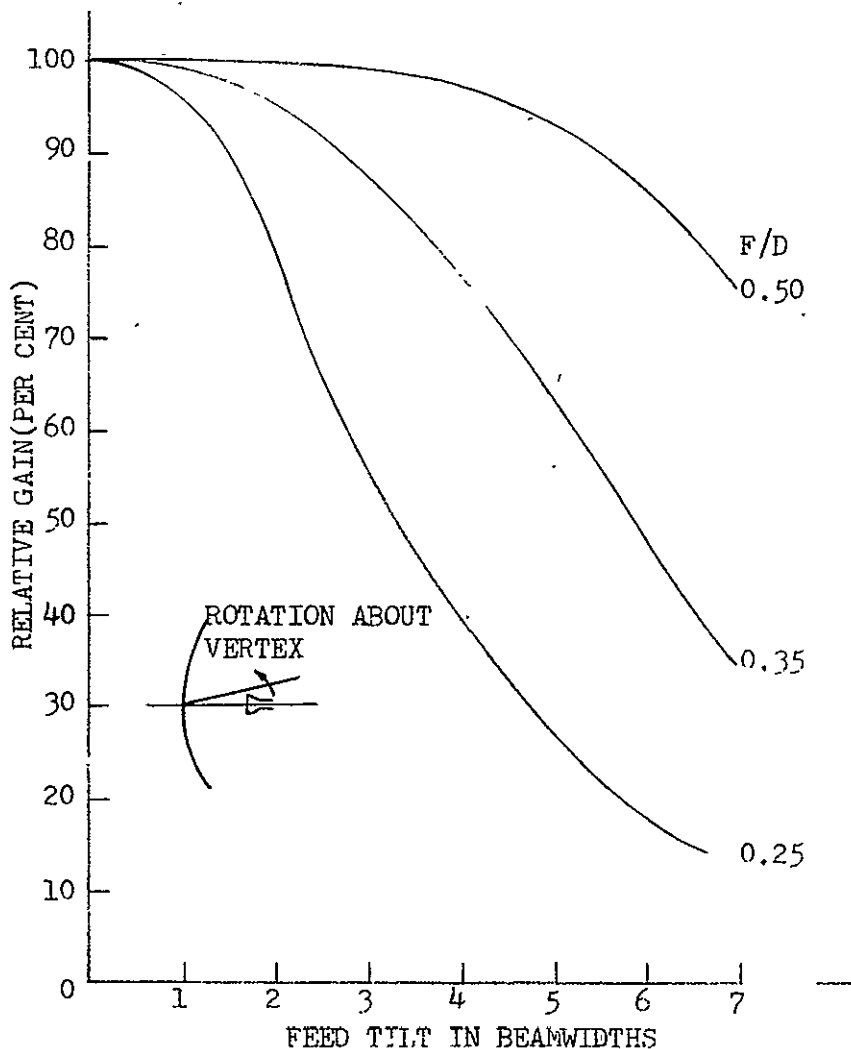
Fig. (2-8)--Gain reduction due to feed tilt.

Recently a number of suggestions[24,25] have been made for automatic

procedures for searching for peak signal from a geostationary satellite.

These are typically described as step-track or hill-climb track and are

being currently evaluated in industry[26] though little information on

customer opinion is available. This technique has the merit of extreme

simplicity and appears to be the most reasonable potential candidate for

use in a low cost station to track highly stabilized synchronous satellites.

The operation principle of the step-track system is very simple.

After signal acquisition, the antenna is commanded to make an initial

angular move. By comparing the received signal level before and after

the move, the direction of the next move can be decided. That is, if

the signal level has increased, the antenna continues to be moved in the

same direction. If the signal level has decreased, the direction of

movement is reversed. This process would be continuous and alternating

between the two orthogonal antenna axes.

A simple system of step-track is suggested here as shown in the

functional diagram of Fig. (2-9) its cost will be analyzed in Chapter 6.

Since integrated circuits will be used to build this system, great cost

saving under mass production can be expected. The dc voltage input into

this system, representing the received signal level, comes from the IF

energy detector. The control signal must operate on the signal strength

data and derive positioning commands. A simple description of each block

element is made as follows to help further understand the functioning

of this system:

A. Input Buffer/Filter

The Input Buffer/Filter provides about 40 dB gain and 5 Hz cutoff
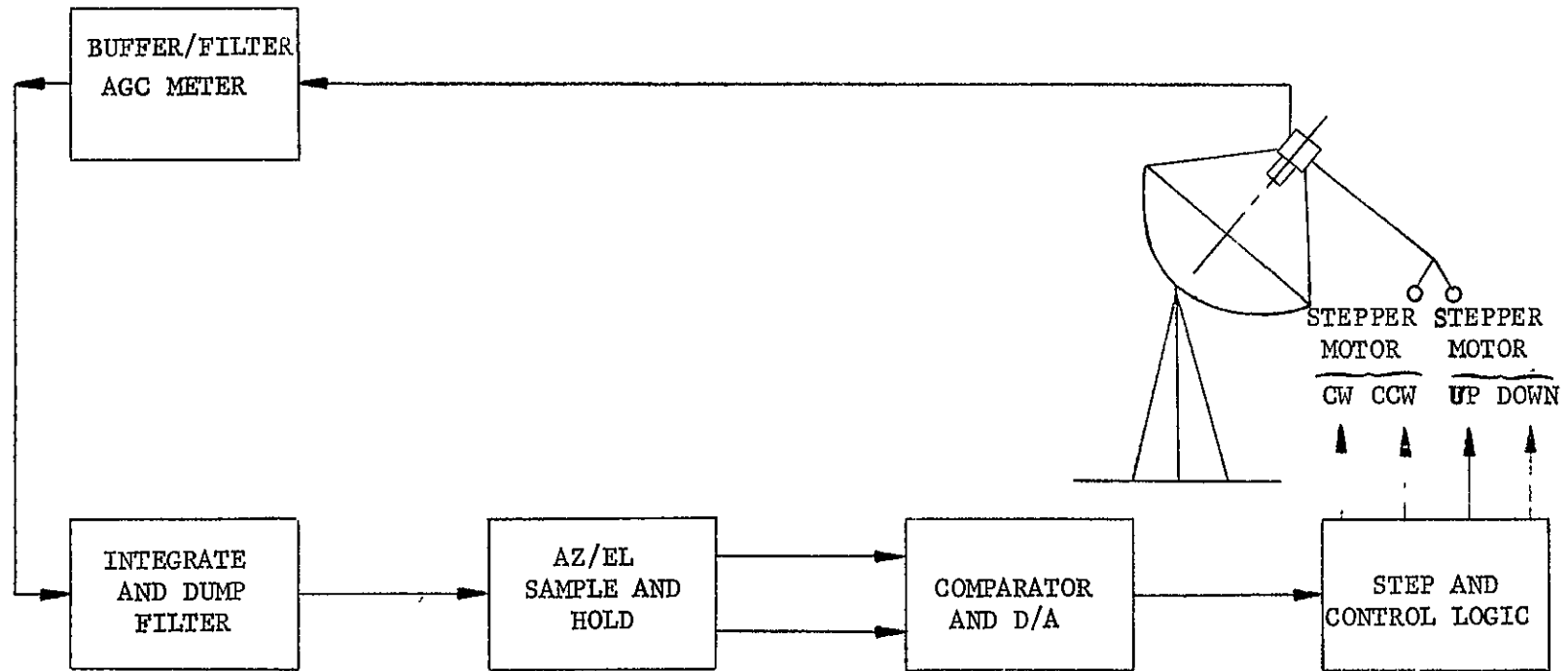
Fig. (2-9)--Basic block diagram of a step-track system.

low pass filtering. Its balanced differential input configuration
allows rejection of common mode noise due to other ground systems,
and presents a high impedance to the input signal. Five Hz
cutoff, low-pass filtering prevents 60 Hz and high frequency
noise from swamping out the buffer amplifier.

B. Integrator

The Integrator circuit determines the average signal levels
following each azimuth and elevation step. The integration of
signal strength variations accomplishes signal noise filtering,
and reduces the effect of periodic ripple due to satellite spin.
A reset capability prepares the integrator for each azimuth
or elevation step cycle.

C. Azimuth/Elevation Sample-And-Hold

A Sample-and-Hold circuit suspends the Integrator output, over
a selected interval, for a duration sufficient to permit com-
parison of signal strength variations and storage of the result-
ant. The Sample-And-Hold circuit design provides accurate
tracking of input signal amplitude and accurate holding over
the selected interval, consistent with the required system
resolution.

D. Comparator

The Comparator evaluates the outputs of the Sample-And-Hold
circuits to determine the relative changes in input signal
strength. The resultant error signal is used by step and
Control Logic circuits for decisions on increment direction.

E. Step And Control Logic

Step and Control Logic circuits direct the various elements of

the step trackers' sequence of operation and stores the choices

of azimuth and elevation increment direction.

CHAPTER 3

EFFECT OF GROUND ANTENNA CHARACTERISTICS ON SATELLITE SPACING

3.1 INTRODUCTION

With the development of effective broadcast satellites using the
synchronous equatorial orbit, concern has grown about efficient use of
this orbit such that both the satellites and the ground stations are
subjected only to harmless interference. Studies on the economic aspects
of direct broadcasting satellite systems show that use of small ground
stations and high satellite effective isotropic radiated power (EIRP)
is more desirable than that of larger ground stations and lower satellite
EIRP. This further stimulates the need to investigate interference among
satellite systems using small ground stations and the development of
low cost techniques to reduce interference. The minimum angle of sep-
aration between satellites in the geostationary orbit sharing the same
frequencies and with specified antenna patterns is determined primarily
by the radiation pattern of the earth station antenna. In this chapter
we will review and propose sidelobe suppression techniques for reflector
type antennas and investigate how the ground station characteristics,
such as antenna size, sidelobe levels and cross-polarization levels
affect the minimum satellite spacings. The CCIR sidelobe model has been
widely used in recent years to study interference between satellite
systems[27,28] and between satellite and terrestrial systems. Unfortun-
ately, the CCIR antenna model is believed to have higher sidelobe levels
than the average ground antennas should have, especially for

small and medium size antennas $(D/\lambda \leq 200)$. Therefore, use of the CCIR model will yield conservative results. Our approach in forming an antenna model is to compute the theoretical pattern taking into account blockage effects, and then to compare the result with typical ground antenna patterns supplied by manufacturers.

To calculate the satellite spacing and interference we assume a homogeneous satellite system in which all the satellites have the same EIRP and identical spacings. For the up-link calculation the transmitting powers are assumed the same for all stations. Under these assumptions, and without counting propagation factors, both down-link interference and up-link interference depend only upon the ground station antenna pattern. In fact, these assumptions lead to a lower limit for the achievable wanted-to-unwanted signal power ratio, since typical proposed systems will generally exhibit 3 to 5 dB greater value of this ratio.

3.2 INTERFERENCE OBJECTIVE AND PROTECTION RATIO

When an unwanted RF interference signal enters the earth station receiver, the quality of the message at the single-channel output of the communication system is degraded. It is therefore necessary to relate the unwanted signal to the message quality so that an allowable level of the unwanted signal can be established.

The output message quality is measured by the single-channel signal-to-noise ratio (S/N) for analog messages. In general, the signal-to-noise ratio is a function of the input wanted-to-unwanted signal ratio P_w/P_u , where P_w is the average power of the wanted signal and P_u is the

average power of the total unwanted RF signal. For the FDM/FM and FDM/AM

message the signal-to-noise ratio is proportional to the wanted-to-unwanted

signal ratio. That is

$$\frac{S}{N} = R \frac{P_w}{P_u} \qquad (3.1)$$

where R is the interference reduction factor.

We assume that technology has reached the state where thermal noise

can be reduced to a small value compared with interference, at least

during normal propagation conditions. Calculations[29] of carrier-to-noise

ratio made by the Bell Telephone Laboratories verify that such an assump-

tion is warranted.

The interference protection ratio (PR) required by a satellite earth

terminal can be defined as the minimum wanted-to-unwanted signal ratio

P_w/P_u (in dB) compatible with the signal-quality objectives after de-

modulation. Two factors determine this required protection ratio:

A. the allowable interference in the overall noise budget.

B. the types of modulation of both wanted and unwanted signals.

The protection ratios for television and telephone systems will be

examined separately in section 3.2.1.

3.2.1 Protection Ratio of An FM Television System

The International Radio Consultative Committee (CCIR) recommended[30]

that the required protection ratio in dB (PR), for just-perceptible inter-

ference upon a color television signal with a given peak-to-peak luminance

signal-to-r.m.s. weighted noise ratio, S/N, should be calculated using

the formula:[*]

$$PR = PC - (49 - S/N), \quad S/N \leq 49 \text{ dB}$$
$$PR = PC \qquad\qquad\qquad S/N \geq 49 \text{ dB}$$

(3.2)

where PC is the "protection constant" given in Table 3-1. The protection ratios versus the signal-to-noise ratio for various FM signals representing different peak-to-peak deviations at reference frequency (Δf) are plotted in Fig. (3-1). For all the curves in Fig. (3-1) we assume the wanted and unwanted signal have the same Δf . The deviation, Δf , and the signal-to-noise ratio for the unwanted signal have only minor effects upon the protection ratio. Over the range of deviations studied, the protection ratio decreases with increasing wanted signal deviation.

Table 3-1

PROTECTION CONSTANT OF FM TV SYSTEM

Wanted signal	Unwanted signal	Protection Constant (dB)
FM, Δf = 8 MHz	AM - VSB	32
	FM, Δf = 8 MHz	36
	FM, Δf = 15 MHz	34
FM, Δf = 16 MHz	AM - VSB	26
	FM, Δf = 10 MHz	28
	FM, Δf = 16 MHz	30
	FM, Δf = 20 MHz	28
FM, Δf = 24 MHz	AM - VSB	23
	FM, Δf = 18 MHz	25
	FM, Δf = 24 MHz	27

[*]Reference to Appendix A for results of subjected assessment tests of co-channel interference.

Very little data exists on the protection ratio required for monochrome

FM transmission. Some preliminary subjective assessments[27] of interfer-

ence between monochrome-television-picture signals made in the British

Post Office laboratories indicate that, for a peak-to-peak deviation

of 8 MHz on the wanted system, the protection ratio is of the. order of

30 dB for the condition of just perceptible video interference, a value

compatible with the protection ratio of the color television system.

Note that use of Fig. (3-1) to determine the protection ratio will

result in just perceptible interference during less than 5% of possible

program picture content. The values for tolerable interference are some

4 or 5 dB lower, as are the values for 50% of possible program picture

contents.
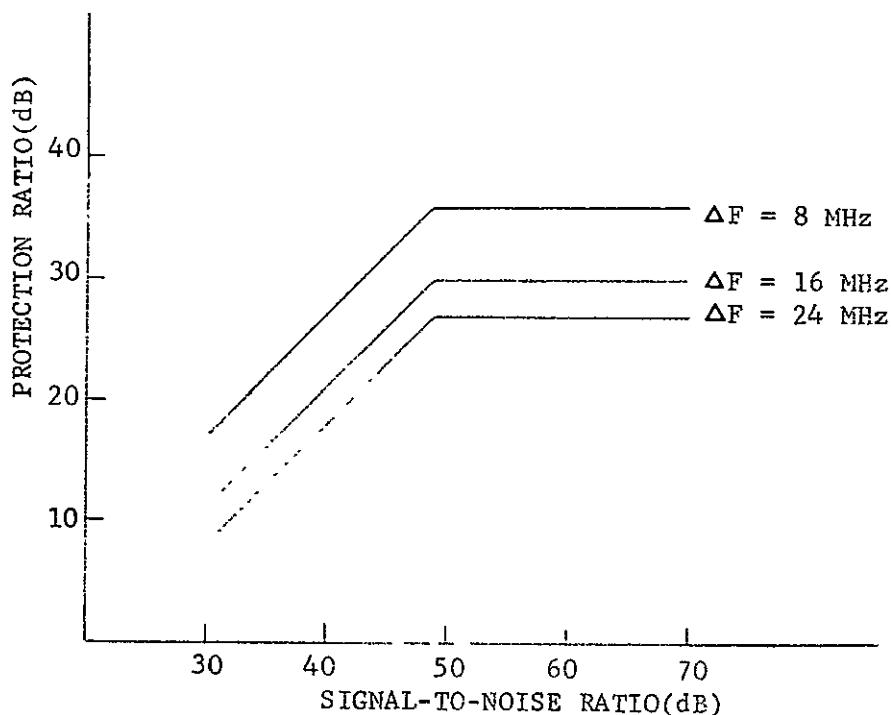
Fig. (3-1)--Protection ratio of FM TV system.

3.2.2 Protection Ratio of a Communication Satellite FM Telephone System

In specifying telephone signal objectives, it is customary to indicate the desired signal-to-noise ratio, S/N, by giving the allowable value of N as a so-called point of 0 relative level where $S \equiv 1$ mW. The CCIR normally gives N in units of pWOp (picowatts at a point of 0 relative level, psophometrically weighted). This unit can be converted to dBmOp (dB above a milliwat at a point of 0 relative level, psophometrically weighted) by using the identities

$$N_{dBmOp} = 10 \log N_{pWOp} - 90 \qquad (3.3)$$

The interference noise power, as recommended by CCIR (Rec. 466), at a point of zero relative level in any telephone channel of a hypothetical reference circuit of a geostationary communication-satellite system employing frequency-modulation, caused by the aggregate of the earth station and transmitters of unwanted satellites should provisionally not exceed:

A. 1000 pW psophometrically-weighted mean power in any hour;

B. 1000 pW psophometrically-weighted one-minute mean power for 20% of any month;

The protection ratios for the telephony system are quite dependent on how the total 1000 pWOp objective is partitioned - i.e., divided between up link and down link — though this is not pointed out in the CCIR recommendation. To calculate the required protection ratio the following formula derived from Eqs. (3.2) and (3.3) are used

$$PR = (- 10 \log NpWOp + 90) - R(dB) \qquad (3.4)$$

The interference reduction factor R for an FM system with modulation indices greater than 1 and for the co-channel case (carrier frequency separation = 0) can be found from reference 31. Tables 3-2 and 3-3 show the protection ratios which are necessary to limit interference to 1000 pWOp and 500 pWOp (divided equally between up link and down link) for 240 voice-channel systems with a range of RF bandwidths. For the offset channel case the required protection ratio is reduced and an improvement of 10 dB in protection ratio is common.

Table 3-2

PROTECTION RATIOS FOR FM TELEPHONY SYSTEMS

NpWOp = 1000 pWOp

RF Occupied Bandwidth Per 240-Channel Carrier, MHz	17	15	12	9	6
Interference - Reduction Factor R(dB)	35	34	32	27.5	27
Required protection Ratio (dB)	25	26	28	32.5	33

Table 3-3

PROTECTION RATIOS FOR FM TELEPHONY SYSTEMS

NpWOp = 500 pWOp

RF Occupied Bandwidth Per 240-Channel Carrier, MHz	17	15	12	9	6
Interference - Reduction Factor R(dB)	35	34	32	27.5	27
Required Protection Ratio (dB)	28	29	31	35.5	36

3.3 EFFECT OF EARTH STATION ANTENNA ON RF INTERFERENCE

3.3.1 Down-Link Interference - Satellites To Earth Station

The RF interference from unwanted satellites sharing the same frequencies under given conditions (i.e., specified antenna directivity patterns for each of the adjacent satellites) is determined primarily by the radiation pattern of the earth-station antenna. To show this let G_0 be the gain of the satellite antenna which transmits the wanted signal with power P_0 and let g_0 denote the gain of the ground station in the direction of the wanted satellite. Then the wanted carrier power Pw received can be expressed in the form

$$Pw = P_0 \left(\frac{\lambda}{4\pi R_0} \right)^2 G_0 g_0 \qquad (3.5)$$

where λ is the wavelength and R_0 is the distance between the wanted satellite and earth station antennas. If P_i and G_i denote the power transmitted and gain of the unwanted satellite, the unwanted signal power (interference) P_u is the sum of the interference from all the unwanted satellites:

$$P_u = \sum_{i=1} P_{ui} = \sum_{i=1} P_i \left(\frac{\lambda}{4\pi R_i} \right)^2 G_i g_i, \; i \geq 1$$

$$\qquad (3.6)$$

where P_{ui} is the interference from an individual unwanted satellite, R_i is the distance between the unwanted satellite and the earth station and g_i is the gain of the earth receiving station antenna in the direction of the unwanted satellite.

Under the following two assumptions:

A. All the satellites have equal effective radiated power in any

   given bandwidth in the direction of the earth station, i.e.,

   $P_i = P_0$ and $G_i = G_0$.

B. The distances between the earth station and the wanted satellite

   and the unwanted interfering satellites are assumed approxi-

   mately the same, i.e., $R_i = R_0$.

Equation (3.6) can be simplified as

$$P_u = P_0 \left(\frac{\lambda}{4\pi R_0} \right)^2 G_0 \sum_{i=1} g_i \qquad (3.7)$$

Assumption (A) is not far away from practice if all the ground stations

are within the satellite antenna beam coverage area. In general, the

edge-of-coverage gain of a wide-coverage satellite antenna using pencil

beam is optimized if it is 4.34 dB below the on-axis gain as shown in

Eq. (2.9). In this case satellite antenna sidelobe structures and levels

have the least effect on interference. The sidelobe level is of interest

only for those satellite antennas providing narrow beam coverage. The

wanted-to-unwanted signal power ratio then obtained is

$$\frac{P_w}{P_u} = \frac{g_0}{\sum_{i=1} g_i} \qquad (3.8)$$

It is apparent that the ratio P_w/P_u can be determined if the earth

antenna patterns are known. In the discussion hereafter we further

assume that the satellites are equally spaced along a geostationary orbit

and only those satellites above the local horizon contribute interference.

(see Fig. (3-2)).
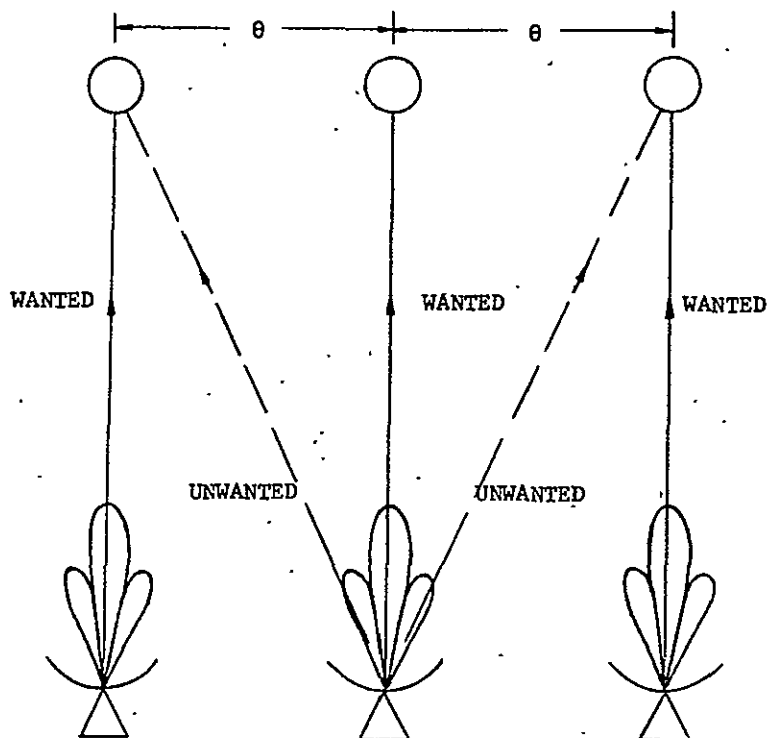
Fig. (3-2)--Down-link interference geometry.

3.3.2 Up-Link Interference-Earth Stations To Satellite

The interference caused by unwanted ground transmitting stations on the satellite's wanted received signal can be treated in the same way as described before. To simplify the problem we assume that:

A. The satellites are equally spaced and have specified patterns;

B. Each satellite has only one corresponding transmitting ground station; and

C. All the transmitting stations are identical.

Following the procedures indicated in the last section we have

$$P_w^u = P_0^u \left(\frac{\lambda}{4\pi R_0^u} \right)^2 G_0^u g_0^u \ . \qquad (3.9)$$

and

$$P_u^u = \sum_{i=1} P_{ui}^u = \sum_{i=1} P_i^u \left(\frac{\lambda}{4\pi R_i^u}\right)^2 G_i^u \, g_i^u \, , \, i \geq 1$$

(3.10)

where the superscript denotes up-link.

If we further assume that the transmitting powers from the unwanted ground stations are the same as P_0^u, that is $P_i^u = P_0^u$, and also assume that $R_i^u = R_0^u$. Then we obtain the wanted-to-unwanted signal power ratio as

$$\frac{P_w^u}{P_u^u} = \frac{g_0^u}{\sum_{i=1} g_i^u}$$

(3.11)

which is again obtainable if the earth station antenna pattern is given.

Although the assumptions which led to Eq. (3.11) are over-simplified, the wanted-to-unwanted signal power ratio calculated from (3.11) represents a lower limit if atmosphere effects are not taken into account. Note that Eq. (3.11) involves the ratio of the gains of separate earth-station antennas in the direction of a single satellite, whereas Eq. (3.8) involves the ratio of the gains of the same earth-station receiving antenna in the direction of the various satellites. If the main beams of the ground stations have the same spacing as that of the satellites, Eq. (3.11) is identical to Eq. (3.8). This can be seen from Fig. (3-3).
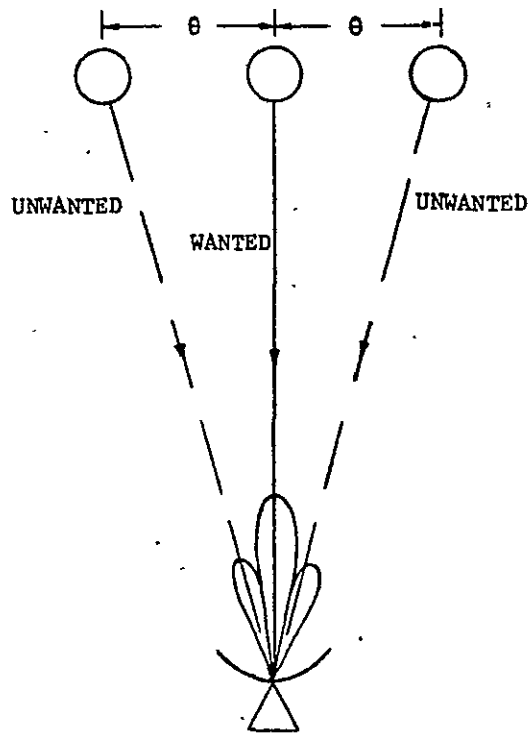
Fig. (3-3)--Up-link interference geometry.

3.4 REDUCTION OF NEAR-IN SIDELOBES IN THE SYNCHRONOUS EQUATORIAL ORBIT

DIRECTION.

3.4.1 Review of Sidelobe Suppression Techniques for a Reflector Type

Antenna

As discussed in the previous sections the earth station antenna

pattern is important-particularly its sidelobe levels-in determining

the amount of interference between satellite systems. The sidelobe

level and the sidelobe structure of a reflector type antenna are the

result of the illumination function of the aperture. A desired illumin-

ation function can be produced by controlling the primary feed pattern

and/or the reflector shape.

In practice, the simpliest method of suppressing sidelobe levels is to have a primary feed illuminating the reflector such that the illumination function at the edge of the reflector is heavily tapered. For the modern shaped-reflector Cassegrain antenna with uniform illumination a sidelobe level of -15 to -17 dB is common. For the conventional prime-focus antenna with 10 dB illumination taper a sidelobe level of -20 dB is common. Although theoretically sidelobe level can be reduced to below -30 dB with heavily tapered edge illumination, in the practical situation it is generally very difficult to achieve. This is caused by feed blockage and feed support structure which both contribute to increased sidelobe levels. The most undersirable effect of using the heavy taper technique is a great reduction in antenna gain.

The general idea behind shaping the reflector is that of constructing an out-of-phase radiator superimposed on the main reflector. If the radiation pattern of this radiator has similar sidelobe structure to that of the main reflector and has proper amplitude, the sidelobe levels of the main reflector can be reduced or completely eliminated.

There are a number of other well known techniques which can be categorized as follows:

A. Aperture blockage compensation technique

B. Active zone suppression technique

C. Absorber ring suppression technique

In the aperture blockage compensation technique,[32] a single radiating element (see Fig. (3-4)) is used as a means of partially compensating for the aperture blockage associated with the antenna feed structure. The relative phase and amplitude of this element are adjusted so as to
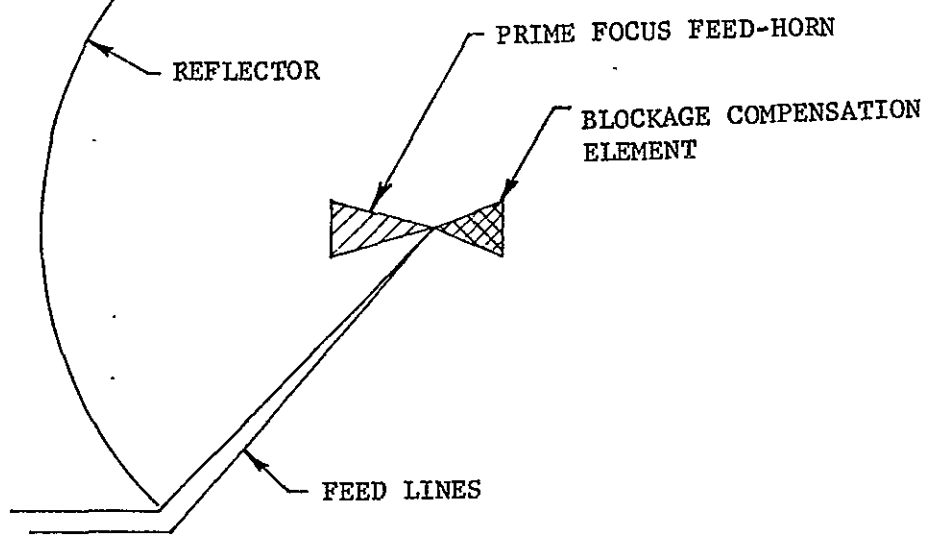
Fig. (3-4)--Antenna configuration for aperture blockage compensation.
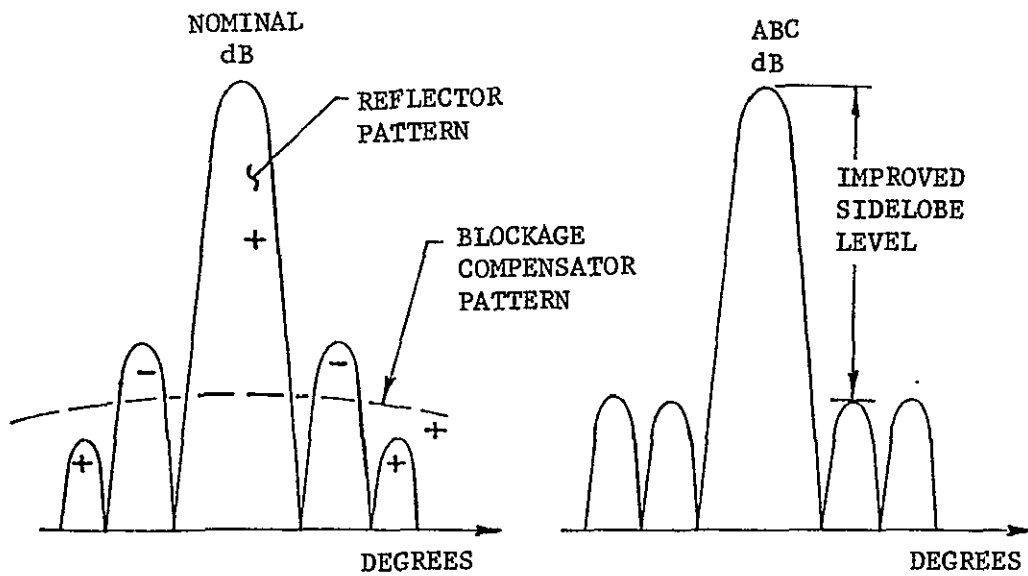
Fig. (3-5)--Suppression of near-in sidelobes by aperture blockage compensation.

suppress the highest near-in sidelobe in the manner depicted in Fig. (3-5).

If further suppression is required, it may be obtained by simultaneously

employing the active zone technique. In this, the reflector is surrounded

by a ring of radiating elements as shown in Fig. (3-6). The diameter

of the ring is chosen so that the lobes of its radiation pattern coin-

cide with the near-in sidelobes of the reflector pattern. Suppression

is again achieved by adjusting the phase and amplitude of the elements

to obtain cancellation. This is illustrated in Fig. (3-7) for a given

plane. The use of the aperture blockage compensation technique is

limited by the radiation pattern of the suppressor, which is generally

very broad, and only 3 dB improvement in sidelobe level can be achieved.

The active zone technique is more effective and a sidelobe reduction of

more than 10 dB has been reported.[33]

The absorber ring technique,[33] in which concentric circular ring-

shape absorbers are installed on the reflector, is one example of using

a passive element to suppress the sidelobes. Each ring can be considered

as a radiation element but 180° out-of-phase relative to the main reflector

radiation field. By adjusting the number of rings and their positions

and sizes, a reduction of sidelobe levels can be achieved. This technique

can reduce the sidelobes to the -30 dB level but unfortunately it also

generally results in an antenna gain loss of more than 2.5 dB.

If, on the other hand, one only intends to reduce the sidelobe

level of the pattern plane directing toward the synchronous equatorial

orbit, the wisdom of using the above-mentioned techniques, which are

either costly or cause a great gain reduction, to suppress sidelobe in

all pattern planes need to be re-evaluated. When only the sidelobe

MAIN REFLECTOR

. COMPLEX
. HEAVY

SIDELOBE
CANCELLATION
ELEMENTS
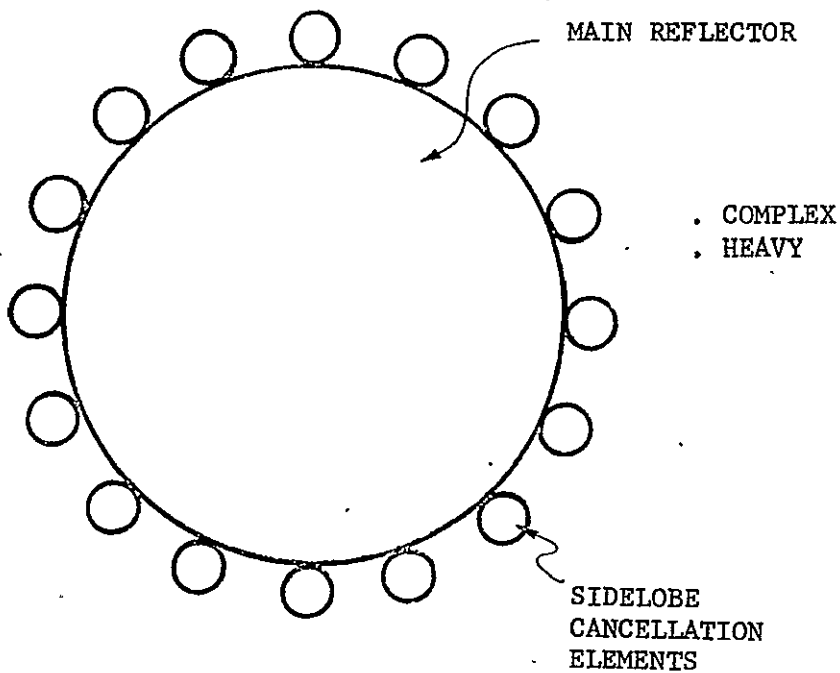
Fig. (3-6)--Antenna configuration for active zone sidelobes
        cancellation.

dB   PATTERN OF REFLECTOR
            WITH APERTURE BLOCKAGE
            COMPENSATION

            ACTIVE ZONE
            PATTERN

                        DEGREES

dB   RESULTANT PATTERN

                        DEGREES
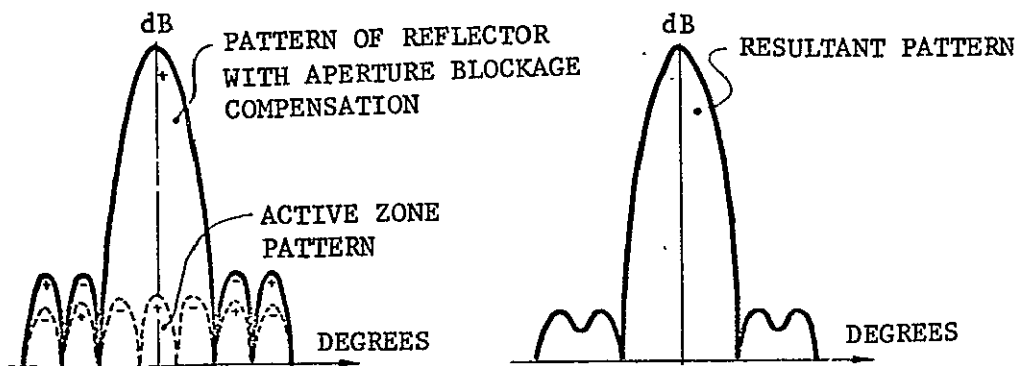
Fig. (3-7)--Suppression of near-in sidelobes by active zone
        cancellation.

levels of one pattern plane (or a limited region around the plane) are to be suppressed, it is sufficient to construct a second radiator with similar sidelobe structure in that plane only.

In the past months Stanford University researchers have proposed a low cost technique to accomplish this by using an array of two rectangular absorbers placed on the reflector. This paper is the first to evaluate this technique experimentally. A brief description of this technique is made in the following section.

3.4.2 Use of an Absorber Array in Sidelobe Suppression

The far field radiation pattern, $g(\theta,\phi)$, of an aperture, A , with illumination function $F(x,y)$ is given by[34]

$$g(\theta,\phi) = \frac{(1 + \cos \theta)}{2} \int_A F(x,y) \, e^{jk\sin \theta(x\cos \phi + y\sin \phi)} \, dxdy$$

The coordinate system is shown in Fig. (3-8).
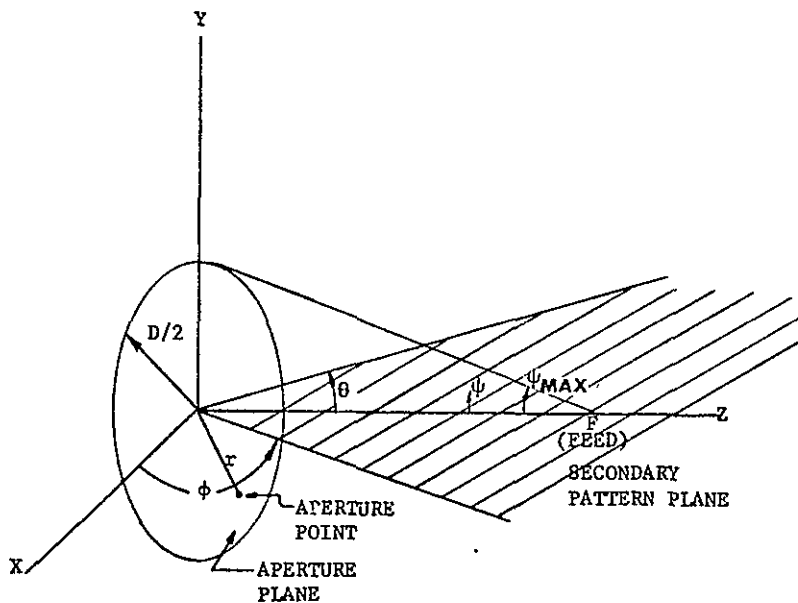
Fig. (3-8)--Coordinate system.

Consider now an array of two rectangular absorbers at the aperture

of a reflector as shown in Fig. (3-9). Assuming that over the exposed

area the presence of the absorbers does not alter the distribution

$F(x,y)$ which would exist in their absence, the absorbers can be regarded

as producing a field 180° out-of-phase with $F(x,y)$ over the area that it

covers as will be seen from the following manipulation:

$$g(\theta,\phi) = \frac{(1 + \cos\ \theta)}{2} \int_{A-2A'} F(x,y)\ e^{jk\sin\theta(x\cos\phi + y\sin\phi)}\ dxdy$$

$$= \frac{(1 + \cos\ \theta)}{2} \int_{A} F(x,y)\ e^{jk\sin\theta(x\cos\phi + y\sin\phi)}\ dxdy$$

$$- \frac{(1 + \cos\ \theta)}{2} \int_{2A'} F(x,y)\ e^{jk\sin\theta(x\cos\phi + y\sin\phi)}\ dxdy$$

$$(3.19)$$
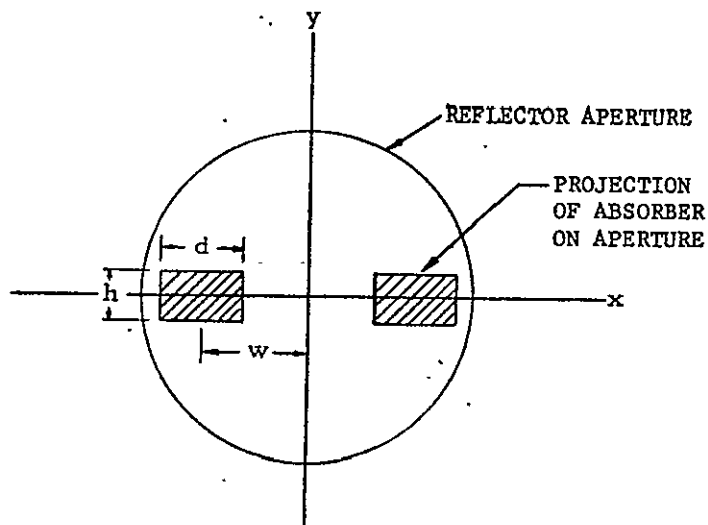
Fig. (3-9)--Absorber array at the aperture of reflector.

where A´ is the area occupied by one absorber and A is the reflector aperture. It is seen explicitly that the absorbers can be regarded as an out-of-phase field superimposed on the original distribution. If the absorbers are small, $F(x,y)$ over them can be considered constant and their radiation pattern, g_{ab} , may be found by using the radiation field of a rectangular aperture and the array factor as derived by Silver:[34]

$$g_{ab}(\theta,\phi) = - \frac{(1+\cos\theta)}{2} \operatorname{sinc}(d\sin\theta\cos\phi/\lambda)\operatorname{sinc}(h\sin\theta\sin\phi/\lambda)$$
$$\cdot 2\cos(2\ w\sin\theta/\lambda)hd \qquad\qquad (3.20)$$

$$g_{ab}(\theta,0) = - \frac{(1+\cos\theta)}{2} \operatorname{sinc}(h\sin\theta/\lambda)2\cos(2\ w\sin\theta/\lambda)hd \qquad (3.21)$$

In general, $F(x,y)$ cannot be considered as a constant and its exact value can be obtained by mapping the feed pattern to the blocked area of the aperture. This can be done by using the relationships between feed pattern angle, ψ , and aperture radius, r , as follows (see Fig. (3-8)).

$$r = 2f\ \tan(\psi/2) \qquad\qquad (3.22)$$

where f is the focal length of the reflector. The amplitude of the feed pattern is multiplied by the space loss factor, L , to obtain the amplitude of the field in the aperture plane.

$$L = \cos^2(\psi/2) \qquad\qquad (3.23)$$

This process can be implemented by the use of a digital computer. Full details of analysis of this technique can be found in reference 35.

To achieve the sidelobe suppression objective the positions and sizes of the absorbers must be so chosen that their radiation pattern has proper amplitude and is similar to but 180 degrees out-of-phase relative to at least the first few sidelobes of the main antenna. The locations of the zeros of the array pattern can be varied by varying the distance, w, between absorbers. The amplitude of the array radiation pattern can be controlled by adjusting the height, h, and the width, d, of the absorbers. Figure (3-10) shows various radiation patterns of the absorber array.

Two examples are worked out here which show the validity and effectiveness of this technique. In the first example, a 50λ reflector is uniformly illuminated. A pair of absorbers whose radiation pattern matches the first few sidelobes of the main antenna (see Fig. (3-11)) is placed on the reflector and the combined radiation pattern of the main antenna and the absorbers at $\phi = 0^{\circ}$ plane is plotted in Fig. (3-12). As shown, the highest sidelobe level is reduced from a level of 17 dB to a level of 26 dB - an improvement of 7 dB. It also can be seen from the figure that the third sidelobe actually increases while the first two sidelobes decrease. This is allowable since our goal is to keep all the sidelobes below a certain level. In order to see how the sidelobes vary in other pattern planes a two-dimensional pattern contour is plotted in Fig. (3-13). It is found that the sidelobe levels are below 27 dB for pattern planes up to $\phi = 30$ degrees. Because the introduction of the absorbers on the reflector, a gain reduction of 1.73 dB is observed, which is much less than that obtained when using absorber ring technique. In the second example, a reflector of 45λ is illuminated
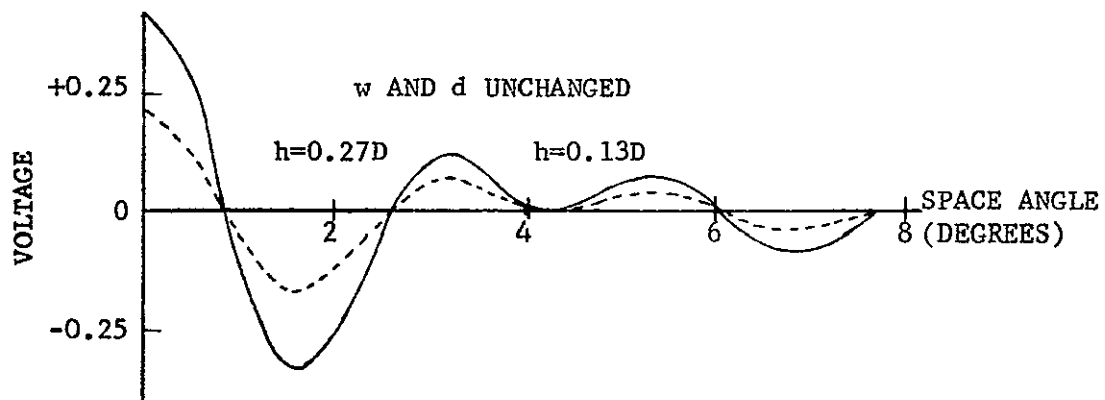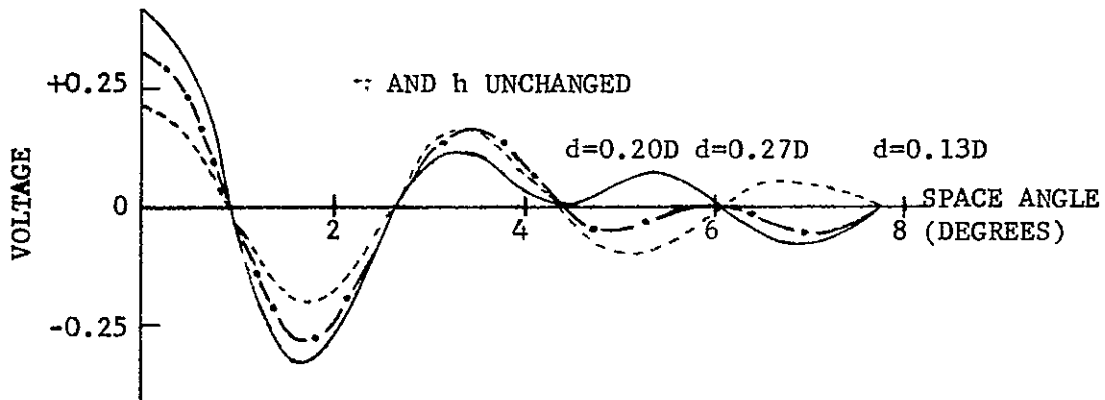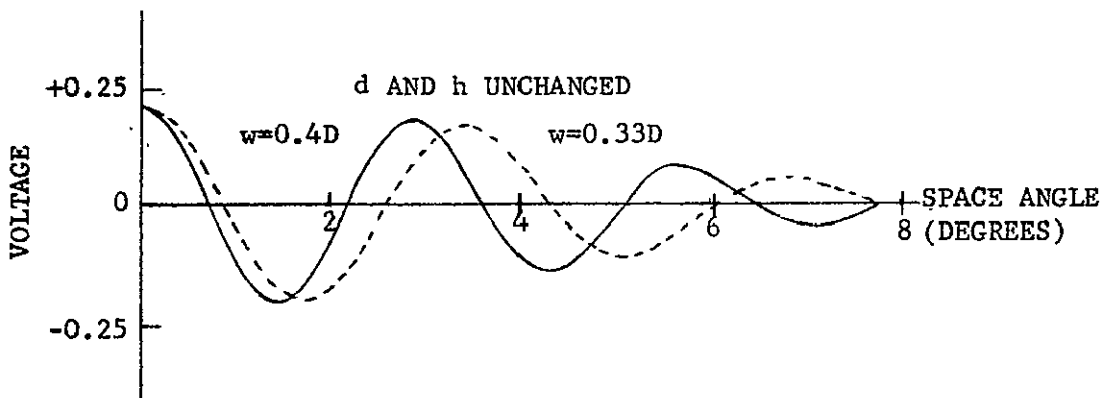
Fig. (3-10)--Absorber array radiation patterns.

Fig. (3-11)--Illustration of matching sidelobe structure -- uniform
illumination.

Fig. (3-12--Radiation.pattern resulting from sidelobe cancellation
-- uniform illumination.
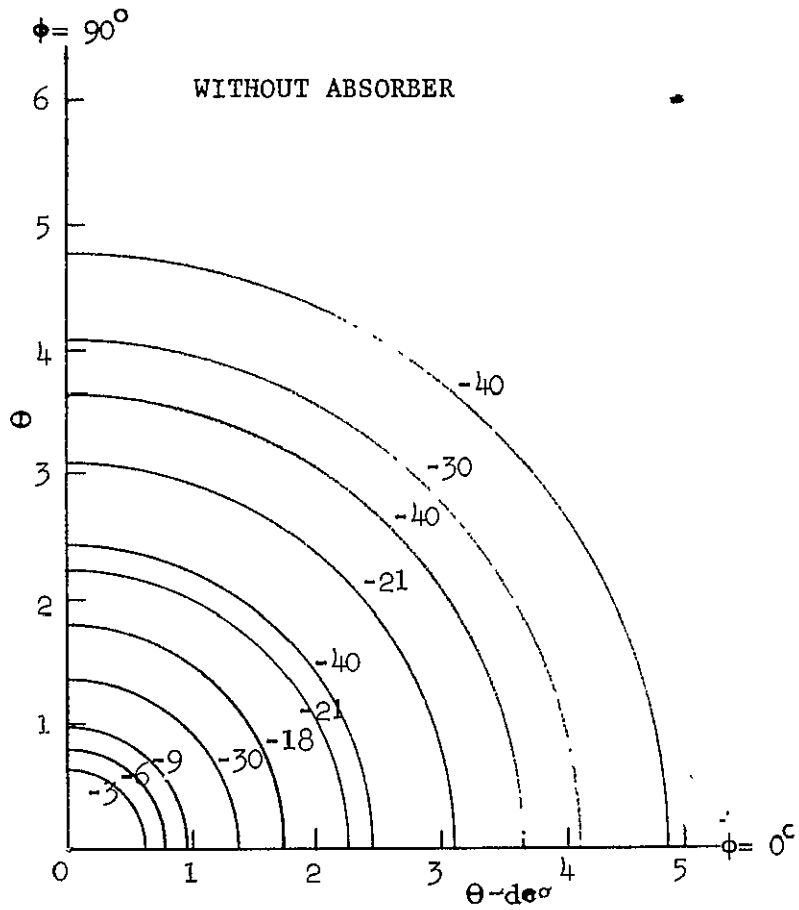
Fig. (3-13)--Two-dimension radiation contours -- uniform illumination.

by the feed of a symmetric beam which gives 8 dB illumination taper at the edge of the reflector. The sidelobe structures of the selected absorber pair and the main antenna are shown in Fig. (3-14). The resultant patterns at $\phi = 0^{\circ}$ and the pattern contours are shown in Fig. (3-15) and Fig. (3-16), respectively. As shown, a 7 dB reduction in sidelobe level is achieved. Antenna gain loss in this case is 0.7 dB. By comparing these two examples we observe that the higher the sidelobe levels the reflector originally has, the greater the antenna gain will be reduced. This is because large absorbers are required to produce large amplitude array pattern lobes to cancel high main antenna sidelobes.

It is noted that the relationship of our model to the actual situation, in which the absorber lies on the curved surface of the reflector, is of course not exact. We are interested at this point in identifying a general approach, the detailed implementation of which is to be experimentally determined. It is also noted that the calculation of radiation patterns assumed no aperture blockage. This was done in order to assess the effectiveness of this technique in suppressing only the reflector pattern sidelobes. In practice, aperture blockage is present and produces a constant amplitude, out-of-phase field in the vicinity of broadside. This field, when superimposed on the main antenna pattern, raises sidelobe levels and fills in nulls. However, it is anticipated that the absorber array technique will correct this effect if blockages are properly located to maintain pattern symmetry.
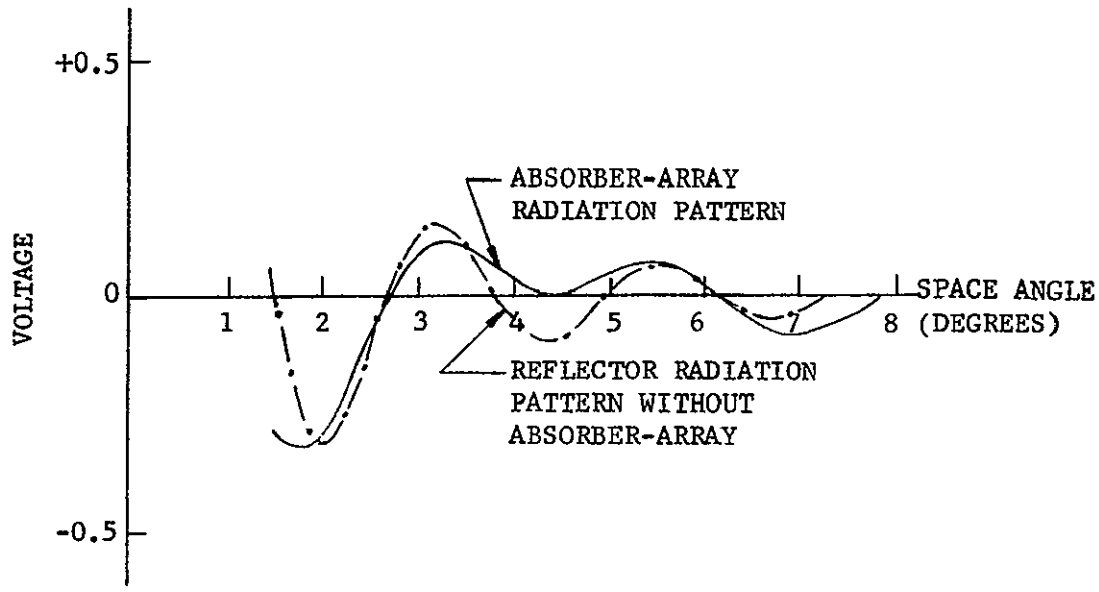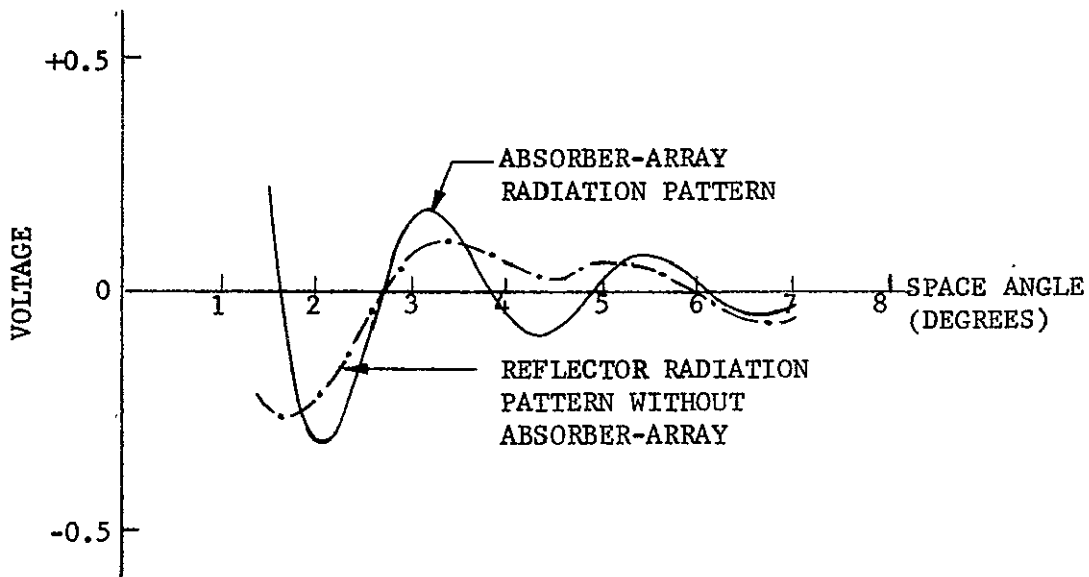
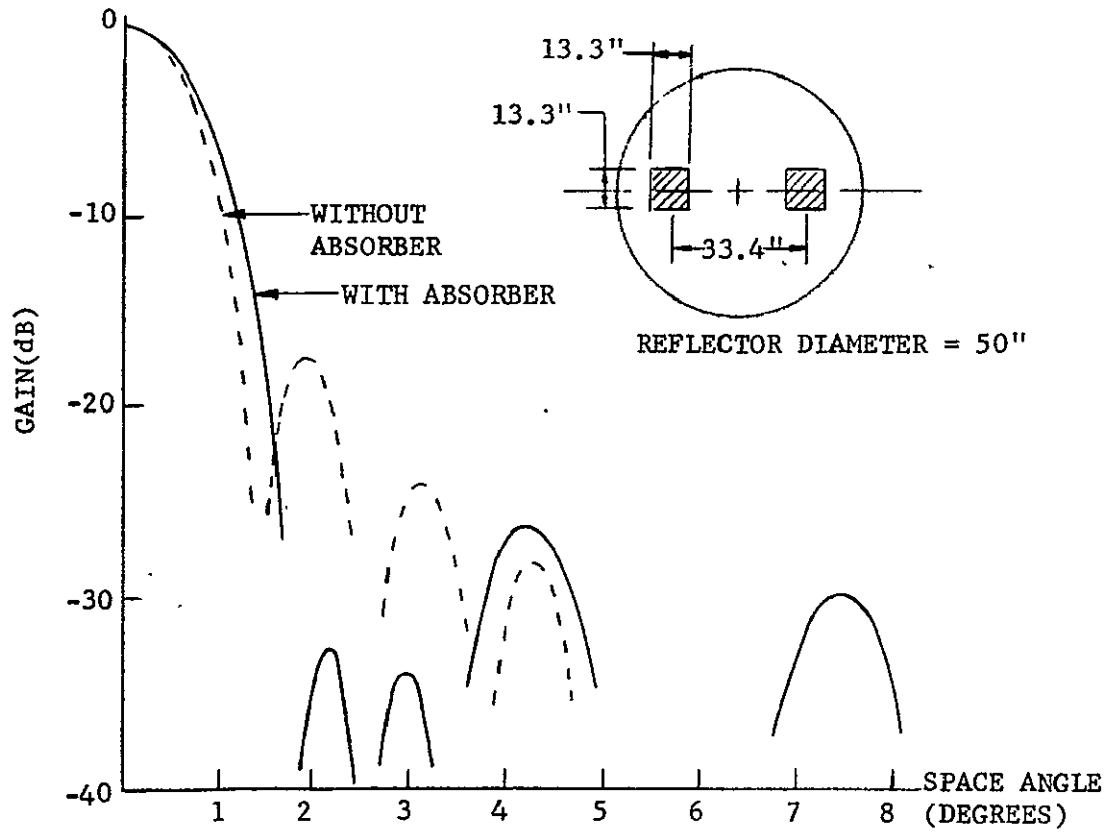Fig. (3-14)--Illustration of matching sidelobe structure -- tapered
illumination.
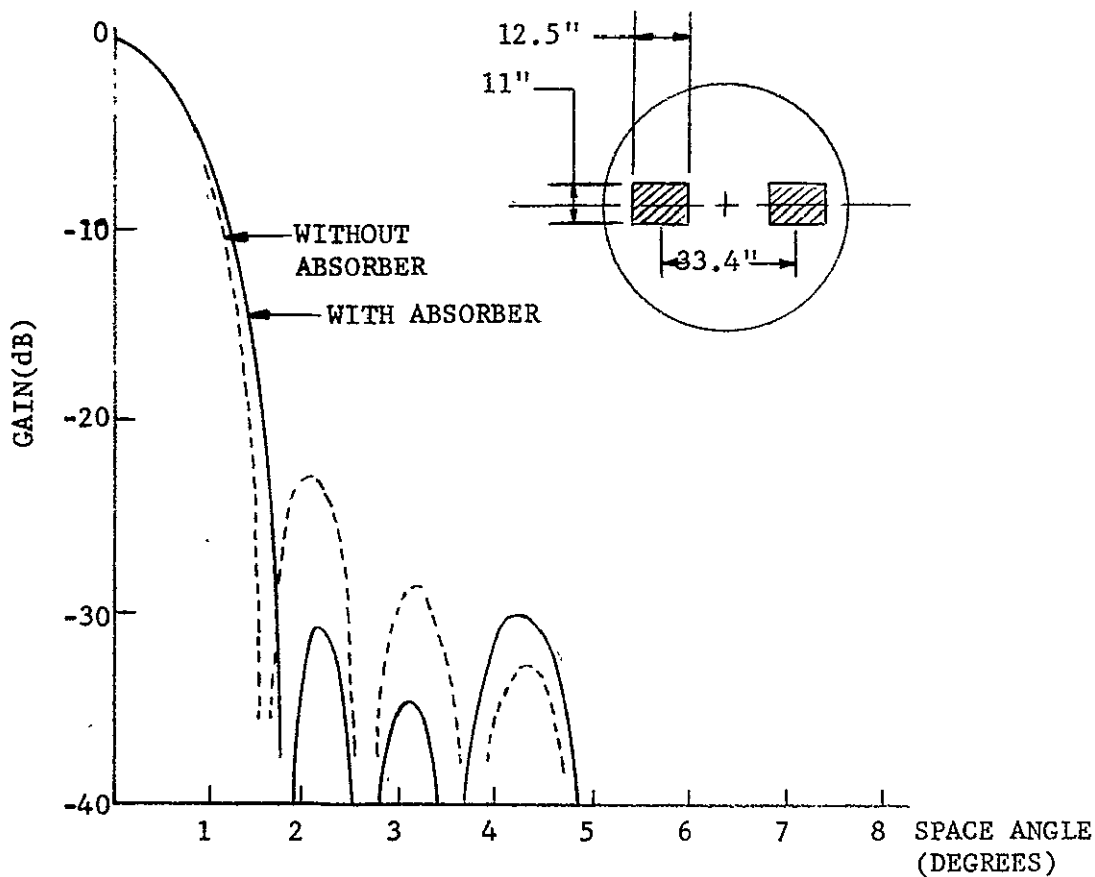
Fig. (3-15)--Radiation pattern resulting from sidelobe cancellation--
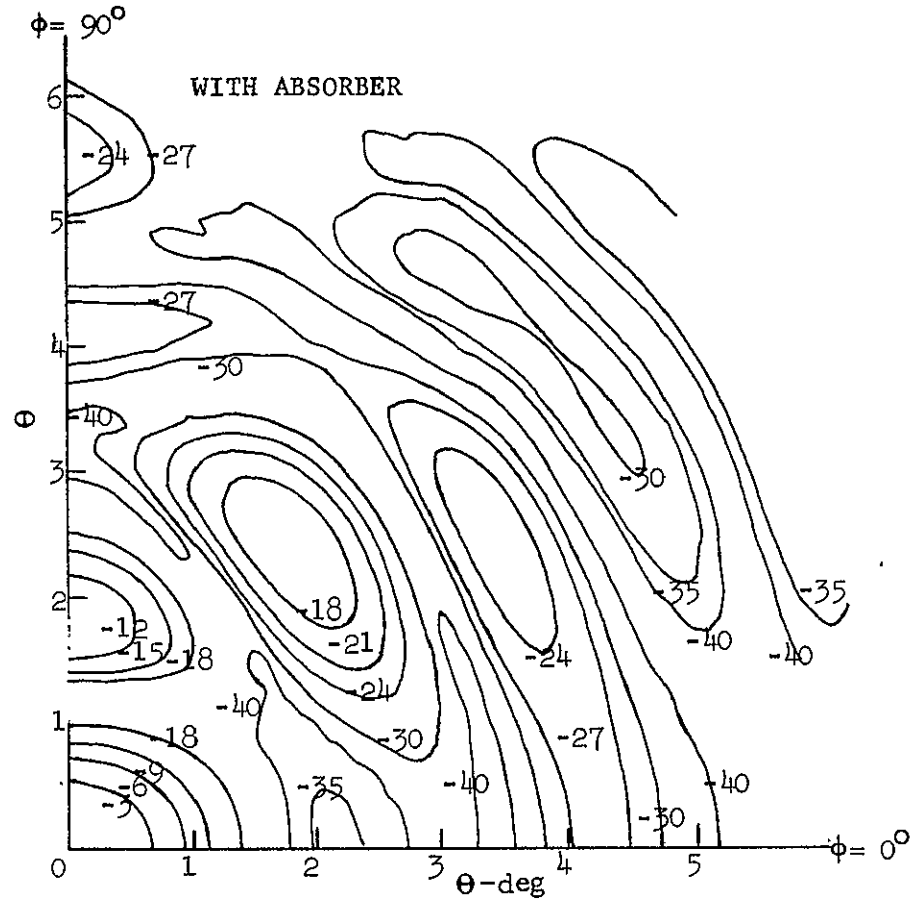tapered illumination.
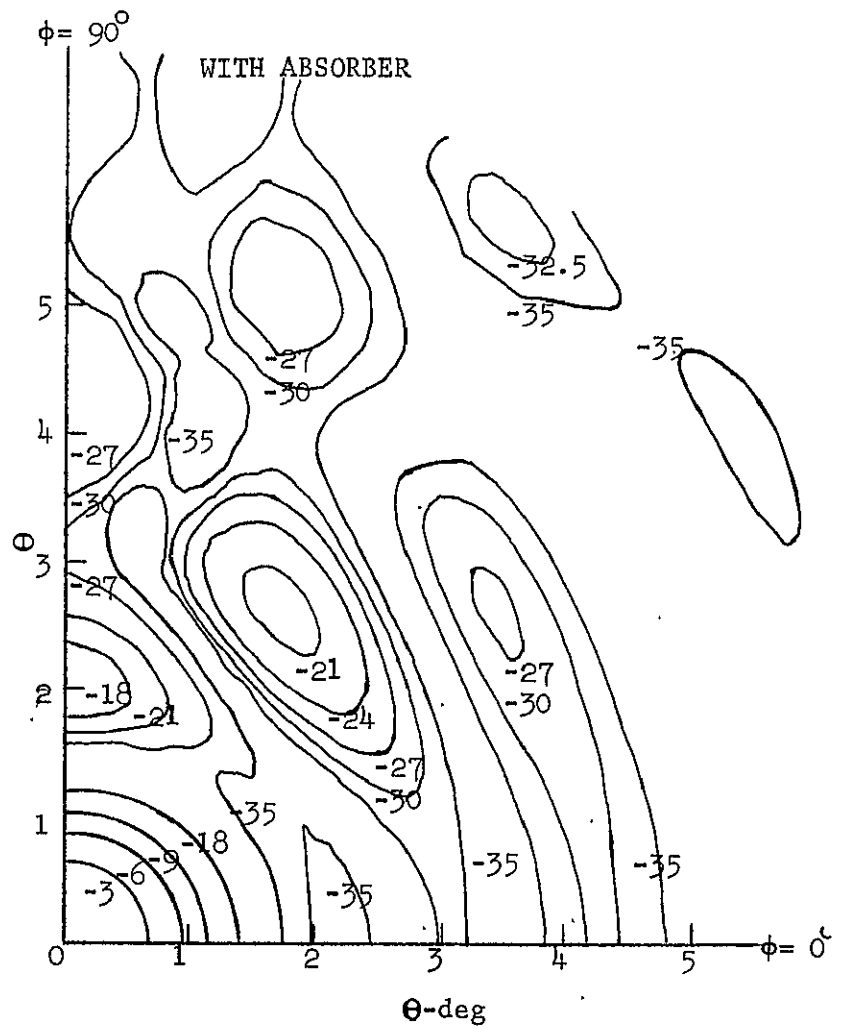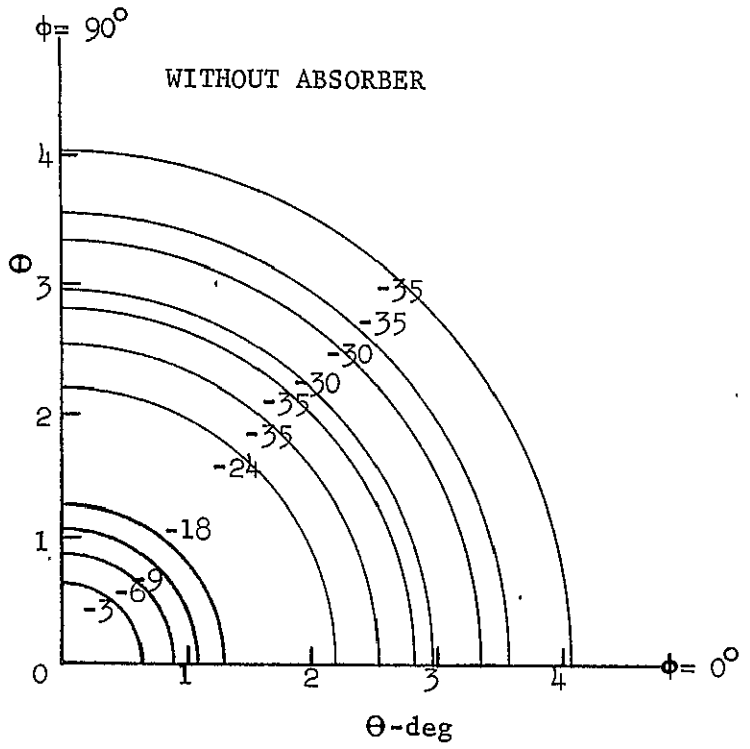
Fig. (3-16)--Two-dimension radiation contours -- tapered illumination.

3.4.3 Experimental Investigation

The objective of the experimentation is to demonstrate sidelobe suppression in a limited pattern planes by applying the absorber array technique. The frequency chosen for experimentation is 10.5 GHz. The testing antenna Figures 3-17 and 3-18 give them credit consists of a 4-foot paraboloid reflector with an F/D of 0.4 and an open-end rectangular waveguide feed. Other features of this antenna are shown in Fig. (3-17). Figure (3-18) shows the reflector with absorbers mounted. The test was conducted at the Philco-Ford Corporation (Palo Alto, California), Western Development Laboratories' 500-foot antenna range (see Fig. (3-19)). This range satisfies the far-field distance requirement at the testing frequency. The block diagram for the antenna pattern measurement test set-up is shown in Fig. (3-20). The pattern recorder used is a standard Scientific Atlanta rectangular recorder (series 1520) with a dynamic range of 70 dB. The signal source is a Hewlett Packard Model 628 signal generator (Model 628). The antenna feed is linearly polarized and therefore tests using circular polarization are precluded.

Before placing absorbers on the reflector the position of the feed is carefully adjusted until patterns in both H- and E-planes have best symmetry and lowest sidelobe levels. The most important feastures of these patterns are as follows:

A. The first sidelobe levels of the H-plane and E-plane patterns are found to be -19.5 dB and -14 dB, respectively.

B. Due to the unsymmetric feed mount, it is not possible to adjust
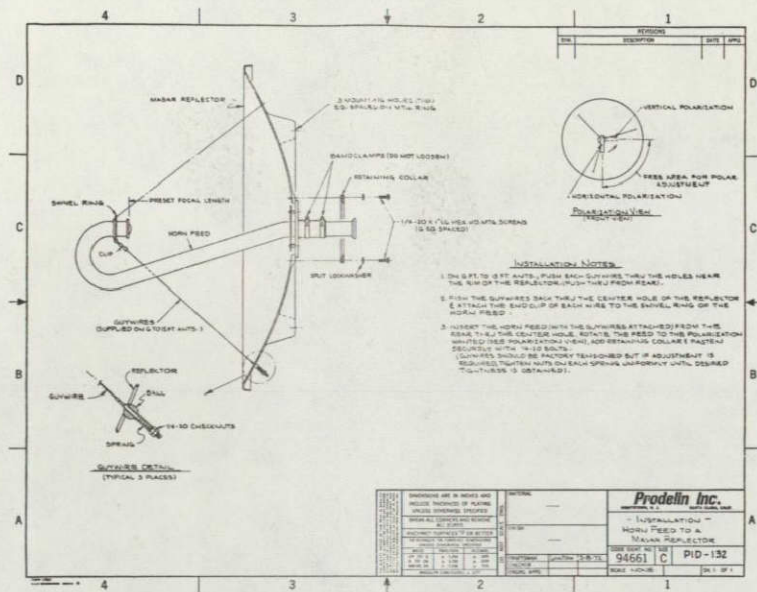
Fig. (3-17)--Features of experimental reflector.

Fig. (3-18)--Reflector with absorbers mounted.
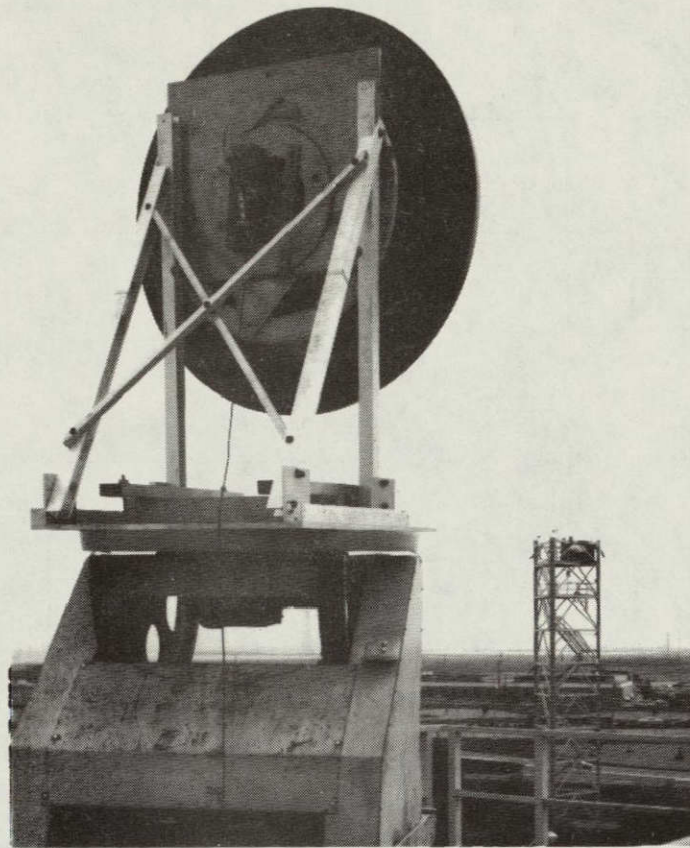
Fig. (3-19)--Antenna range.

the sidelobes on each side of the boresight axis to have the same levels.

C. No deep nulls exist between the main beam and the first sidelobes, and between the first sidelobe and the second sidelobe, suggesting that a phase error exists and that the first sidelobes are not 180° out-of-phase with respect to the main beam.

Because of the high first sidelobe level it is expected that antenna gain would have to be greatly reduced to achieve a 10 dB reduction in the first sidelobe levels, as has been pointed out before. The lack of symmetry and the presence of shallow nulls make it unlikely that the use of a symmetric absorber array pattern will match the main reflector pattern effectively to a wide range of angle.

ANTENNA
UNDER TEST

LINEAR OR
CIRCULAR SOURCE

BORESIGHT

500 FT.

BOLOMETER

PATTERN RECORDER

(SA SERIES 1520)

VARIABLE ATTENUATOR

FREQUENCY METER

DIRECTIONAL COUPLER

CRYSTAL DETECTOR

TWT (HP 493)

POWER METER

SIGNAL SOURCE (HP 628)
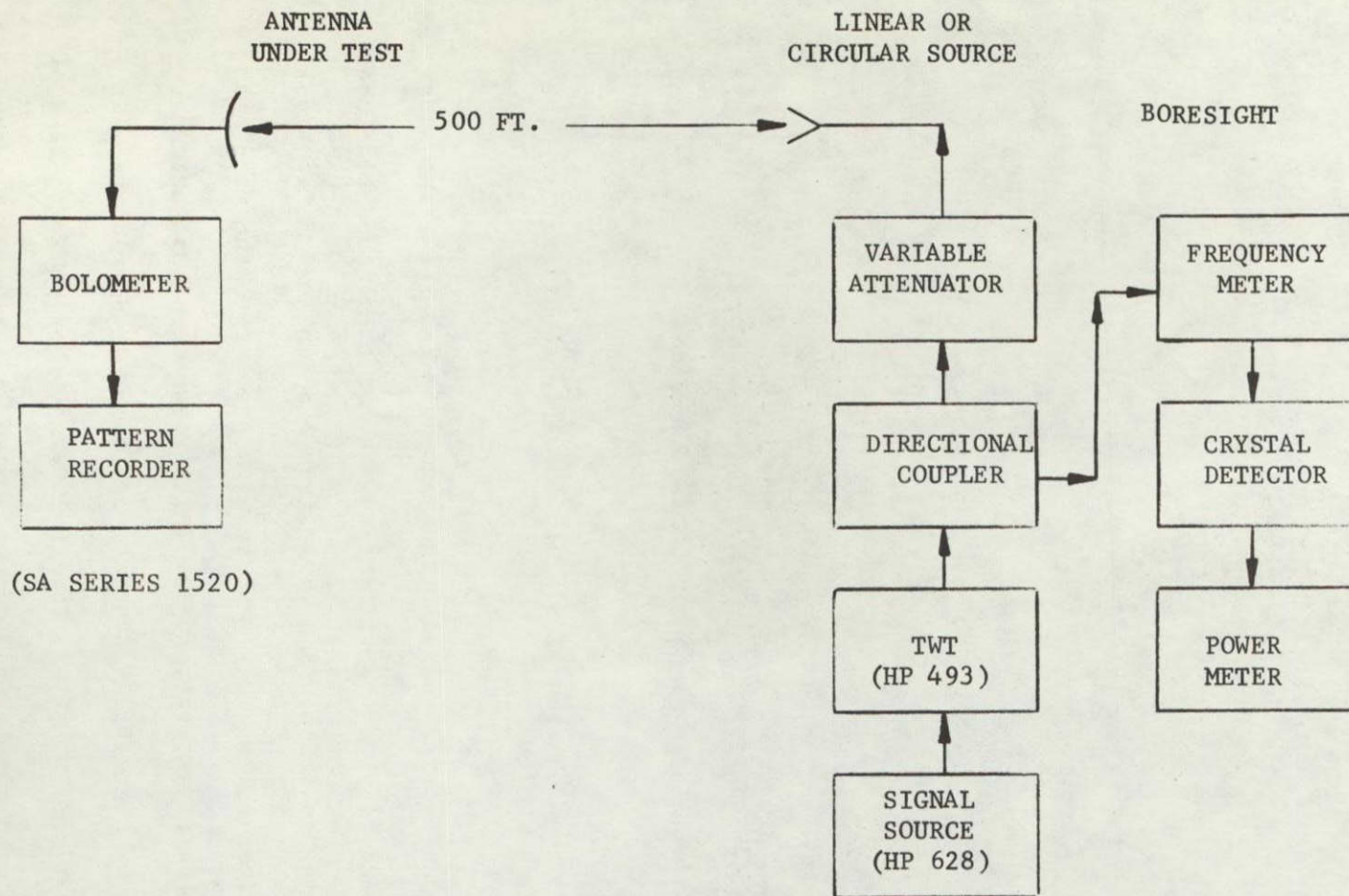
Fig. (3-20)--Test set-up for pattern measurements.

The absorber used (Emerson Cummings AN 74) has a thickness of 0.375 inch and a transmission coefficient of less than 1% at the testing frequency. Two cases have been studied; in the first case the absorbers are placed on the H-plane (y-direction). Due to reasons just discussed, in each case we only intend to adjust the position of the absorbers to match the first sidelobe of the irregular main beam antenna pattern. The amplitude of the array pattern is varied by varying the height and the width of the absorbers. Some of the experimental results are shown in Fig. (3-21) to Fig. (3-26). Radiation patterns in planes of 2.5° and 5° relative to the location of the absorbers are also recorded. As shown an array element spacing of 26 inches and an absorber size of 9×13 inches reduces the first sidelobes 8-12 dB in the H-plane and 5 dB in the E-plane to pattern planes up to 5°. The antenna gain reduction is about 1.7 dB. Figure (3-27) to Fig. (3-28) shows patterns for different absorber spacing or absorber size. The cross-polarization patterns in the principal planes are also recorded and found to have little change in the presence of the absorbers.

At this point it is worth mentioning again Goebels' work using expensive active zone techniques to suppress the sidelobes. Instead of employing the entire ring elements he used only two elements in his experiment to suppress sidelobes in only one pattern plane. In that respect, it is very similar to the case we investigated. Results showed that by controlling the phase and amplitude of the suppressors he was able to reduce the sidelobes below the -35 dB level. However, we must note that the radiation patterns of the antenna he used originally had low sidelobes (about -26 dB) and good symmetry.
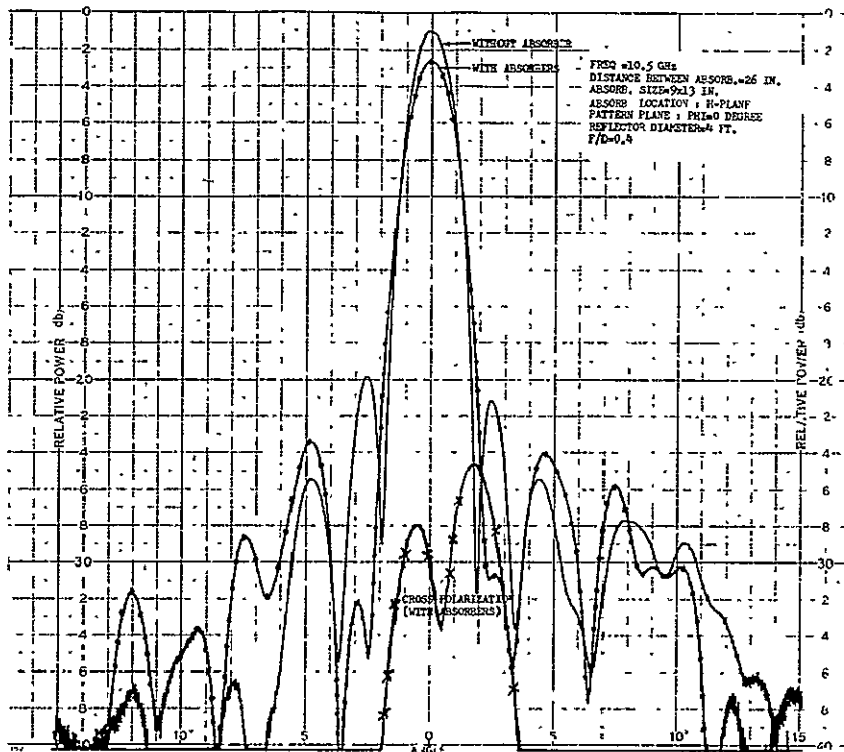
Fig. (3-21)--Measured radiation patterns of a reflector -- with and without absorber.
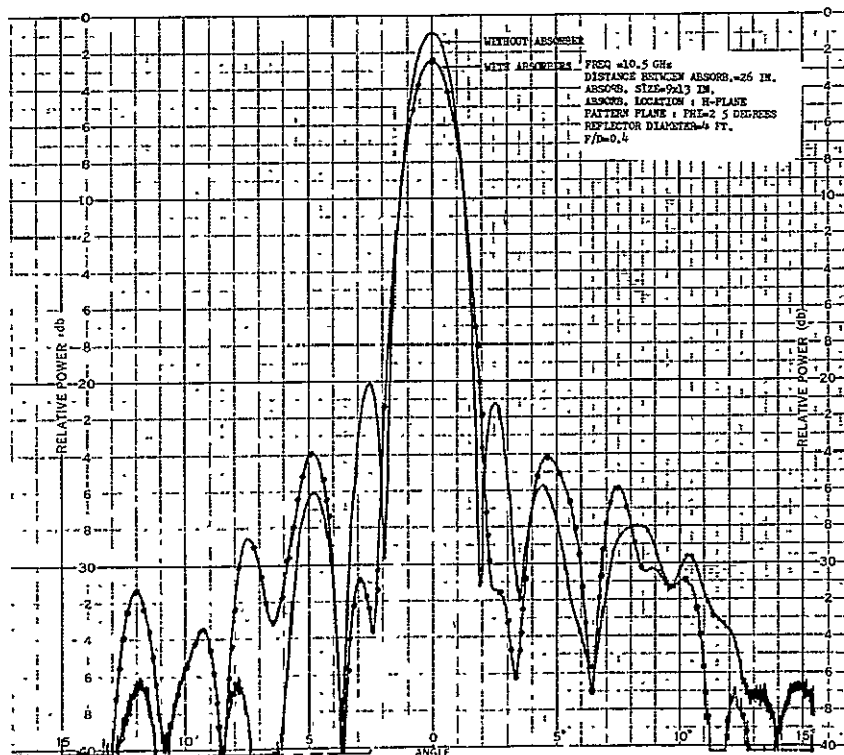
Fig. (3-22)--Measured radiation patterns of a reflector -- with and without absorber.

- 70 -
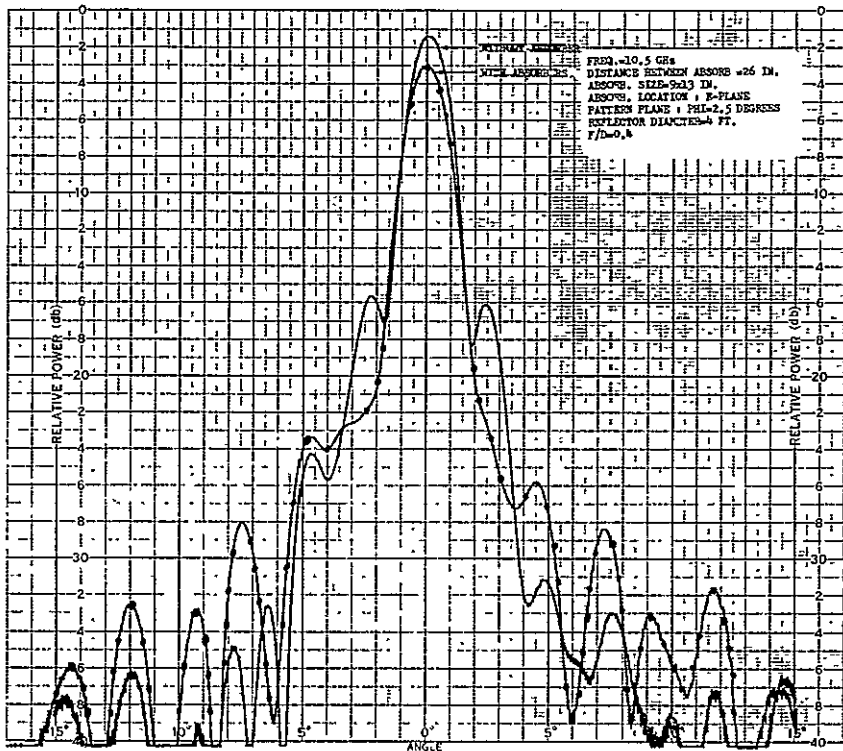
Fig. (3-25)--Measured radiation patterns of a reflector -- with and without absorber.
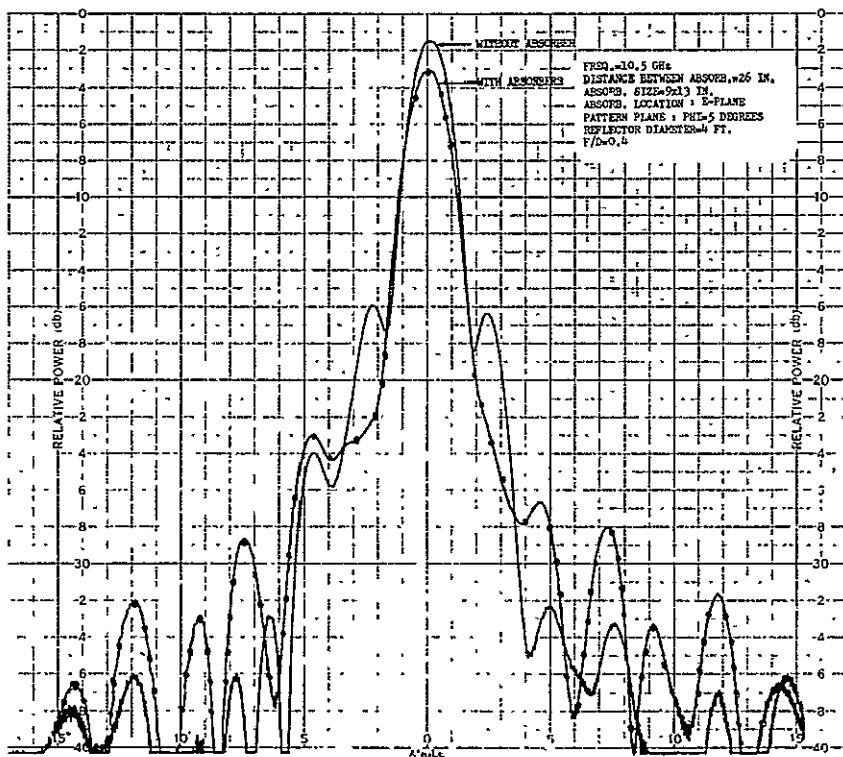
Fig. (3-26)--Measured radiation patterns of a reflector -- with and without absorber.
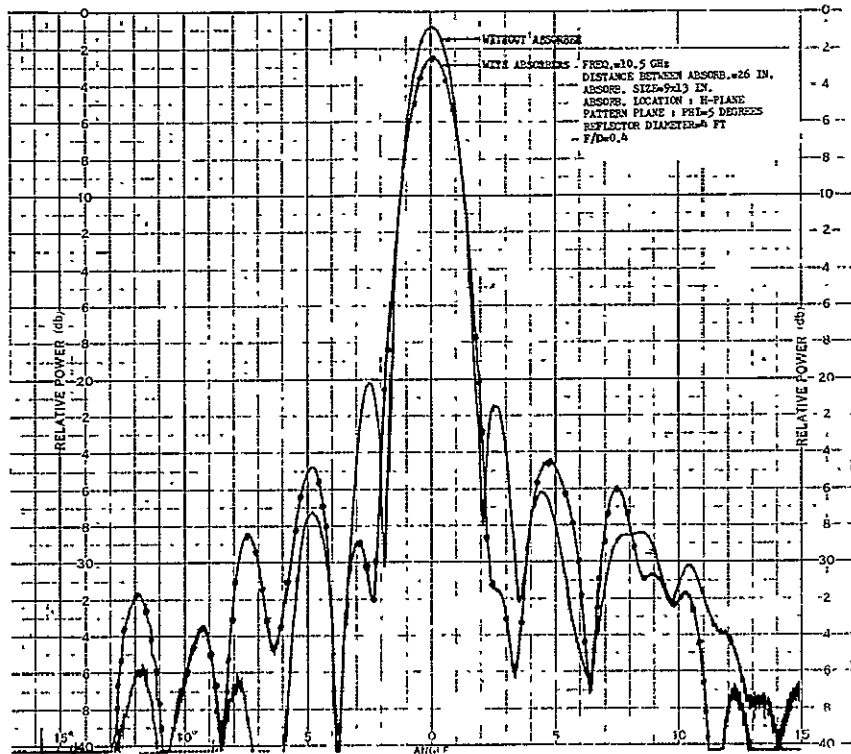
Fig. (3-23)--Measured radiation patterns of a reflector -- with and without absorber.
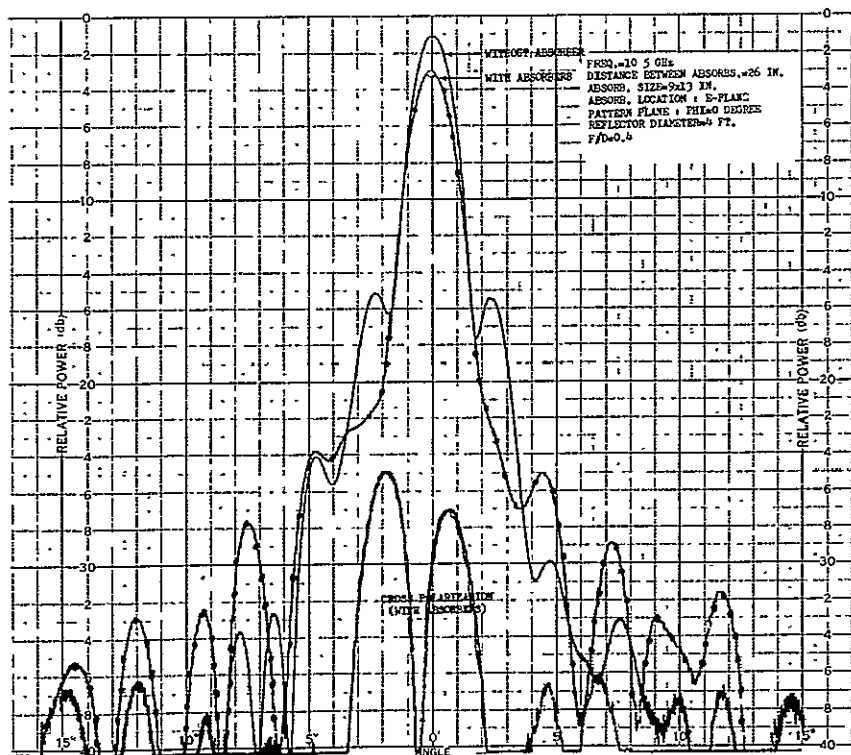
Fig. (3-24)--Measured radiation patterns of a reflector -- with and without absorber.
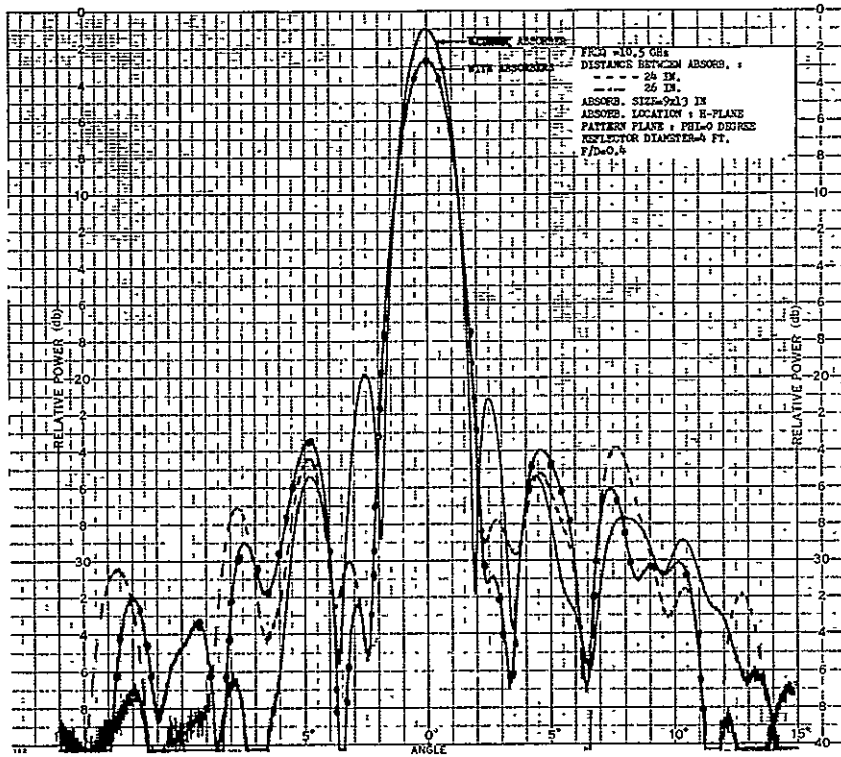
Fig. (3-27)--Measured radiation patterns of a reflector -- with and with-
out absorber.
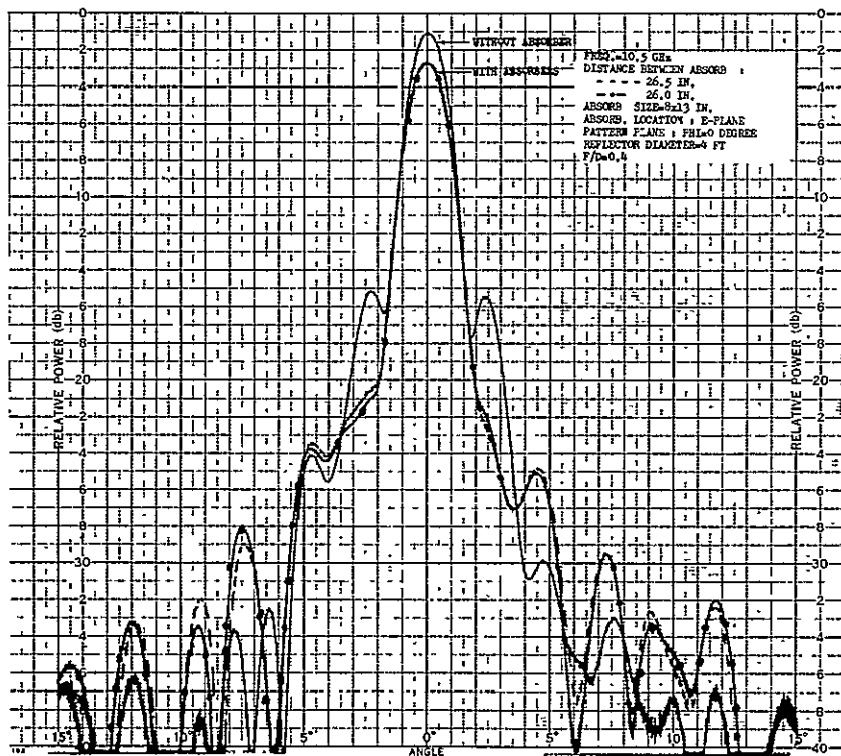
Fig. (3-28)--Measured radiation patterns of a reflector -- with and with-
out absorber.

- 73 -

3.5 ANTENNA PATTERN AND SATELLITE SPACING

As discussed before the earth station antenna pattern is particularly important in determining the amount of interference between satellite systems. The lack of published measured patterns[36] for the reflector type antennas in representative sizes and the correct frequency bands poses a most difficult problem in studying interference between satellite systems. A major effort was made during the period of this study to investigate the antenna characteristics of some existing ground stations, or their scale models, through some experienced companies in this field, including:

A. Philco Ford Corporation's Western Development Laboratories (Palo Alto, California)

B. Radiation Inc, (Melbourne, Florida)

C. Prodelin Inc. (Santa Clara, California)

Since we are more interested in small ground stations, the antenna sizes selected in this study have a D/λ up to only 150. Our approach is to set up representative antenna pattern models to compare the measured patterns supplied by industries with the theoretically predicted patterns including feed blockage effect and feed support scattering. Sidelobe locations and levels are carefully examined, resulting in the horizontal lines as shown in the antenna pattern models (figure a of Fig. (3-29) to (3-31)), for reflectors with uniform illumination (which is typical in modern shaped reflector Cassegrain system) and with 9 dB-taper illumination (which is typical in a conventional prime-focus system).
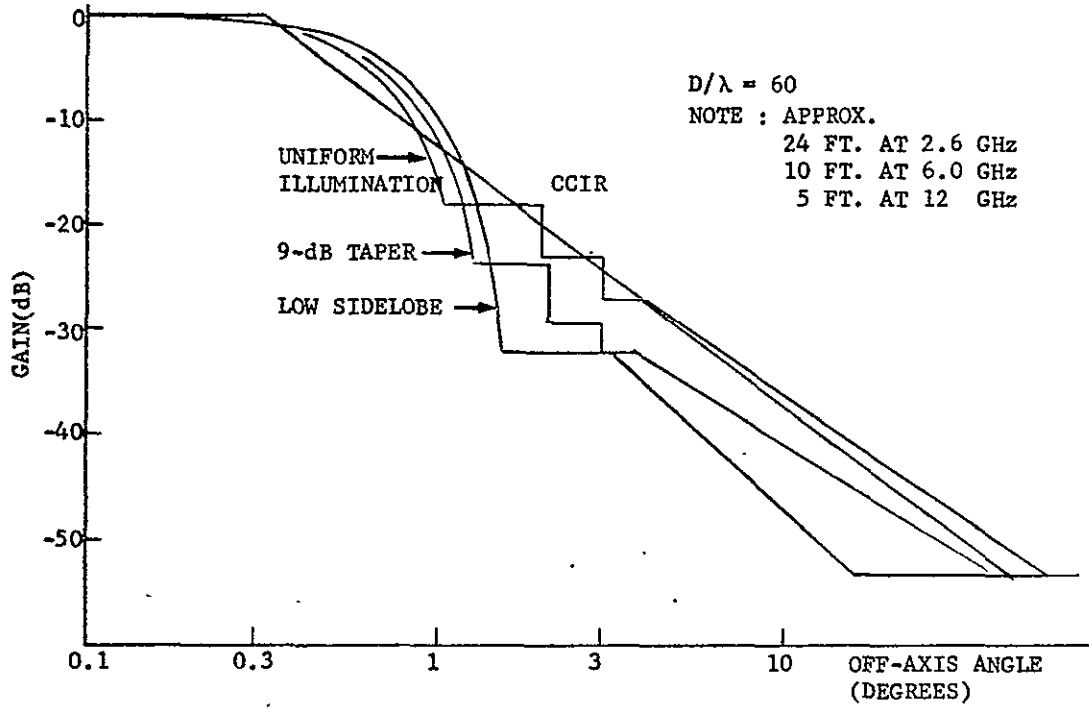
Fig. (3-29a)--Antenna pattern model (D/λ = 60).
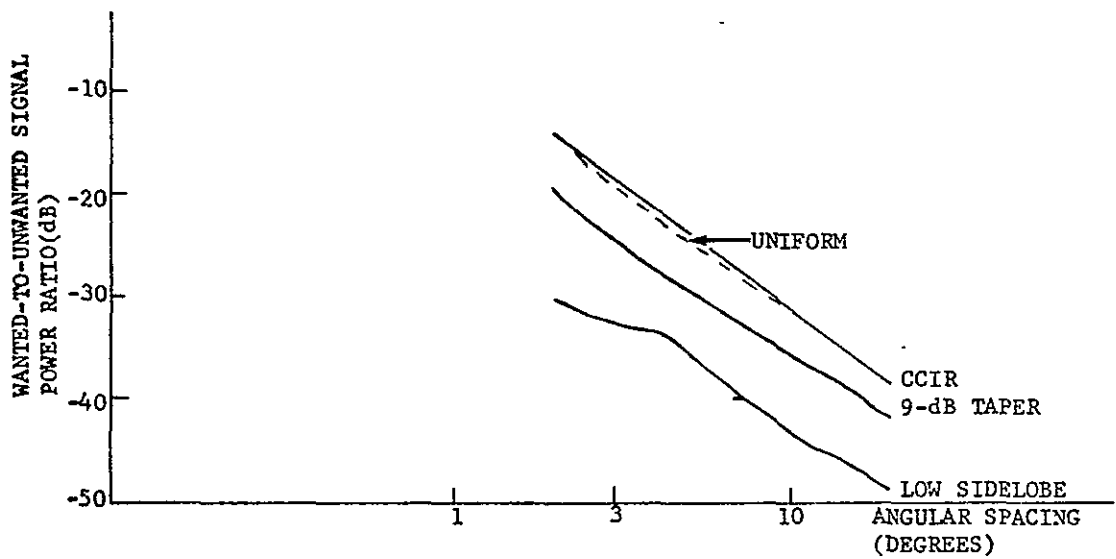
Fig. (3-29b)--Interference level vs satellite spacing -- D/λ = 60.
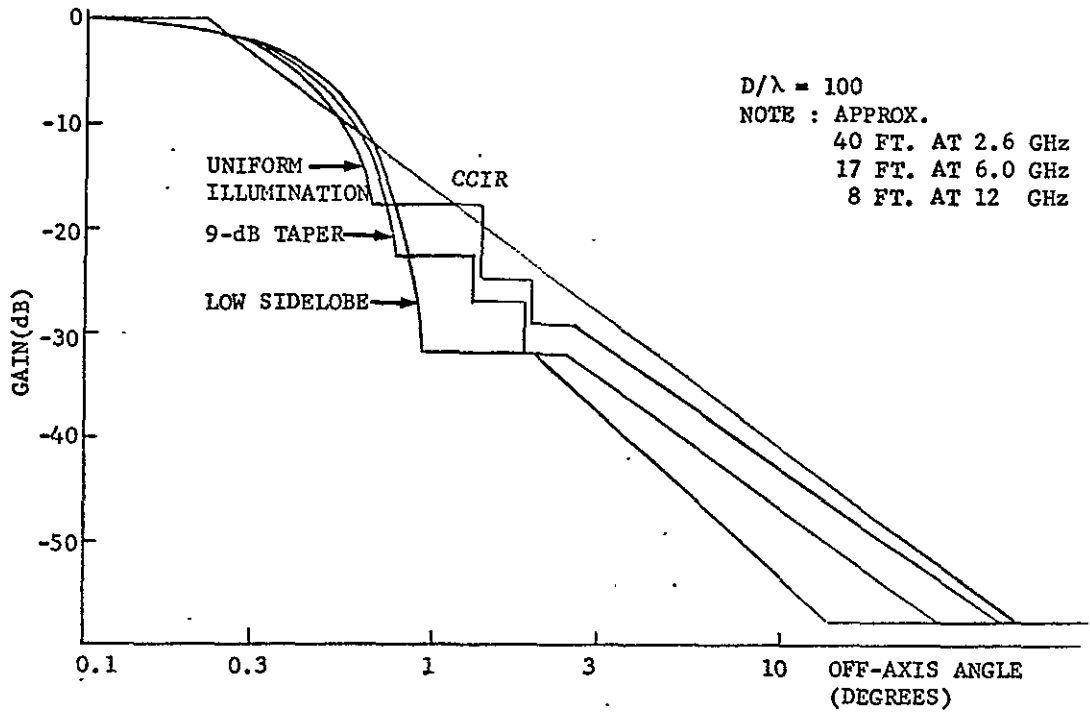
Fig. (3-30a)--Antenna pattern model (D/λ = 100).
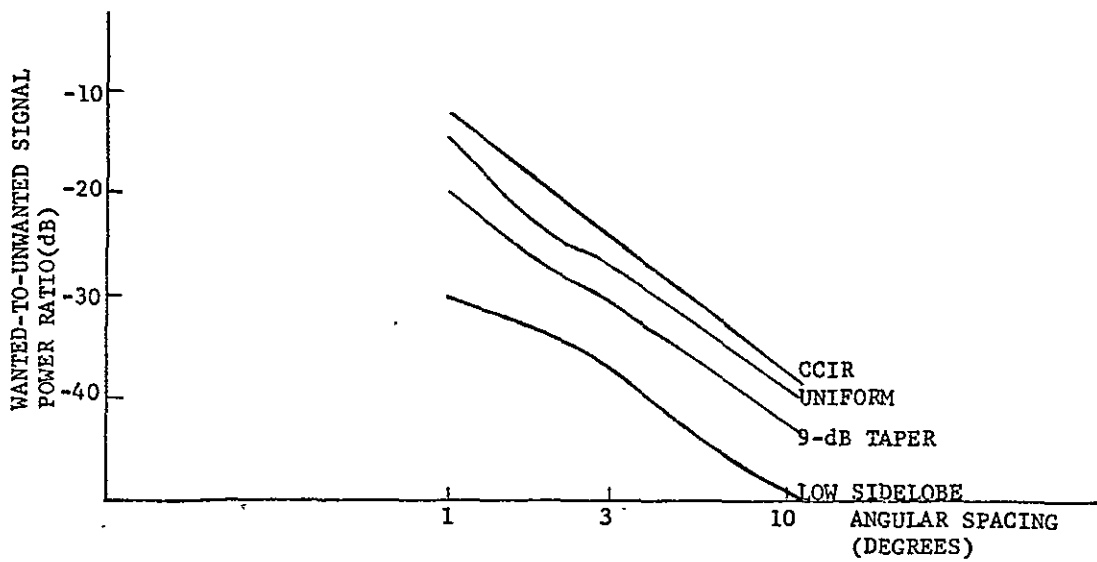
Fig. (3-30b)--Interference level vs satellite spacing -- D/λ = 100.

D/λ= 150
NOTE : APPROX.
60 FT. AT 2.6 GHz
25 FT. AT 6.0 GHz
12 FT. AT 12 GHz
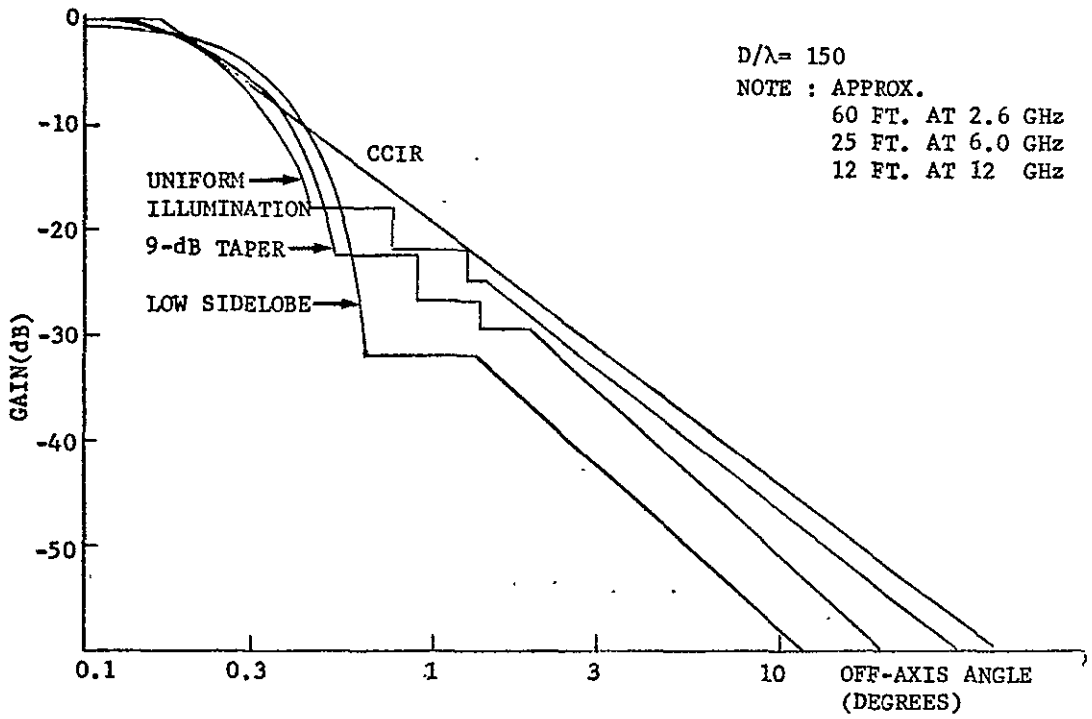
Fig. (3-31a)--Antenna pattern model (D/λ = 150).
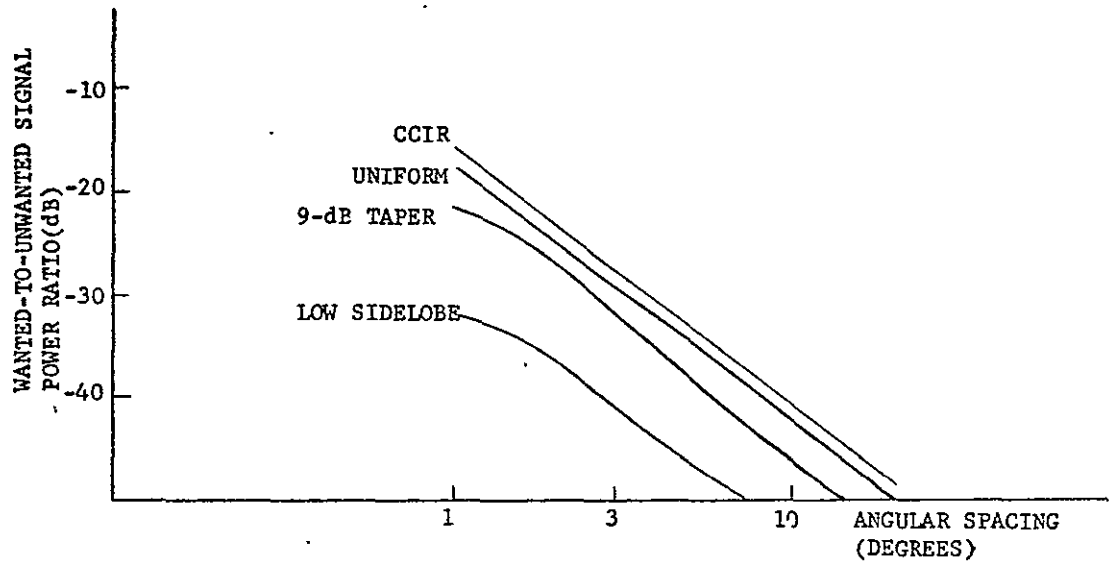
Fig. (3-31b)--Interference level vs satellite spacing.

For communicating with satellites in a geostationary orbit, it may be enough for the ground stations to have low sidelobes in the direction of the geostationary orbit. Therefore, antenna pattern models having low sidelobes, based on the absorber array technique are included in Fig. (3-30) to (3-32). For the purpose of comparison CCIR models are also plotted, in which the sidelobe levels are given by:

$$G(\theta) = (32 - 25 \log \theta) \text{ in dB} \qquad (3.24)$$

where $G(\theta)$ is the gain relative to an isotropic antenna. As shown, CCIR models have the highest sidelobe levels. It is noted that CCIR reference pattern represents peak sidelobe levels for antennas with $D/\lambda > 100$, and hence will be more unsuitable for smaller diameter ground antennas.

It is worth noting that the unmanned receiving stations (without auto-tracking) will be installed in the future for domestic communication satellite systems, the antenna will be designed to maximize the off-axis gain instead of the on-axis gain, to accommodate satellite drifting and pointing errors. In this case more illumination taper at the edge of the reflector is needed and an improvement in sidelobe level can be expected.

The wanted-to-unwanted signal ratios are calculated by the use of Eq. (3.8) or Eq. (3.11). The satellites are assumed to be equally spaced on the geostationary orbit. The interference from unwanted satellites within $70°$ of the wanted satellite is summed up. In fact, only satellites close to the first few sidelobes produce a significant contribution to interference. The results are plotted in the bottom figures of Fig. (3-29)

D/λ = 115
D = 15 FT.
FREQUENCY = 7500 MHz

CROSS POL.

RELATIVE POWER (db)

ANGLE
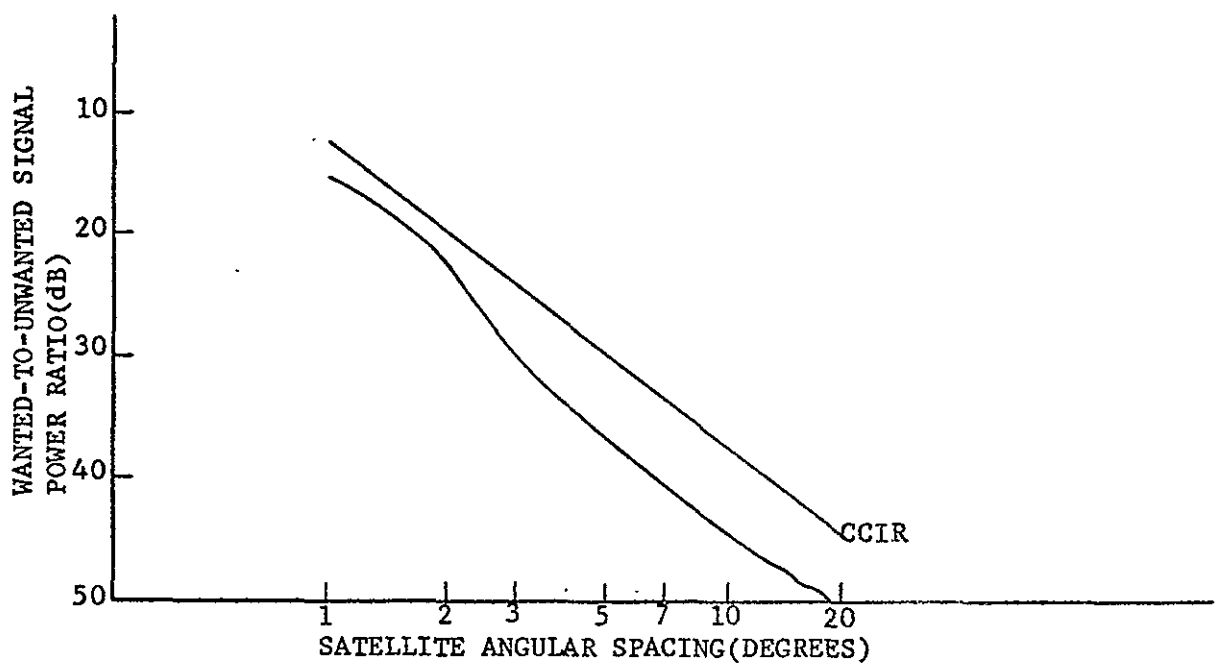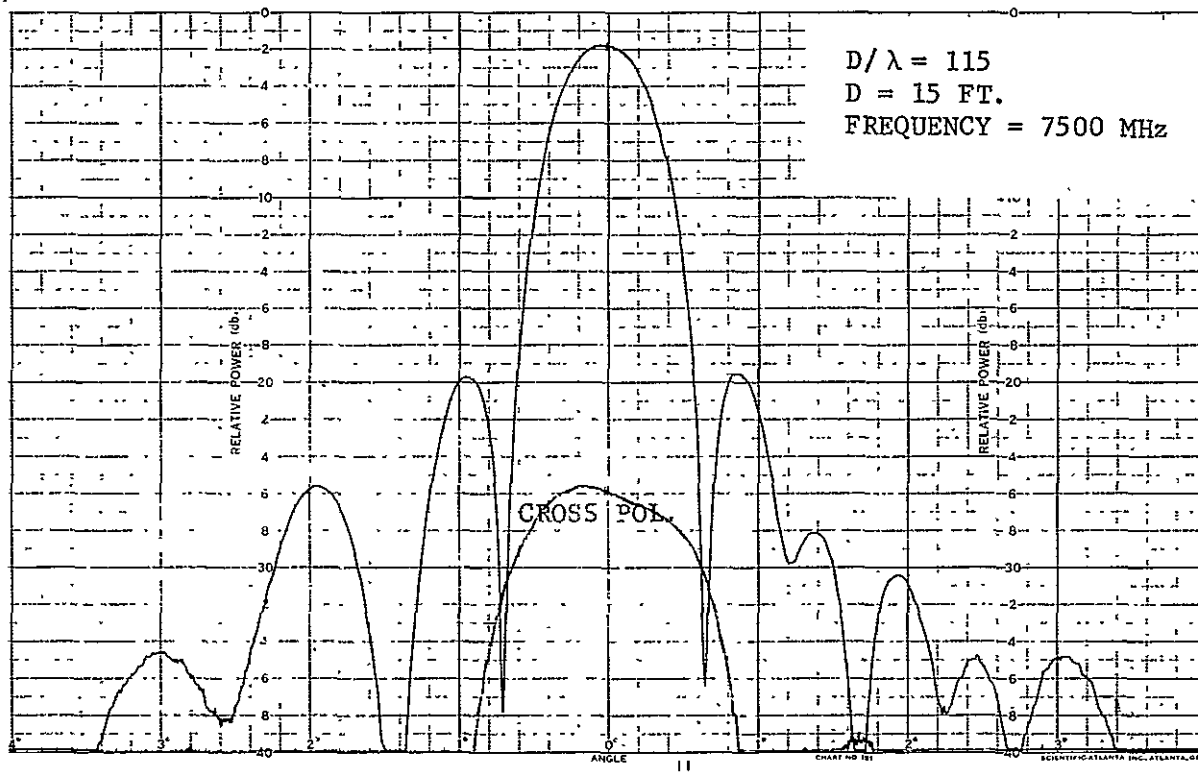
Fig. (3-32)--Interference level vs satellite spacing -- using
measured pattern.

to (3-31). As is expected, the low-sidelobe model offers great improvement in efficient utilization of the orbit. For example, if 17 foot antennas at 6 GHz were used to transmit signals to satellites in orbit; CCIR guidelines would require satellite spacing of at least 8° if noise from unwanted signals were to be kept 35 dB lower than the wanted signals. Using conventional prime focus antennas, satellite spacings of 5° would be allowed. And using our special low-sidelobe antennas, spacing of 2.5^{o} would be allowed. Note that a margin must be made to account for pointing error and propagating and fading factors.

A calculation based on a measured pattern $(D/\lambda = 115)$ was made. The result is shown in Fig. (3-32). It comes close to the predicted value for satellite spacings greater than 3° as seen by comparing with Fig. (3-30) $(D/\lambda = 100, 9$ dB taper curve).

3.6 EFFECT OF POLARIZATION DISCRIMINATION ON SATELLITE SPACING

It has been recognized that the proper use of orthogonal linear polarizations or opposite sense circular polarizations can permit smaller satellite spacings. The potential advantages of using polarization isolation depend on the cross polarization pattern level in the receiving antenna. For the paraboloid antenna the cross-polarized component is generated by the curved surface of the reflector and by feed and feed support scattering. Furthermore, the primary feed itself is necessarily imperfect and radiates a certain amount of cross-polarized field. Many techniques have been reported to reduce the cross-polarization level. For example, a primary feed[37,38] with equal E-plane and H-plane patterns has lower cross-polarized pattern levels than those produced by a

conventional waveguide primary feed. COMSAT[39] has used so-called

polarization-selective gratings over the antenna aperture to reduce the

cross-polarized component level in a system using linear polarization.

In this report we do not intend to dwell on how we can reduce the cross-

polarized field level. Instead, we are investigating and predicting the

realistic cross-polarization level achievable at this stage of technology

by examining some specific reflector-type of spacecraft and ground

station antennas.

The cross-polarization characteristics of linearly polarized reflector

antennas have been investigated by the CCIR[40] and COMSAT.[41] Both reported

that the average cross-polarized sidelobe level is from 10 to 15 dB

smaller than the co-polarized level, up to an angle of $40°$ off axis for

a D/λ ranging from 60 to 140. To confirm this we also made measurements

at x-band using a 4 foot parabolic antenna. A typical principal and

cross-polarized pattern is shown in Fig. (3-33).
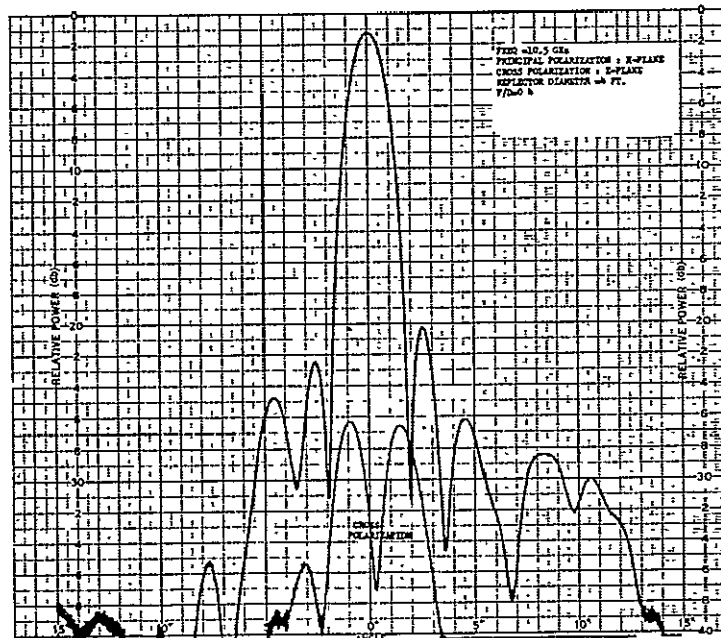
Fig. (3-33)--Measured linear polarization pattern.

The cross-polarization level of the circularly polarized wave in general is higher than that of linear polarization, depending on the axial ratios (ellipticity) and orientation of both the receiving and transmitting antennas. In general, the isolation between two circularly polarized (or more precisely "elliptically polarized") waves of opposite sense is given by[42]

$$F = \frac{(1+r_1^2)(1+r_2^2) - 4r_1r_2 + (1-r_1^2)(1-r_2^2)\cos\psi}{2(1+r_1^2)(1+r_2^2)} \quad (3.25)$$

where

F = polarization coupling factor

r_1 = axial ratio of incident wave (power)

r_2 = axial ratio of receiving antenna

ψ = angle between the major axes of the two polarization ellipses

The maximum and minimum isolation (in dB) has been calculated and is plotted in Fig. (3-34). As shown in the figure, the maximum discrimination occurs when the major axes of the unwanted incident signal and the receiving antenna are orthogonal, and the minimum occurs when the major axes are aligned. If the axial ratios of the satellite and ground antenas can be maintained within 3 dB regardless of their orientation, a discrimination of better than 9 dB would be assured. If they can be maintained within 1 dB, the minimum isolation will be 19 dB. For modern satellites the earth coverage antenna (not necessarily a reflector type antenna) can easily be designed with an axial ratio ≤ 3 dB. For example, the INTELSAT IV[43] earth coverage beam has an axial ratio ≤ 3 dB within $34°$ of the main beam and the Pioneer 10 antenna[44] also has an AR ≤ 3 dB. For
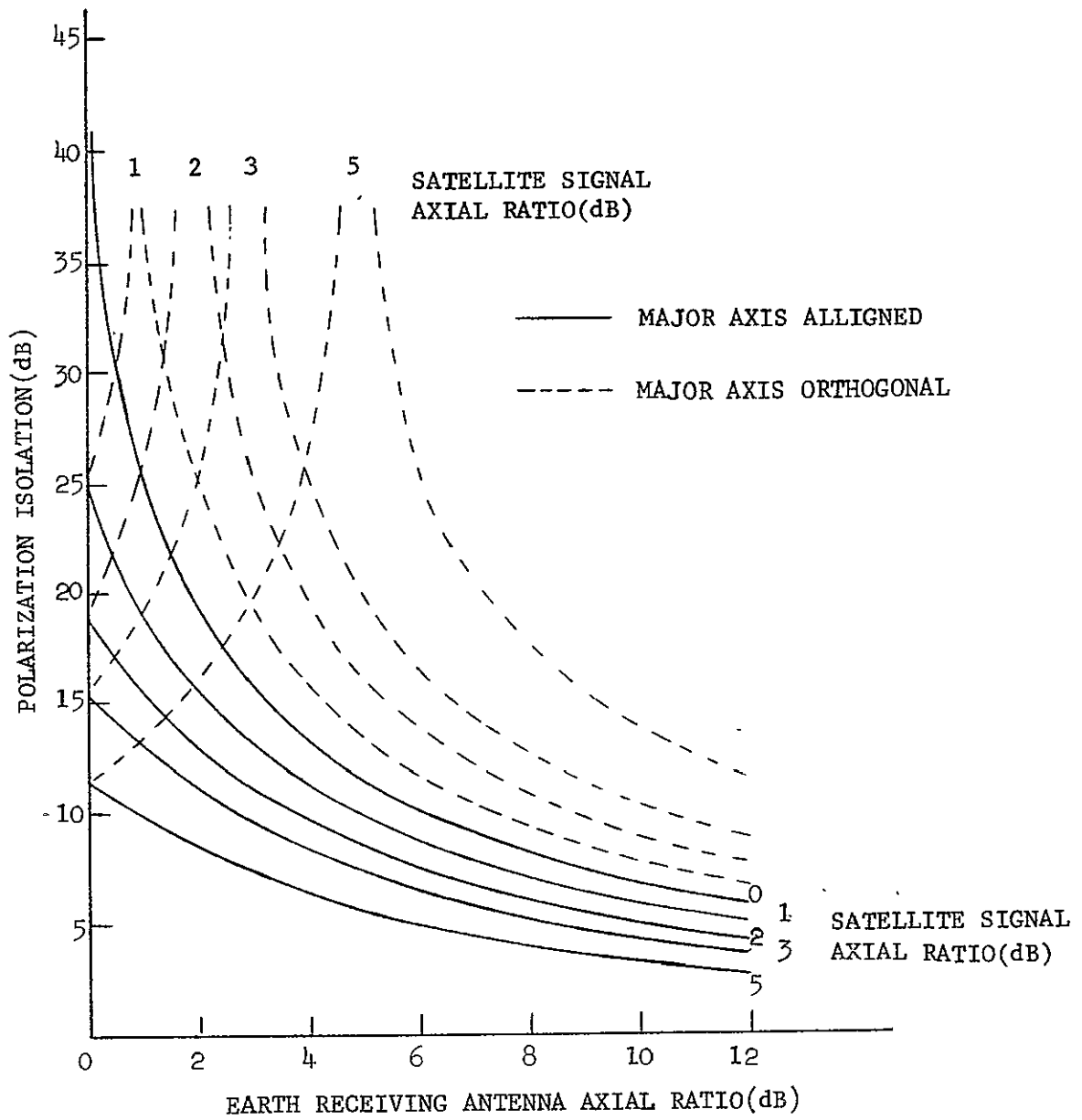
Fig. (3-34)--Polarization isolation between circularly polarized waves.

reflector-type earth station antennas the CCIR Study Group has claimed

that no reliable polarization advantages can be gained in the angular

range of most interest i.e., 1° to 10°. The validity of this statement

has been questioned after examining some existing ground antenna secondary

patterns supplied by Philco-Ford Corporation's Western Development

Laboratories Division and by Radiation Inc. (See Fig. (3-35) to (3-36).

These are prime focus type antennas with conventional conical horn feeds.

All these antenas have large blockage. A careful study of their patterns

confirms that substantial amounts of additional isolation still can be

gained up to a few sidelobes by using opposite sense circular polarization,

even though these antennas are not an optimum design for such cross-

polarization rejection. It is believed that the cross-polarized field

pattern level can be held lower if a feed with equal E- and H-plane

patterns (such as a corrugated horn) is used, and the feed support

properly designed.

The next question raised is to what extent the satellite spacings

can be reduced if an average additional isolation is acquired from

polarization discrimination. To illustrate, let us assume that the

wanted-to-unwanted signal power ratio (W/U) falls off with satellite

spacing θ approximately as θ^{-n}. Most curves in Fig. (3-29) to

Fig. (3-31) follow this approximate variation. For example, $n = 2.5$

for CCIR's sidelobe model. Let

$$W/U \;=\; y \;=\; K\,\theta^{-n} \tag{3.27}$$

D = 12.5 FT.
F = 2100 MHz
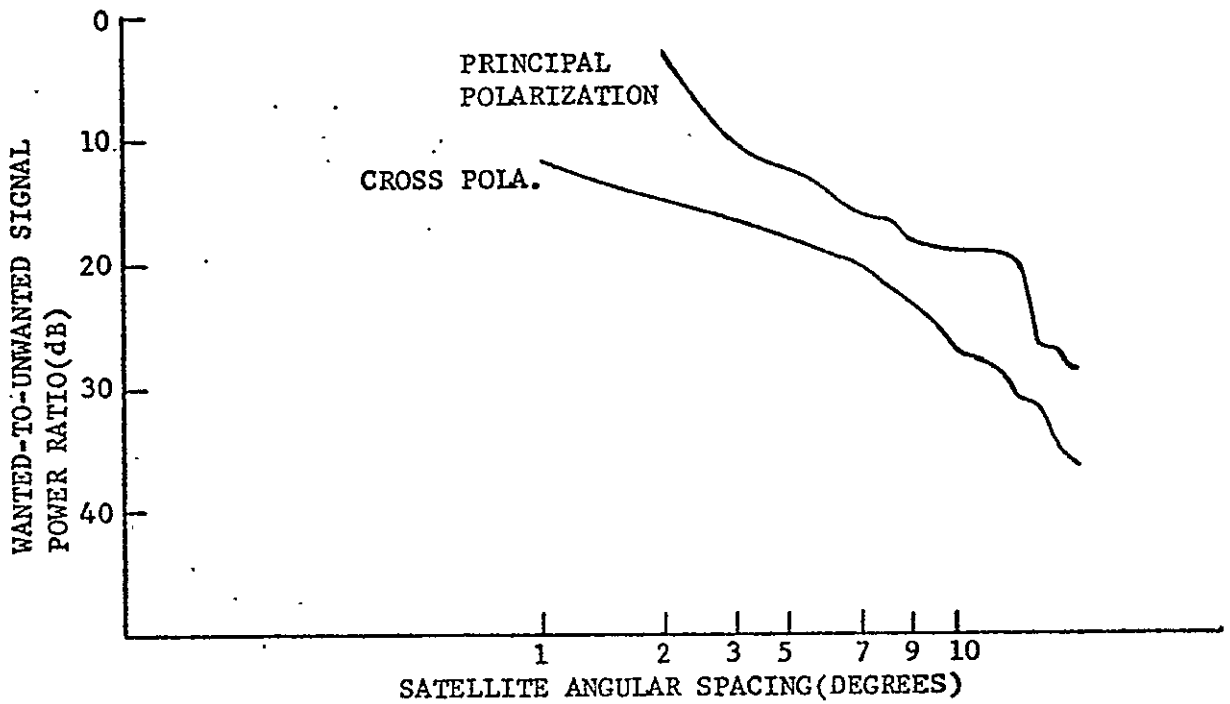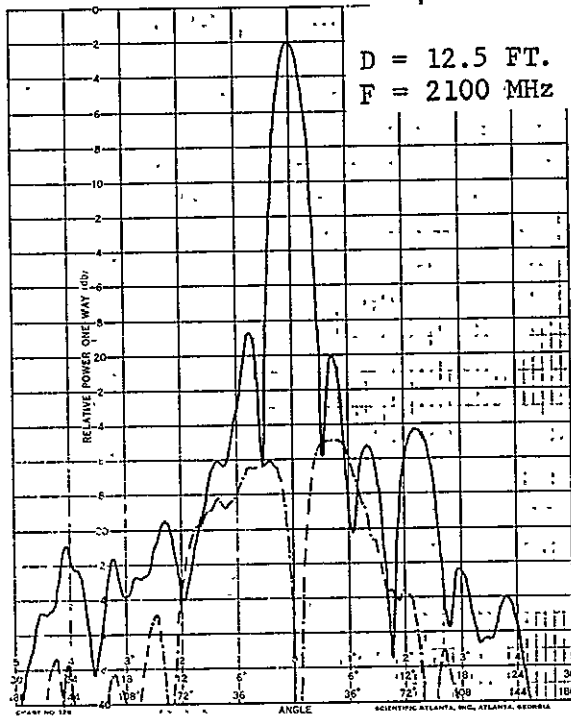
Fig. (3-35)--Polarization isolation — using measured pattern.

REFLECTOR DIAMETER
= 15 FT.
FREQUENCY = 7400 MHz

CROSS POL.

RELATIVE POWER (db)

RELATIVE POWER (db)

ANGLE

CROSS POLA.

PRINCIPAL
POLARIZATION

WANTED-TO-UNWANTED SIGNAL
POWER RATIO(dB)

10

20

30

40

50

1   2   3 5   7 9 10

SATELLITE ANGULAR SPACING(DEGREES)
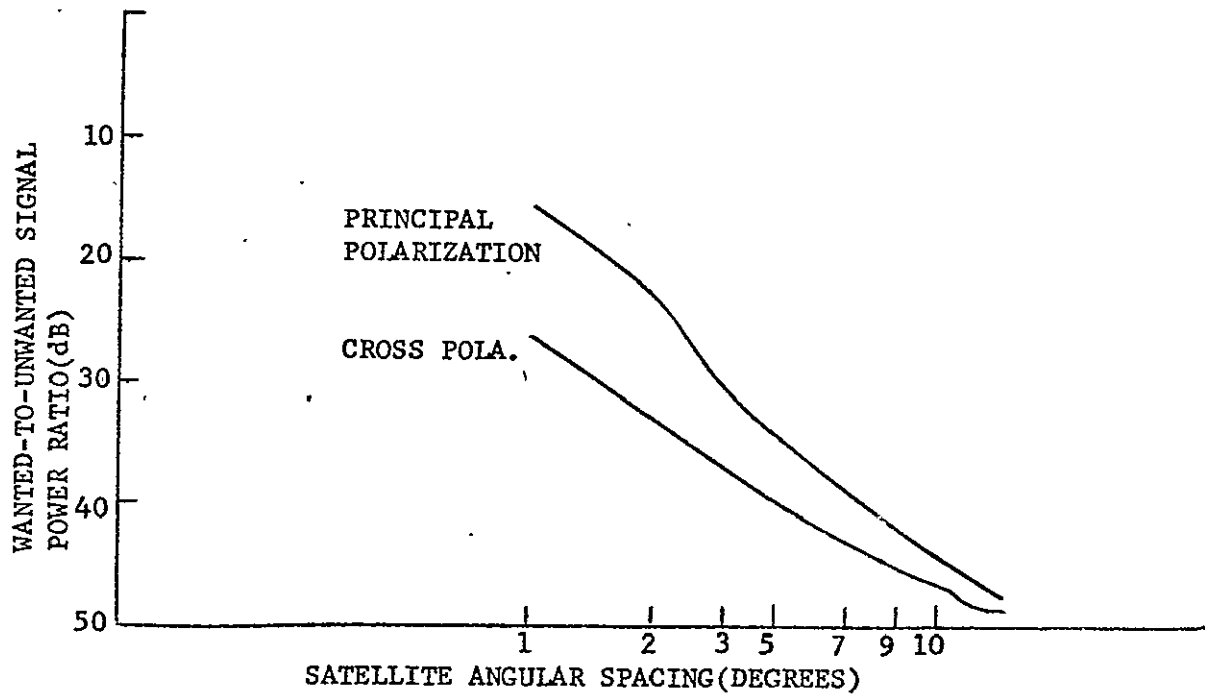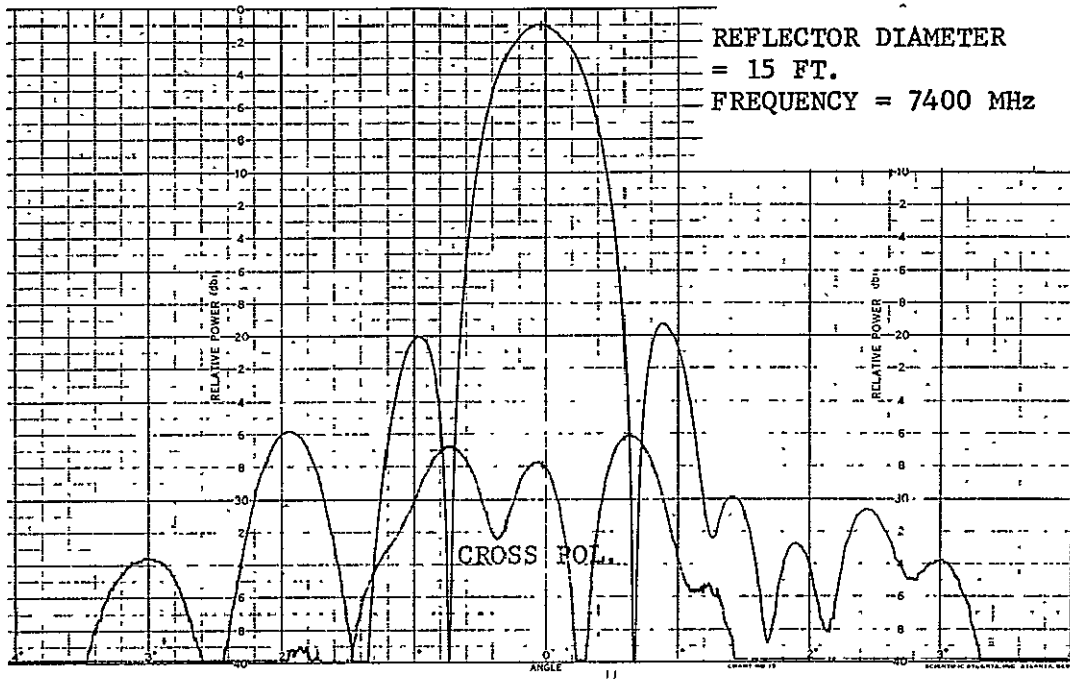
Fig. (3-36)--Polarization isolation — using measured pattern.

where

θ is the satellite spacing,

K is a constant

In terms of dB we have

$$10 \log y = Y = 10 \log K - 10 \, n \log \theta \qquad (3.28)$$

Let's now assume that for a satellite spacing $\theta = \theta_o$, the corresponding W/U ratio is $Y = Y_o$. That is

$$Y_o = 10 \log K - 10 \, n \log \theta_o \qquad (3.29)$$

If we now introduce the additional isolation P (in dB) obtainable from polarization discrimination, the W/U ratio will increase to a value equal to $Y_o + P$, which reduces the original spacing θ_o to a value θ_p . Again from Eq. (3.28) we have

$$Y_o + P = 10 \log K - 10 \, n \log \theta_p \qquad (3.30)$$

Substituting Eq. (3.29) into (3.30) we obtain

$$\frac{\theta_o}{\theta_p} = 10^{P/10n} \qquad (3.31)$$

For a homogeneous system employing orthogonally-polarized antenas between neighboring satellites, the spacing can at most be reduced to one half of the original spacing. Equation (3.31) is plotted in Fig. (3-37) for various values of n. For the CCIR sidelobe model (n = 2.5) Fig. (3-37) indicates that an additional isolation of 7.5 dB from polarization discrimination is required to reduce the satellite spacing to half of its original value. For illustration, the wanted-to-unwanted signal power ratio is calculated using the principal and cross-polarized patterns

- 87 -

supplied by Philco-Ford Corporation, and Radiation Inc., and the results are shown in the lower curves of Fig. (3-35) and (3-36). As shown, a substantial reduction in satellite spacing is possible if polarization isolation is used.
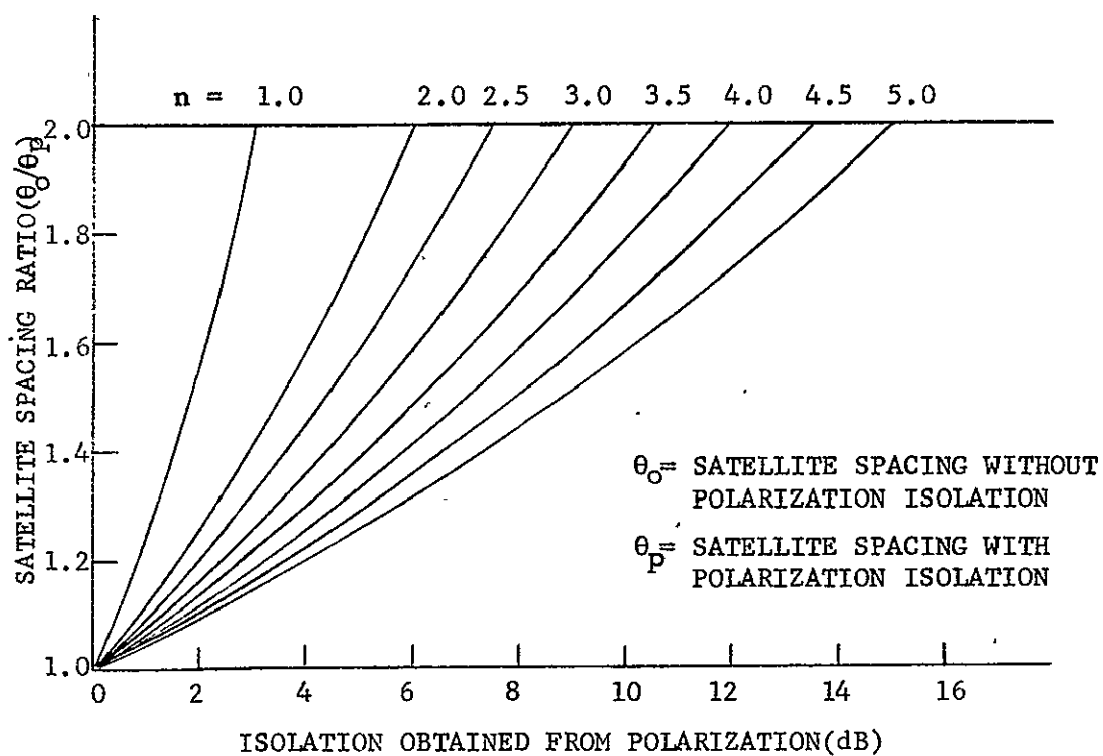
Fig. (3-37)--Satellite spacing reduction vs additional isolation obtained from polarization isolation.

CHAPTER 4

ZONED REFLECTOR ANTENNAS FOR A

LOW COST SATELLITE GROUND STATION

4.1 INTRODUCTION

Parabolic reflector antennas are most widely used in satellite

ground stations to obtain a narrow beam and high gain. However, a precise

parabolic reflector can be very expensive to manufacture. In the past,

Stanford University researchers[45] have demonstrated successfully a low

cost seven-foot pseudo parabolic reflector made of ten radial petal

plates which operates in the 2.6 GHz band. This configuration is too

expensive for use in the 12 GHz band because it requires more than 20

petals to obtain good performance. In this report we are proposing a

seven-foot zoned parabolic reflector antenna and a stepped cone-section

antenna for the 12 GHz band. The zoned parabolic reflector can be mass

produced as an inexpensive stamped unit and the stepped cone-section

reflector can be made at low cost from flat metal sheets in moderate

quantity. The zoned parabolic reflector is a more rigid structure than

a full parabolic one since each step of the zone is an edge stiffened

parabola. Consequently it has approximately the same rigidity as a full

parabolic reflector with a series of backup rings at each step. Because

of this inherent rigidity the skin of the shaped reflector can be thinner

than that for an unsupported full parabolic reflector.

4.2.1 Formulation

The zoned parabolic reflector consists of sections of paraboloids with different focal lengths but same focus point (Fig. 4-1). For proper design the zoned parabolic reflector must satisfy two conditions:

(1) Each zone must individually focus incoming parallel rays to a common focal point.

(2) The contributions from all zones must arrive at the focal point in phase.

Because the zoned reflector is a surface of revolution its design can be entirely developed in just two dimensions by working in a single axial cross section plane. Once conditions (1) and (2) are satisfied in a single axial cross section plane, they will be satisfied in all axial cross section planes.
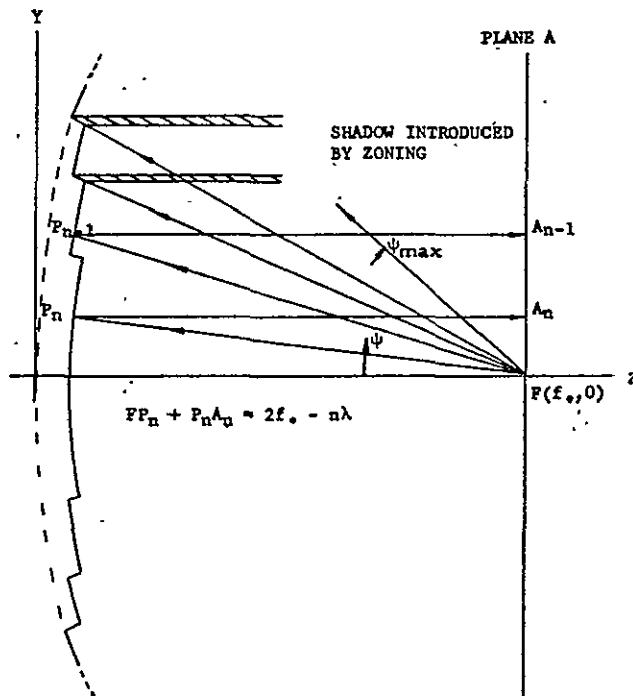
Fig. (4-1)--Zoned parabolic reflector.

In order to maintain a plane wavefront at the reflector aperture A the rays originating from the focus should differ in path by an integral number of wavelength, that is,

$$FP_0 + P_0A_0 = 2f_0$$
$$FP_1 + P_1A_1 = 2f_0 - \lambda$$
$$\cdot$$
$$\cdot$$
$$\cdot$$
$$FP_n + P_nA_n = 2f_0 - n\lambda \qquad (4.1)$$

Where subscripts 0, 1, 2, ..., n designate zones, f_0 is the focal length of the original unzoned reflector and λ is the wavelength. It follows immediately that the focal length, fn , of each zone relates to the focal length of the unzoned reflector by

$$f_1 = f_0 - \frac{\lambda}{2}$$
$$f_2 = f_0 - 2 \cdot \frac{\lambda}{2}$$
$$\cdot$$
$$\cdot$$
$$\cdot$$
$$f_n = f_0 - n \cdot \frac{\lambda}{2} \; . \qquad (4.2)$$

Let y, z be the rectangular coordinate system with the origin at the vertex of the unzoned paraboloid and the z-axis of the axis of revolution. In these coordinates the equation of each zone can be described by

$$y^2 = 4f_n \left(z - n \cdot \frac{\lambda}{2} \right) \qquad (4.3)$$

where fn is as given in (4.2). The vertex of each zone is displaced from the unzoned reflector by an integral number of half wavelengths.

The depth of each step is made as small as possible and arranged to lay in the same plane to simplify machining the stamping molds and for

ease of assembly and installation. It is therefore apparent that we must choose a plane perpendicular to the z-axis passing through the vertex of the last zone--nth zone. That is, all the zones lie on the plane of

$$Z = n \cdot \frac{\lambda}{2} \qquad \qquad (4.4)$$

The surface of each zone can also be expressed in terms of polar coordinates ρ_n, ψ_n

$$\rho_n = \frac{2f_n}{1 + \cos \psi_n} = f_n \sec^2 \left(\frac{\psi_n}{2} \right) \qquad (4.5)$$

The end points of each zone can be easily determined by the use of (4.3) and (4.5). As the number of zones increases, the depth of the reflector decreases. However, the diffraction effect and shadowing loss becomes severe. The choice of n is therefore determined by the trade-off between the performance and cost.

Since f_n is a function of λ, the chromatic aberration is obtained by differentiation of (4.2)

$$df_n = - \frac{n}{2} d\lambda \qquad \qquad (4.6)$$

where df_n denotes the decrement of the focal length of n-th zone due to an increment of the wavelength, $d\lambda$. The dependence of f_n on the wavelength makes the zoned reflector antenna frequency sensitive. For a feed slightly off focus the effect can be simulated by entering a phase distribution that is equal to

$$\Phi(\psi_n) = \frac{2\pi}{\lambda} d\cos(\psi_n)_{degree} \qquad (4.7)$$

where d is the feed displacement along axis away from the reflector.

4.2.2 GAIN AND EFFICIENCY CALCULATIONS

Although it has been thought that the zoned reflector can be fabricated at low cost under mass production, in that it can be stamped out, two penalties may result. The first is that Eq. (4.2) shows the focus length, f_n , depends on the wavelength at the operating frequency and zoned reflectors are, therefore, inevitably frequency-dependent in their behavior, the second penalty is that shadowing will occur. This is shown in Fig. (4-1) where the rays FPA and FP'A', which are together on reaching the reflector, have undergone considerable separation at the step. In transmission the aperture illumination is zero between P and P' ; in reception the energy incident between P and P' does not reach F and is therefore lost. The gain of a zoned reflector is therefore always less than that of the unzoned reflector from which it is derived.

For convenience the relationships between feed pattern angle and aperture radius are rewritten as follows

$$r = 2f_n \tan\left(\frac{\psi_n}{2}\right)$$

$$\rho_n = f_n \sec^2\left(\frac{\psi_n}{2}\right) \tag{4.8}$$

The amplitude of the feed pattern is multiplied by the space loss factor, L , to obtain the amplitude of the field in the aperture plane.

$$L = \cos^2\left(\frac{\psi_n}{2}\right) \tag{4.9}$$

The total radiated power contained in a feed pattern is equal to

$$P_T = \int_0^{2\pi} d\phi' \int_{-1}^{1} W(\psi,\phi') \, d(-\cos\psi) \tag{4.10}$$

where ϕ', ψ are the ordinary spherical coordinates. The radiated

power intercepted by the reflector is

$$P_R = \int_0^{2\pi} d\phi' \int_{-1}^{-\cos(\psi max)} W(\psi, \phi') \, d(-\cos\psi) \qquad (4.11)$$

The antenna geometry together with the coordinates is given in Fig. (4-2).
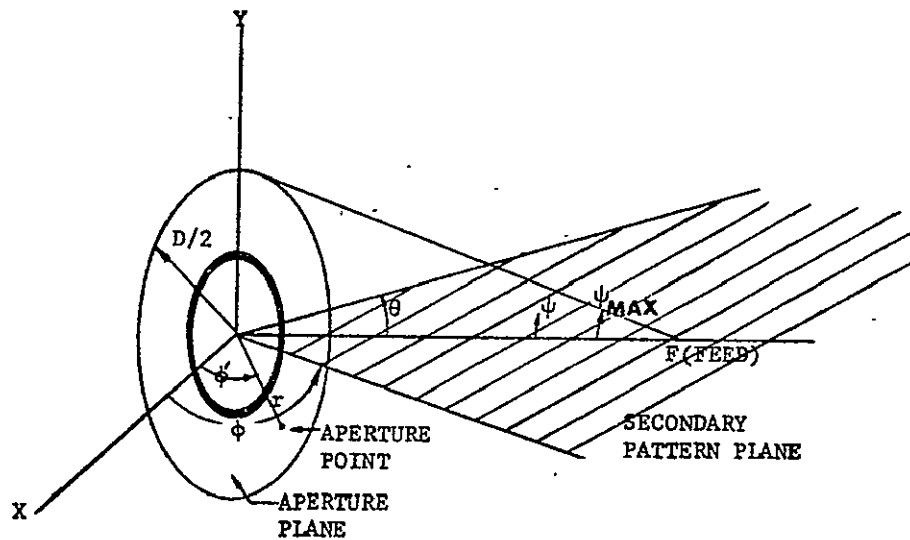
Fig. (4-2)--Coordinate system.

The fields at the equally spaced points along each radial are

determined by interpolating the input radial distribution. The aperture

field, W(volts/m), is analyzed as a Fourier series as follows:

$$W(r, \phi') = A_0(r) + \sum_{\ell=1}^{N/2} A_\ell(r) \cos(\ell\phi') + \sum_{\ell=1}^{N/2} B_\ell(r)\sin(\ell\phi')$$

$$(4.12)$$

where N = Number of feed pattern planes entered, $0 \le N \le 16$. Note

that if $N = 0$, then only the $A_0(r)$ term is calculated, $0 \le r \le D/2$,

where D is the diameter of the reflector.

A_1 , B_1 are Fourier coefficients:

$$A_\ell(r) = \frac{1}{\pi} \int W(r,\phi') \cos(\ell,\phi')d\phi'$$

$$B_\ell(r) = \frac{1}{\pi} \int W(r,\phi') \sin(\ell,\phi')d\phi' \qquad (4.13)$$

The apparent on-axis voltage (i.e., assuming the aperture phase is zero and no blockage) is found by

$$V_0 = 2\pi \int |ReA_0(r)^2 + ImA_0(r)^2|^{1/2} r\, dr \qquad (4.14)$$

The actual on-axis voltage is found to $Vaxis = (P_0^2 + Q_0^2)^{1/2}$ where

$$P_0 = 2\pi \int_0^R (ReA_0(r))r\,dr$$

$$Q_0 = 2\pi \int_0^R (ImA_0(r))r\,dr \qquad (4.15)$$

The actual on-axis voltage with shadow is found by

$$V'_{axis} = ((P_0 + BP_0)^2 + (Q_0 + BQ_0)^2)^{1/2} \qquad (4.16)$$

where BP_0 and BQ_0 are the corresponding real and imaginary voltage components contributed by the shadow region. The total radiated power (from the aperture) is

$$P = 2\pi \int_0^R \left\{ ReA_0(r)^2 + ImA_0(r)^2 + \frac{1}{2} \sum_{\ell=1}^{N/2} +(ReA_0(r)^2 + ImA_0(r)^2 \right\} r\,dr$$

$$(4.17)$$

Then the aperture efficiency is equal to

$$A_{eff} = \frac{V_0^2}{PA} \qquad (4.18)$$

where $A = \pi R^2$, area of the aperture. When the amplitude and phase are constant across the aperture, the aperture efficiency becomes unity. The phase efficiency is defined as

$$P_{eff} = \left(\frac{V_{axis}}{V_0}\right)^2 \qquad (4.19)$$

We define the blockage efficiency due to the presence of shadowing by

$$B_{eff} = \left(\frac{V'_{axis}}{V_{axis}}\right)^2 \qquad (4.20)$$

The gain of an antenna is

$$G = A_{eff}\, P_{eff}\, B_{eff}\, \frac{4\pi A}{\lambda^2} \qquad (4.21)$$

The radiation pattern is calculated according to the conventional diffraction field integral, which is given by[34]   ,

$$G(\theta,\phi) = \int_0^R dr \int_{-\pi}^{\pi} d\phi' \, rW(r,\phi')\exp\left\{j\left[Kr\sin\theta\cos(\phi-\phi')\right]\right\} \qquad (4.22)$$

where ϕ is held constant for each integration

$K = 2\pi/\lambda$

$r,\phi' = $ polar coordinates in the plane of the aperture

$R = $ radius to the aperture periphery

$\theta,\phi' = $ pattern coordinates

$W(r,\phi') = $ Complex amplitude distribution function over the circular

aperture. It is represented by an array of Fourier series coefficients.

When the shadow is present, the blocked pattern is computed as the sum of $G(\theta)$ plus the contributions calculated for the shadow. To calculate contribution from the shadow, the shadow region is assumed sufficiently narrow that they are essentially line sources with a distribution equal to the aperture field along their center lines. The aperture field at any given point, r, ϕ', on a given ring is found by directly summing the Fourier series

$$W_{shad}(r,\phi') = A_0(r) + \sum_{\ell=1} A_\ell(r)\cos(\ell\phi') + \sum_{\ell=1} B_\ell(r)\sin(\ell\phi')$$

(4.23)

Where ϕ' represents the azimuth to the center line of the shadow under consideration. The far field pattern for the shadow is of the form below for a line source

$$S = \int^R W_{shad}(r)\exp(Kr\cos(\phi-\phi'))dr \qquad (4.24)$$

These must be computed for each ϕ' and summed. The previous analysis excludes the phase deviations of the wave front due to scattering from the edges of the zone step.

The forgoing analyses can be implemented by the use of a digital computer.

4.2.3 Design Example

A seven-foot parabolic reflector consisting of seven zones with $F/D = 0.48$ has been designed for use in the 12 GHz band. The detailed

geometry is shown in Fig. (4-3). The total shadow area contributed by six zone steps is less than 1% of the reflector radiation aperture.

A multimode horn feed is used to illuminate the reflector and the blockage efficiency due to the presence of shadowing at the zone steps is calculated to be 81%, and a gain loss of -0.92 dB. The far field secondary pattern of a circularly polarized wave is plotted in Fig. (4-4) to be compared with that of the unzoned reflector. It is interesting to see that the first side lobe of the secondary pattern of the zoned reflector is about 10 dB below that of the unzoned reflector. The remaining sidelobes, however, are higher for the zoned reflector. This phenomenon is a result of superimposing the radiation patterns of the shadow area on the radiation pattern of the reflector aperture. The positions of the shadow areas are a very important factor in changing the sidelobe structure.
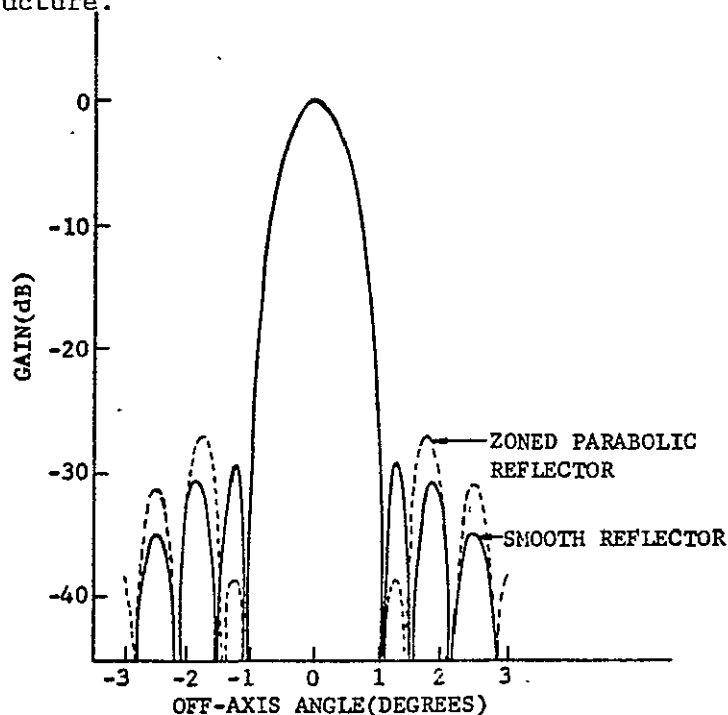
Fig. (4-4)--Compuated radiation pattern of zoned parabolic reflector.
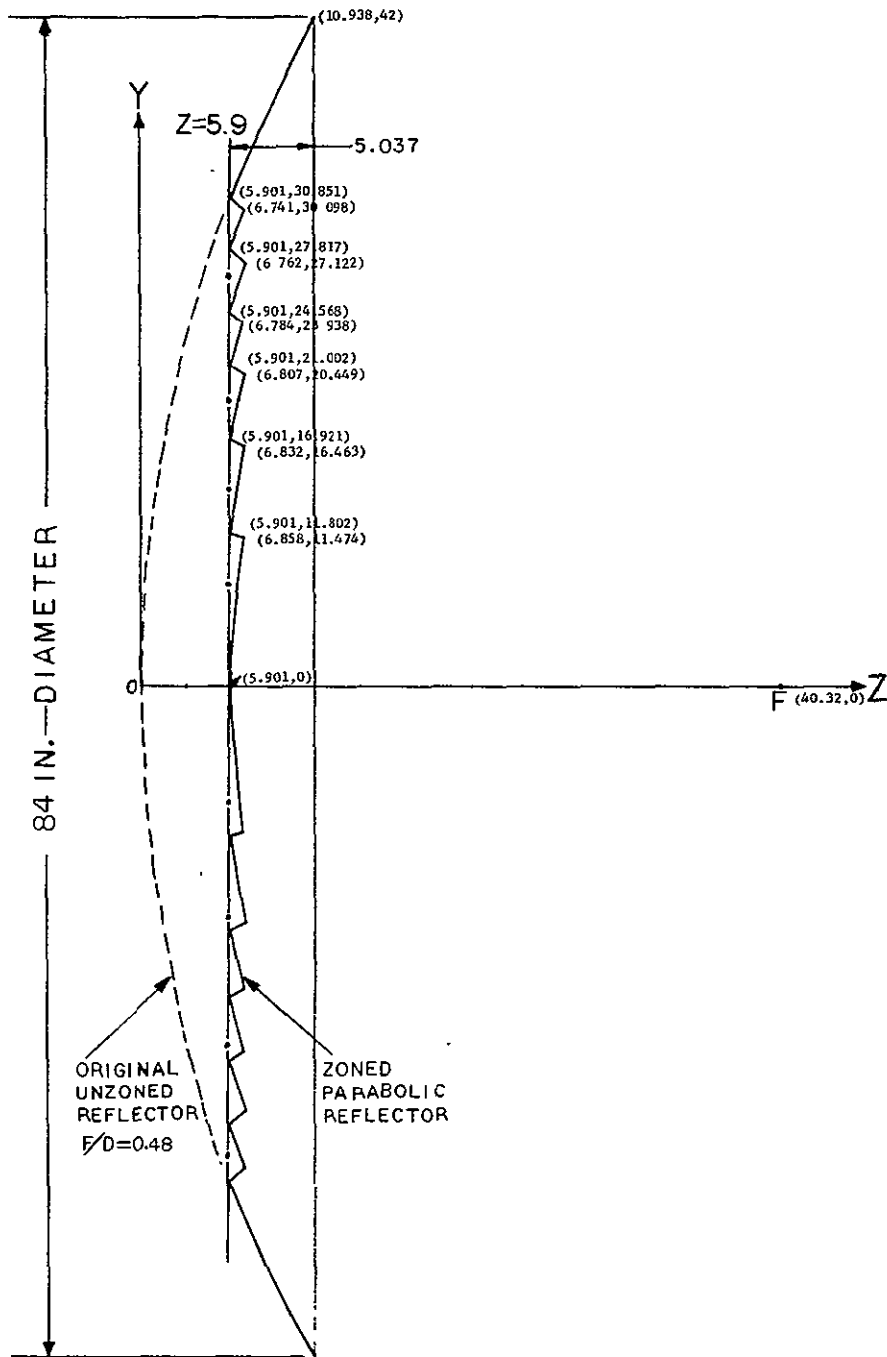
Fig. (4-3)--A design of 7-ft zoned parabolic reflector.

It has been noted in Eq. (4.6) that the focal lengths of each zone.
change with frequency. When operating at frequencies other than the
design center a phase error is introduced in the reflector aperture and
gain loss is observed. For a 10% band width the gain loss due to this
factor is found to be 0.2 dB.

4.3   STEPPED CONE-SECTION REFLECTOR

If the parabolas are replaced by flat surfaces in the zoned parabolic
reflector, the surface consists of a series of cone-shaped sections. For
a small quantity where tooling costs for the parabolic sections would
have a significant effect on unit price this reflector can be made from
flat metal sheets with some gain penalty.

Because the surface of this reflector deviates from the surface of
a paraboloid, gain reduction due to the phase error at the aperture is
expected. Again in this case the design can be entirely developed in
just two dimensions by working in a single axial cross section plane.
To derive the aperture phase error, let us describe each cone-section
be a line L with the equation

$$L \; : \; y \; = \; mz + b \hspace{3cm} (4.25)$$

where m is the slope and b is the y-intercept. All the rays origin-
ating from the focus and reflecting by the reflector can be considered
as coming from the image of the focus, according to the law of reflection.
Referring to Fig. (4-5) the image of the focus (f,0) is a line, L',
perpendicular to L , that is

$$L' \; : \; y \; = \; -\frac{1}{m} z + \frac{f}{m} \hspace{3cm} (4.26)$$

Let (Z, Y) be the image of the focus, then the distances to L from the focus and its image are the same

$$\frac{mf + b}{-(1 + m^2)^{1/2}} = \frac{mZ - Y + b}{(1 + m^2)^{1/2}}$$

$$mZ - Y = - mf - 2b \qquad (4.27)$$

Since (Z, Y) is on L', we have

$$- \frac{1}{m} Z - Y + \frac{f}{m} = 0$$

$$Z + mY = f \qquad (4.28)$$

From (4.27) and (4.28) we obtain

$$Z = \frac{- m^2 f + f - 2mb}{m^2 + 1}$$

$$Y = \frac{2mf + 2b}{m^2 + 1} \qquad (4.29)$$

Let $Z = Z_A$ be the aperture plane, then Z_A is shown to be

$$Z_A = \frac{D/2 - b}{m} \qquad (4.30)$$

For a true parabolic reflector the ray from the focus will travel a distance d_0 to the aperture plane, where d_0 is given by

$$d_0 = f_0 + Z_A , \text{ where } f_0 \text{ is the focal length} \qquad (4.31)$$

The distance, d_i, between the image, (Z, Y), and a point, (Z_A, y) is given by

$$d_i = \left[(Z - Z_A)^2 + (Y - y)^2 \right]^{1/2} \qquad (4.32)$$

The phase error $E(m, b, y)$ is defined as

$$E(m, b, y) = d_i - d_0 \qquad (4.33)$$

This phase error can, therefore, be minimized by looking for a set of m and b such that the following integral

$$I(m,b) = \int_{Y_1}^{Y_0} E^2(m,b,y)2\pi y\,dy \qquad (4.34)$$

is a minimum. This is equivalent to requiring that

$$\frac{\partial I(m,b)}{\partial m} = 0$$

$$\qquad (4.35)$$

$$\frac{\partial I(m,b)}{\partial b} = 0$$
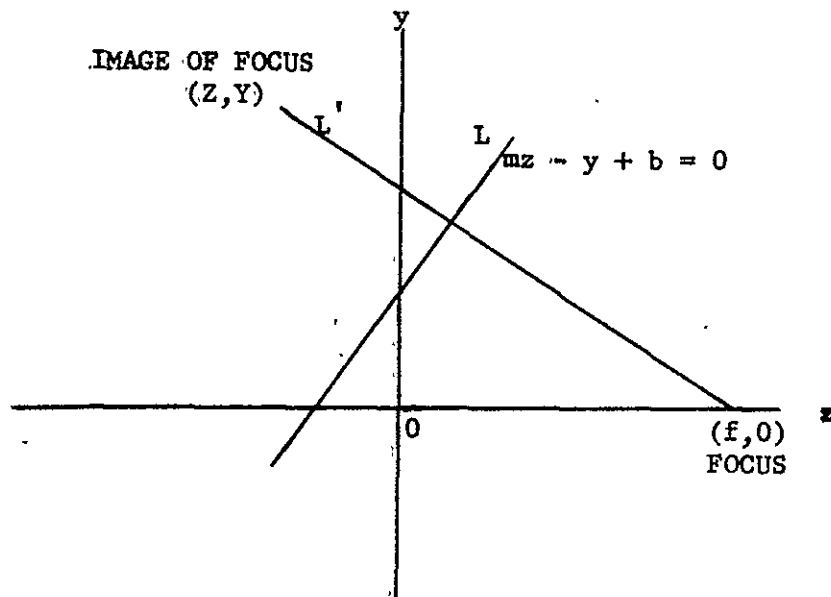
Fig. (4-5)--Image of focus with respect to individual flat zone.

Although m and b can be obtained by solving Eq. (4.14), it is not considered to be a simple matter because of the complexity of $I(m,b)$. Because we only expect to make a minor adjustment of m and b', it is more practical and easier, by the use of a digital computer, to adjust m and b directly until a tolerable phase error is achieved, for example, $E(m, b, y) > 1/16 \lambda$.

A design is shown in Fig. (4-6), which is derived from the seven-foot zoned parabolic reflector of section 4.2. The parabolas of the first and the last zones are each approximated by two straight lines, which introduce a phase error less than 0.07λ across the corresponding zone aperture. Parabolas of other zones are approximated by lines connecting the end points directly, introducing a phase error less than 0.03λ. We arrive at a configuration of nine cone sections.

The gain loss due to phase error for this particular reflector is found to be 0.5 dB. The secondary pattern is shown in Fig. (4-7). As shown, the sidelobe levels are increased and there are shoulders on the radiation pattern. This is because of the phase error incurred by using stepped-cone sections instead of confocal paraboloid sections. This phase error results in the following effects: (1) a drop in gain, (2) an increase in the side-lobe levels, and (3) fill-in of the null between main beam and sidelobes. Furthermore, if the stepped-cone reflector has a tapered illumination, a small phase error results in a more pronounced increase in the sidelobe levels.

We conclude that the flat section reflector is more attractive than the true parabolic reflector from the metal working cost point of view, but not from the gain and interference point of view. However, as a
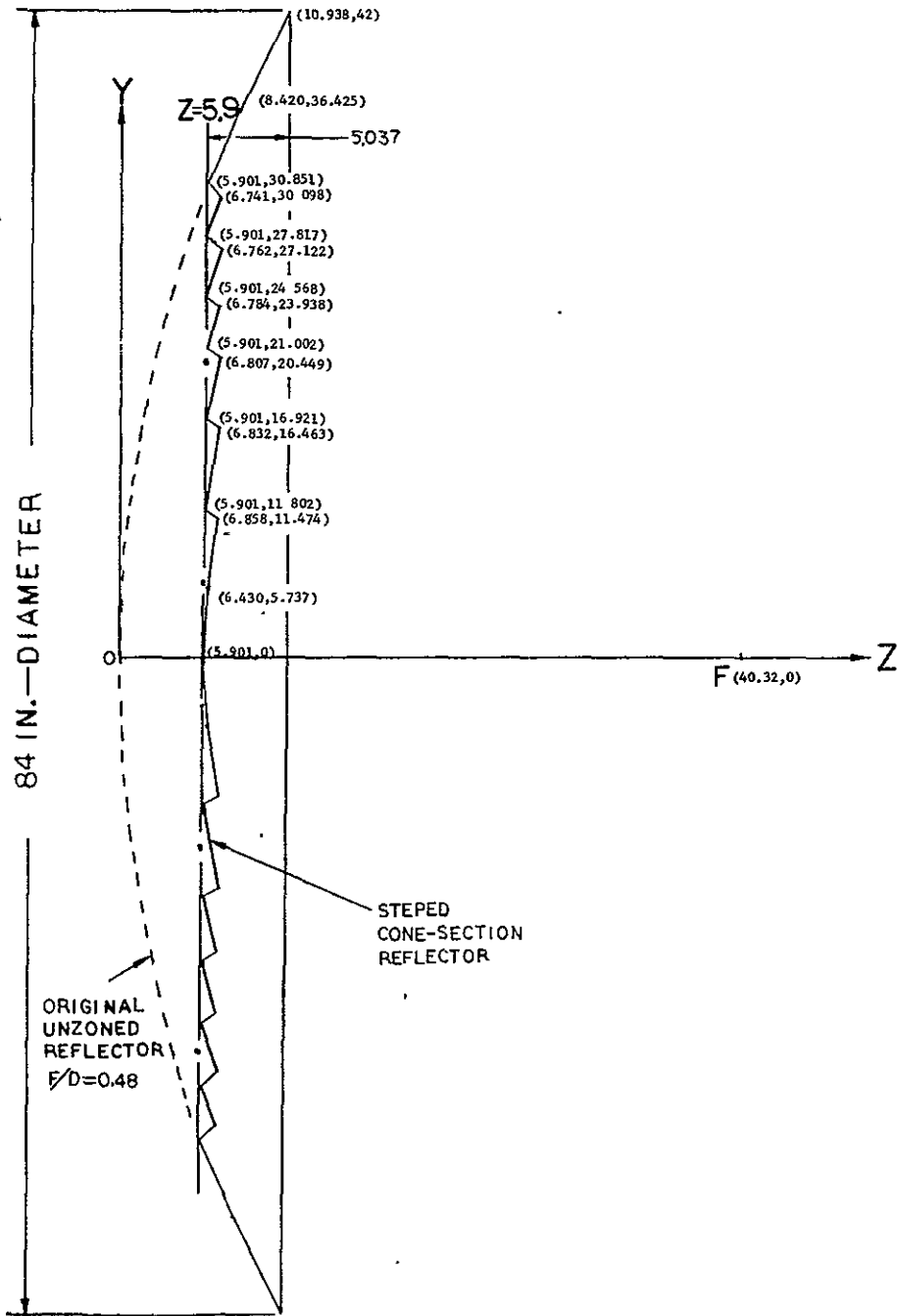
Fig. (4-6)--A design of 7-ft stepped cone-section reflector.

high gain satellite antenna is recommended for use in broadcast satellite systems, the gain penalty suffered by using flat section reflectors at the ground station may not severely degrade the signal quality. For instance, a 30-foot reflector antenna[46] will be used on NASA's Applied Technology Satellites (ATS) Models F & G to transmit educational television programs at 2.5 GHz, which yields a gain of 42 dB. This compares with a gain of perhaps 25 dB for conventional 4-5 foot satellite antenas in this frequency band. The differential gain allows use of a smaller ground station antenna for the same signal quality. Furthermore, this may allow one to use the absorber array technique to suppress the side-lobes of the flat section reflector, as discussed in Section 3.4.2.
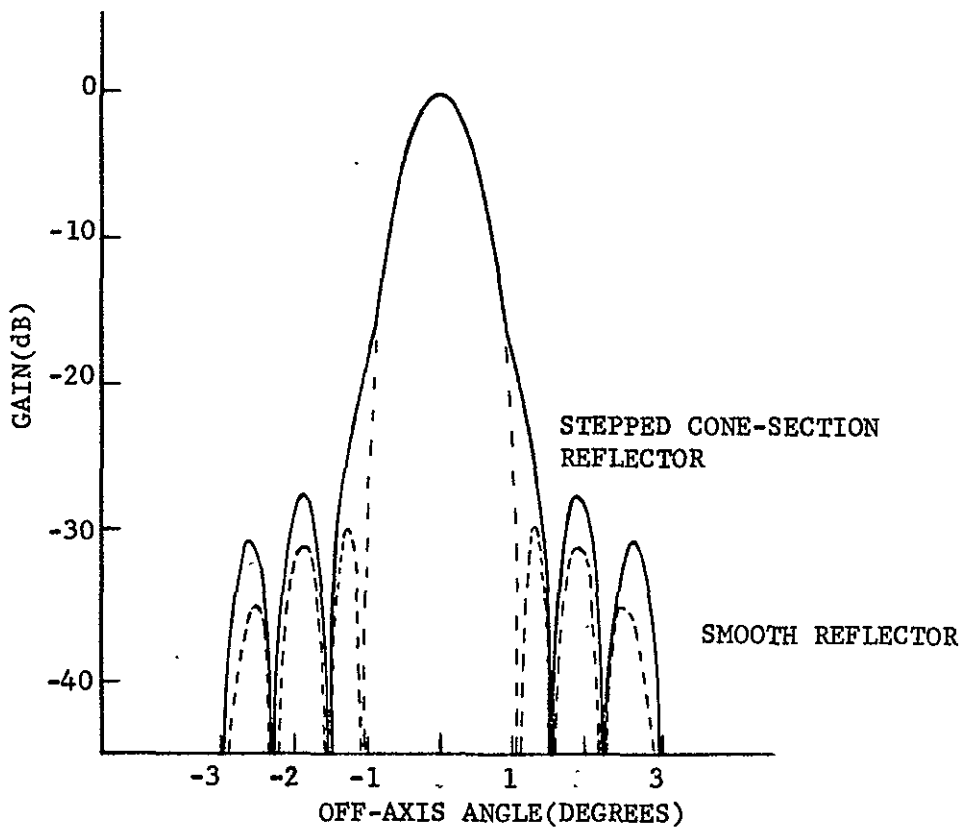
Fig. (4-7)--Computed pattern of stepped cone-section reflector.

CHAPTER 5

A MASS PRODUCIBLE 12 GHz ANTENNA FEED SUBSYSTEM-EXPERIMENTAL MODEL

5.1 INTRODUCTION

This chapter presents the design of a mass producible 12 GHz antenna feed subsystem to be used in either a prime focus or a Cassegrain antenna system. It consists of a multimode feed horn, a waveguide capacitive-type pin polarizer, a nonuniform waveguide high-pass filter and a field-shaping waveguide-to-coaxial-line coupling probe as shown in Fig. (5-1a). The use of waveguide components enables the entire feed subsystem to be fabricated as an integral part through die casting as shown in Fig. (5-1b), resulting in cost saving under mass production conditions. The waveguide system also yields the lowest insertion loss compared with other alternatives. However, it usually has undesirably long length for use in a prime focus system and, therefore, one of the design goals is to minimizd each component's length. None of the component designs discussed in this chapter will require tuning and all have repeatable performance.

The experimental model with the components assembled is shown in Fig. (5-2).

5.2 MULTIMODE FEED HORN

One of the major design criteria for achieving good efficiency in both the prime focus and cassegrain systems is for the primary feed to have equal E-and H-plane response and a low sidelobe pattern. Equal E and H plane patterns reduce the cross polarized energy and also result
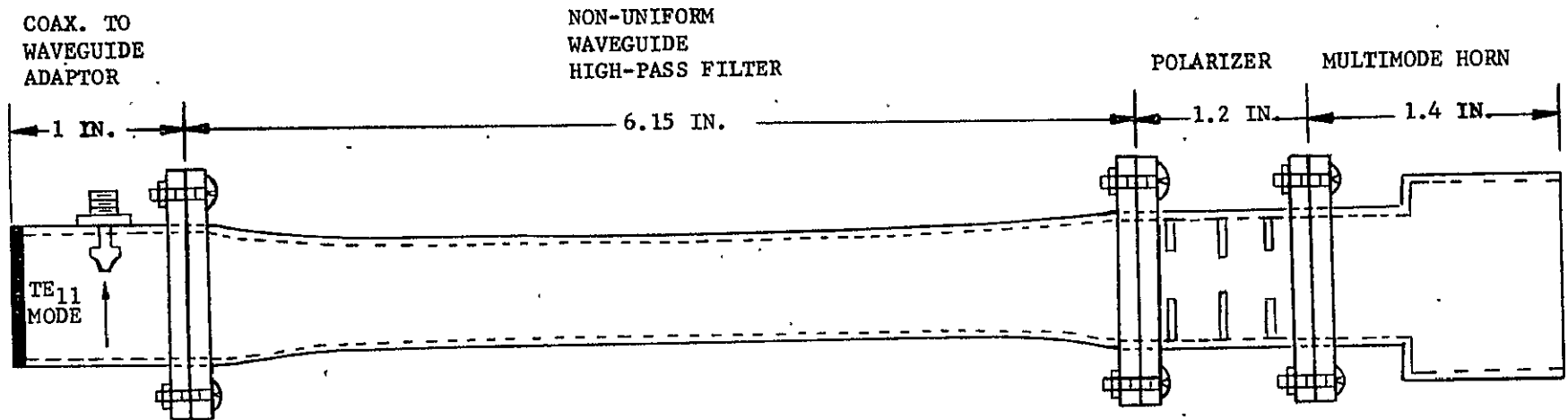
Fig. (5-1a)--Assembly diagram of a 12 GHz antenna feed.
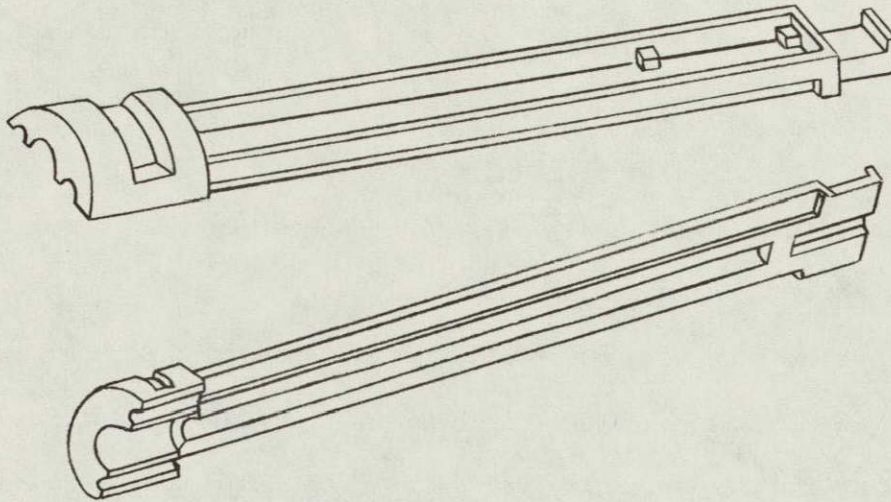
Fig. (5-1b)--Typical proposed die-casting package.
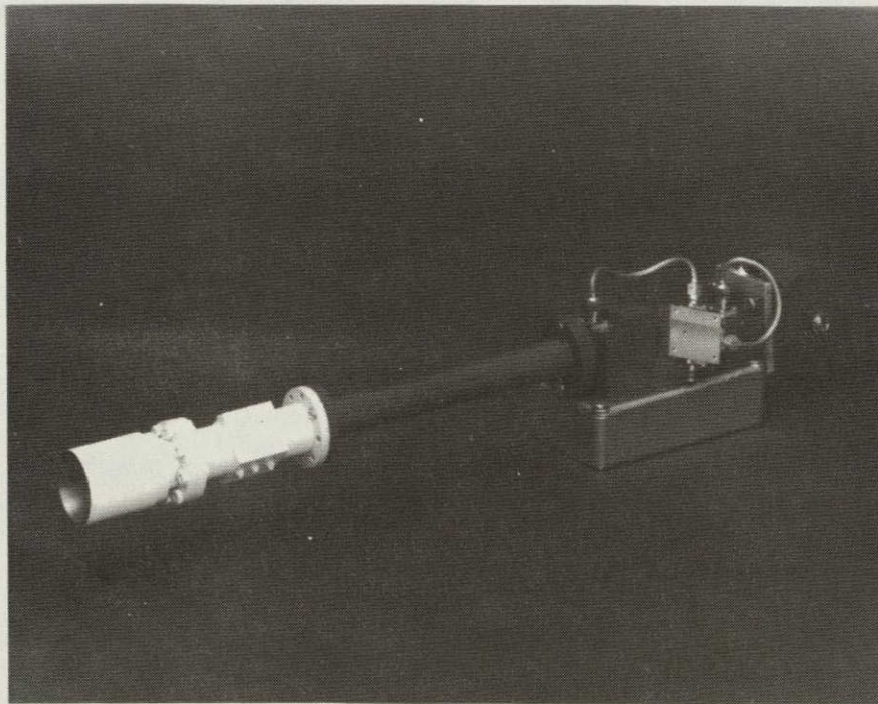
Fig. (5-2)--Experimental model of the 12 GHz antenna feed.

in the same amplitude distributions in both planes. A low sidelobe
pattern reduces spillover loss. For instance, a corrugated wall conical
horn, which has all these features, has been widely used in modern
communication ground stations. The overall antenna efficiency has been
found to be more than 75% over a 60% band for a cassegrain system, com-
pared to 65% at best with a conventional conical horn.

Because the Educational Television ground station program emphasizes
low cost and the antenna operates over a very narrow frequency band, other
alternatives may achieve comparable performance to the corrugated horn
at lower cost. One candidate is the conical horn with a step discon-
tinuity.[48] The discontinuity will excite the TM_{11} mode to shape the
TE_{11} dominant mode pattern.

For a prime focus system the multimode open-end circular waveguide
feed may be used. For the cassegrain system the multimode circular
conical horn is used. Analysis leading to the design of a wide flare
minimum length multimode horn will be presented.

5.2.1 Sidelobe Suppression and Beam Equalization of a Conical Horn
      Pattern Obtained by Using the TM_{11} Mode

The first side lobe of a conical horn pattern in the E-plane is much
higher than that in the H-plane. In addition, the beamwidth of the E-plane
pattern is narrower than that of the H-plane. The explanation for this
effect is simply that the field in the E-plane exhibits fringing and
does not taper down to zero at the horn edge. It has been proven that
the excitation of a TM_{11} mode will suppress the sidelobe and broaden
the pattern in the E-plane. The physical insight to this concept can

be gained by examining the TE_{11} and TM_{11} mode electric field pattern in a circular waveguide as shown in Fig. (5-3). It can be seen that, if the
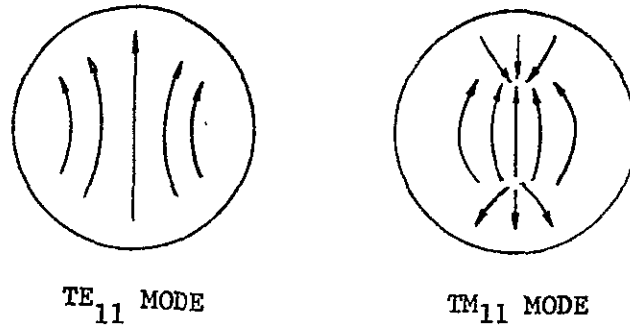
TE$_{11}$ MODE   TM$_{11}$ MODE

Fig. (5-3)--TE$_{11}$ and TM$_{11}$ modes E field pattern in a circular waveguide.

TE_{11} and TM_{11} modes have proper phase and field strength, the combination of these two modes will result in very weak field on the edge of the horn in the E-plane. The edge diffraction and the effective radiation aperture are then reduced, resulting in a lower side lobe level and a broader pattern in the E-plane.

The circular waveguide mode will be used to analyze the radiation pattern produced by the coexistence of the TE_{11} and TM_{11} modes. This is a good approximation for a conical horn of small flare angle. Assuming that mismatches of these two modes at the waveguide open-end are negligible, their patterns are given by[49]

$\underline{TE_{11}}$ Modes:

$$E_\theta \propto \left(1 + \frac{\beta_{TE_{11}}}{k} \cos\theta\right) J_1(Kb) \frac{J_1(kb\sin\theta)}{\sin\theta} \sin\phi \frac{e^{-jkR}}{R}$$

$$(5.1)$$

and

$$E_\phi \propto \left(\cos\theta + \frac{\beta_{TE_{11}}}{k\cdot}\right) J_1(Kb) \frac{J_1'(kb\sin\theta)}{1 - \dfrac{ksin\theta}{k}^2} \cos\phi \frac{e^{-jkR}}{R} \qquad (5.1)$$

$\underline{TM_{11}}$ $\underline{Mode}$:

$$E_\theta \propto \cos\theta + \frac{\beta_{TM_{11}}}{k} \frac{J_1'(Xb)J_1(kb\sin\theta)}{1 - \left(\dfrac{X}{ksin\theta}\right)^2} \sin\phi \frac{e^{-jkR}}{R} \qquad (5.2)$$

$$E_\phi = 0$$

Where

k = free space propagation constant

b = radius of circular aperture

K = 1.841/b

X = 3.832/b

$\beta_{TE_{11}}$ = $(k-k^2)$

$\beta_{TM_{11}}$ = $(k-X^2)$

The E-plane pattern is found to be: ($\phi = 90^o$)

$\underline{TE_{11}}$ $\underline{Mode}$:

$$E_\theta \propto 1 + \frac{\beta_{TE_{11}}}{k} \cos\theta \quad J_1(Kb) \frac{J_1(kb\sin\theta)}{\sin\theta} \frac{e^{-jkR}}{R} \qquad (5.3)$$

$\underline{TM_{11}}$ $\underline{Mode}$:

$$E_\theta \propto \cos\theta + \frac{\beta_{TM_{11}}}{k} \frac{J_1'(Xb)J_1(kb\sin\theta)}{1 - \left(\dfrac{X}{ksin\theta}\right)^2} \frac{e^{-jkR}}{R}$$

$$(5.4)$$

The H-plane pattern is obtained by setting $\phi = 0°$.

$\underline{TE_{11}\ \text{Mode}:}$

$$E_\phi \propto \left(\cos\theta - \frac{\beta_{TE_{11}}}{k}\right) J_1(Kb) \frac{J_1'(kb\sin\theta)}{1 - \left(\dfrac{k\sin\theta}{k}\right)^2} \frac{e^{-jkR}}{R} \qquad (5.5)$$

$\underline{TM_{11}\ \text{Mode}:}$

$$E_\phi \equiv 0 \qquad\qquad\qquad\qquad\qquad (5.6)$$

It becomes clear that the H-plane pattern of the TE_{11} mode is not affected by the existence of the TM_{11} mode since the ϕ component of the TM_{11} mode pattern is identically equal to zero. We now introduce a conversion factor C defined as

$$C = \frac{\left|E_\rho^{TM_{11}}\right|}{\left|E_\rho^{TE_{11}}\right|} \quad (\text{at}\quad \rho = b,\ \phi = 90°) \qquad (5.7)$$

where

$\rho,\ \phi$ = cylindrical coordinates

$E_\rho^{TE_{11}},\ E_\rho^{TM_{11}}$ = radial components of the TE_{11} and TM_{11} modes

It is easy to prove that by comparing E_θ component of TE_{11} and TM_{11} mode patterns and C, the resultant pattern is given by:

$\underline{\text{E-plane}}$

$$E_\theta(TE_{11} + TM_{11}) = \frac{\left(\left(1 + \dfrac{\beta_{TE_{11}}\cos\theta}{k}\right) - C\dfrac{\cos\theta + \dfrac{\beta_{TM_{11}}}{k}}{1 - (X/k\sin\theta)^2}\right)\dfrac{J_1(kb\sin\theta)}{k\sin\theta}}{1 + \dfrac{\beta_{TE_{11}}}{k}}$$

$$(5.8)$$

H-plane

$$E_\phi(TE_{11} + TM_{11}) = \left(\cos\theta + \frac{\beta_{TE_{11}}}{k}\right) \frac{J_0(kb\sin\theta) - J_2(kb\sin\theta)}{\left(1 + \frac{\beta_{TE_{11}}}{k}\right)\left(1 - \left(\frac{k\sin\theta}{k}\right)^2\right)}$$

(5.9)

Note that E_θ and E_ϕ have been normalized to the on-axis $(\theta = 0)$ field amplitude. Radiation patterns in other planes can be obtained in a similar manner.

To illustrate the effect of C on the E-plane beam shape, pattern plots as a function of aperture size are presented in Fig.(5-4). The use of the TM_{11} mode to shape the TE_{11} mode pattern is verified after reviewing those figures. As the aperture size is close to the TM_{11} mode cutoff wavelength (e.g., $D/\lambda = 1.25$), a large conversion factor is needed to equalize the E- and H- pattern at the -10 dB point. As the aperture size increases, the necessary magnitude of the conversion factor decreases drastically. For example, $C > 1$ for $D/\lambda = 1.25$, but $C = 0.7$ for $D/\lambda = 1.75$. C remains essentially constant (has a value between 0.6 and 0.7) for $D/\lambda \geq 1.75$. Figure (5-5) indicates the variation of C with the normalized aperture size, or equivalently, it shows the dependence of the necessary magnitude of C on the frequency.
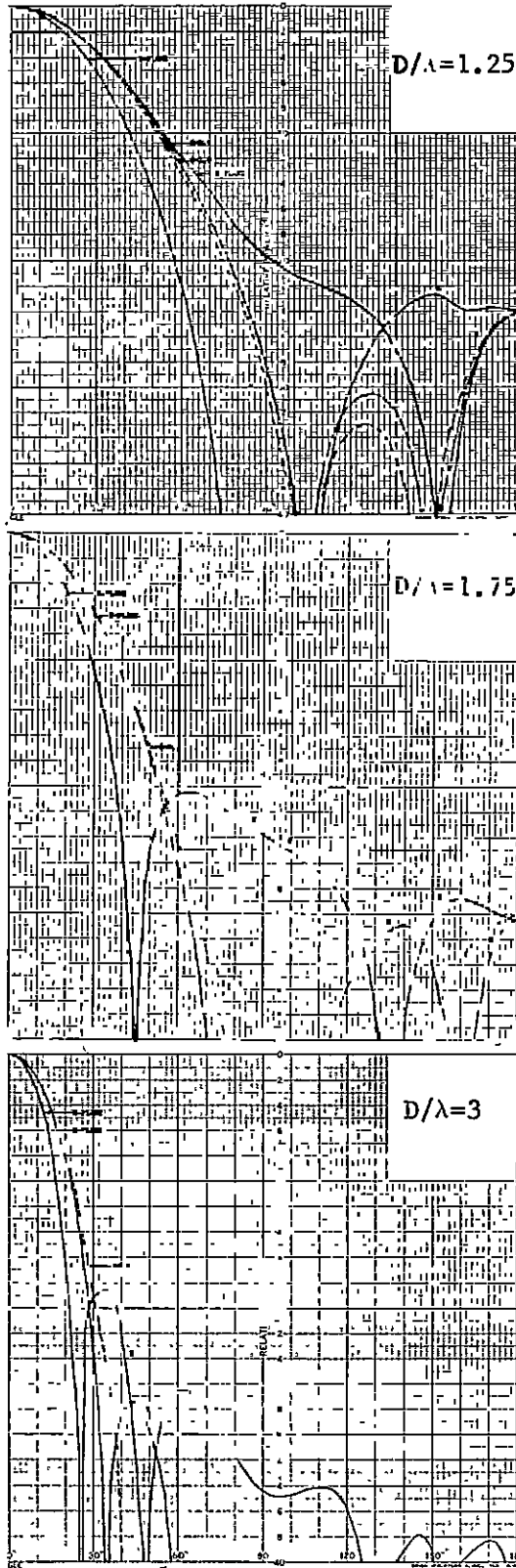
Fig. (5-4)--Calculated radiation patterns of multimode waveguide
radiators.
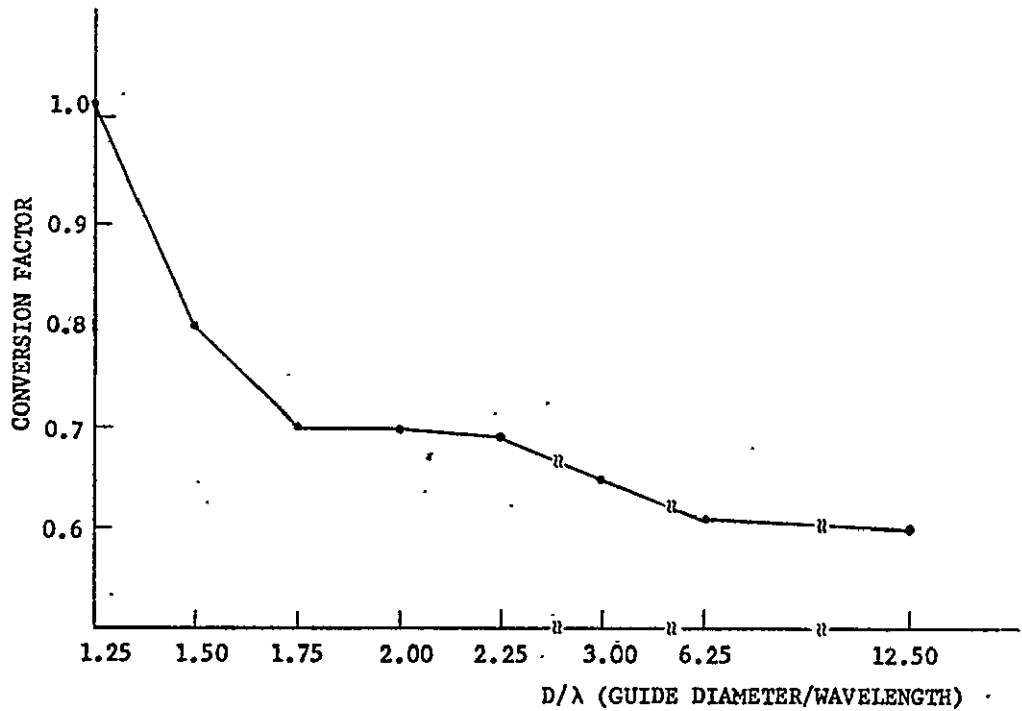
Fig. (5-5)--Variations of conversion factor for equalizing E - and H-plane pattern at the - 10 dB point.

5.2.2 Design Considerations

The conversion factor of a step discontinuity, C_s , as derived in Appendix A is given by

$$C_s = 0.754 \frac{J_1(3.832\frac{a}{b})}{\cdot J_1(1.841\frac{b}{a})} \qquad (5.10)$$

As shown, C_s is a function of step size. In deriving C_s the trans-verse E-field components at the discontinuity are assumed the same as the incident TE_{11} mode. As a result the phase front is unchanged and the TE_{11} and TM_{11} modes are in phase. For the flare angle change in a horn, the higher order mode must be excited such that the curved phase front is matched. Thus, we cannot expect the TM_{11} mode will be in phase

with the TE_{11}[50] dominant mode. Tomiyasu[51] showed that in this case the complex conversion factor (which indicates phase) is

$$c_f = j \ 1.76 \times 10^{-7} \frac{D}{\lambda} \alpha \qquad (5.11)$$

Where: α is the flare angle in degrees

D is the diameter of the horn throat

The TE_{11} and TM_{11} modes are, therefore, in phase quadrature. Figure (5-6)
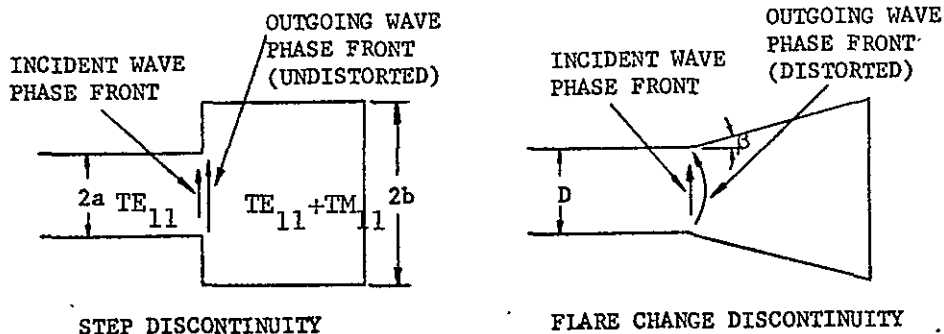
Fig. (5-6)--Phase front change at waveguide discontinuities.

illustrates the phase front change of a wave at a step discontinuity and at a horn flare change discontinuity.

The TE_{11} and TM_{11} modes must be in phase at the horn aperture to enable the additive combination of their far field components to produce the desired pattern. The factors affecting the differential phase shift between these two modes are:

(a) the phase of the generated modes at each discontinuity as discussed above

(b) the length of the oversized waveguide and horn.

The differential phase shift, $\Delta\phi_{guide}$ between TE_{11} and TM_{11} modes in the oversized waveguide section is given in radians by

$$\Delta\phi_{guide} = \frac{2\pi\ell}{\lambda}\left(\left(1 - \left(\frac{1.841\lambda}{2\pi a}\right)^2\right)^{1/2} - \left(1 - \left(\frac{3.832\lambda}{2\pi a}\right)^2\right)^{1/2}\right) \quad (5.12)$$

where

ℓ = guide length

a = guide radius

The differential phase shift, Δ_{horn}, between the TE_{11} and TM_{11} modes in the horn section is given in radians by

$$\Delta\phi_{horn} = \frac{2\pi}{\lambda \sin\alpha}\left(\left(r_A^2 - \left(\frac{1.841\lambda}{2\pi}\right)^2\right)^{1/2} - \left(\frac{1.841\lambda}{2\pi}\right)\cos^{-1}\frac{1.841\lambda}{2\pi r_A}\right.$$

$$- \left(r_0^2 - \left(\frac{1.841\lambda}{2\pi}\right)^2\right)^{1/2} + \left(\frac{1.841\lambda}{2\pi}\right)\cos^{-1}\frac{1.841\lambda}{2\pi r_0}$$

$$- \left(r_A^2 - \left(\frac{3.832\lambda}{2\pi}\right)^2\right)^{1/2} + \left(\frac{3.832\lambda}{2\pi}\right)\cos^{-1}\frac{3.832\lambda}{2\pi r_A}$$

$$\left. + \left(r_0^2 - \left(\frac{3.832\lambda}{2\pi}\right)^2\right)^{1/2} + \left(\frac{3.832\lambda}{2\pi}\right)\cos^{-1}\frac{3.832\lambda}{2\pi r_0}\right)$$

$$(5.13)$$

where

α = half horn flare angle

r_0 = horn throat radius

r_A = horn aperture radius

As shown, the differential phase shifts are a frequency sensitive parameter, which cause the multimode horn to be a narrow-band radiator.

The conversion factor appearing in Eq. (5.8) is actually a resultant of the conversion factor of all discontinuities.[52] Referring to Fig. (5-7) the step discontinuity at junction 1 excites a TM_{11} mode
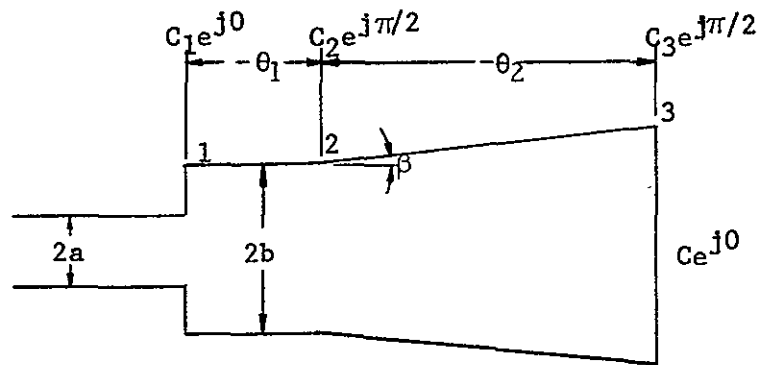
Fig. (5-7)--Multimode conical horn.

with complex amplitude $C_1 e^{j0}$ times that of TE_{11} mode. Similarly, at junctions 2 and 3 the TM_{11} mode amplitude relative to TE_{11} mode are $C_2 e^{j\pi/2}$ and $C_3 e^{j\pi/2}$ respectively. In general the C's are small and to a first order approximation we may assume that the resultant complex conversion factor at the aperture $C e^{j0}$, is the sum of the conversion factors at each junction.

$$Ce^{j0} = C_1 e^{j0} e^{-j(\theta_1 + \theta_2)} + C_2 e^{j\pi/2} e^{-j\theta_2} + C_3 e^{j\pi/2}$$

(5.14)

Note that all the phase are relative to TE_{11} mode.

$$C = C_1 \cos(\theta_1 + \theta_2) - jc\sin(\theta_1 + \theta_2) + C_2 \cos(\pi/2 - \theta_2)$$
$$+ jC_2\sin(\pi/2 - \theta_2) + jC_3$$

(5.15)

which is equivalent to the following set of equations:

$$C_1 \sin(\theta_1 + \theta_2) = C_2 \cos\theta_2 + C_3 \qquad (5.16)$$

$$C_1 \cos(\theta_1 + \theta_2) = C_2 \sin\theta_2 + C \qquad (5.17)$$

The parameters involved in this set of simultaneous equations are C, C_1, C_2 and θ_1, θ_2. The question remaining in the design is what parameters can be suitably pre-set. It is observed that the adjustment of the flare horn section is much more difficult to accomplish than that of the circular waveguide section (between junction 1 and 2). Therefore, if we can find a proper flare angle and horn length such that its effect on the resultant conversion factor, $Ce^{j\theta}$, is negligible, then it only remains to adjust the circular waveguide section to obtain the desired conversion factor magnitude at the aperture. From (5.16) and (5.17) we obtain magnitude C_1

$$C_1 = ((C_2 \cos\theta_2 + C_3)^2 + (C - C_2 \sin\theta_2)^2)^{1/2} \qquad (5.18)$$

$$\tan(\theta_1 + \theta_2) = \frac{C_2 \cos\theta_2 + C_3}{-C_2 \sin\theta_2 + C}$$

For a qualitative analysis let's assume that $C_2 \approx C_3$. If we choose $\theta_2 \approx 180^o$, we will have

$$C_1 \approx C$$

$$\theta_1 + \theta_2 \approx 360^o \qquad (5.19)$$

It is obvious in this case, C only depends on C_1; that is, C is directly controlled by C_1, which is a function of b/a. Note that in our analysis we assume the circular waveguide and the horn section are lossless so that the conversion factor will not change as the waves

propagate. This is not strictly true, however, since the conversion factor is defined as the ratio of mode amplitudes which will be attenuated at a different rates for different modes. Although C_2 will not be exactly equal to C_3 in a practical situation the choice of $\theta_2 \approx 180^{\circ}$ will minimize the effect of the flare horn.

5.2.3 Experimental Results

Two multimode horns have been designed as shown in Fig. (5-8a) and (5-9a): one is an open-end waveguide type with $D/\lambda = 1.25$ for use in a prime focus system and the other is a horn type with $D/\lambda = 3.0$ for use
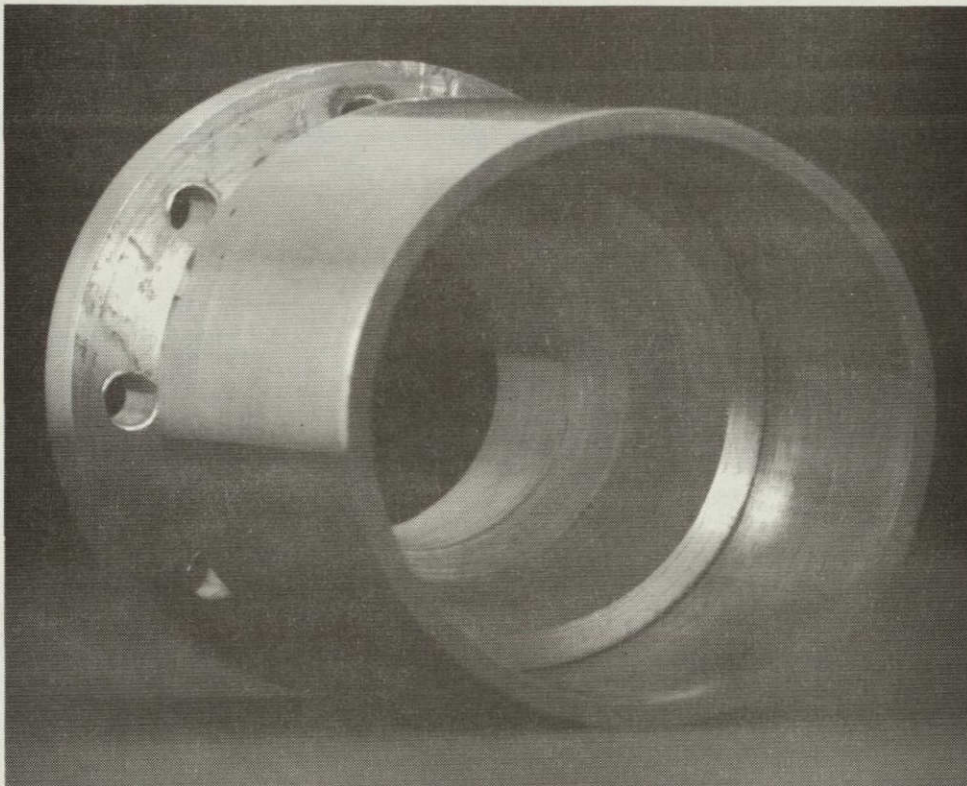
Fig. (5-8a)--Experimental model of 12 GHz multimode waveguide feed.
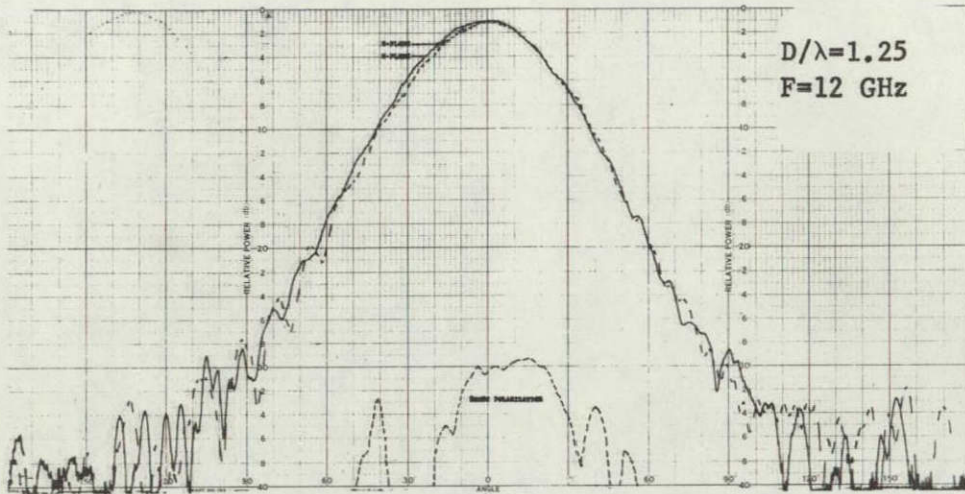
Fig. (5-8b)--Measured E- and H- plane pattern of the 12 GHz
multimode waveguide feed.
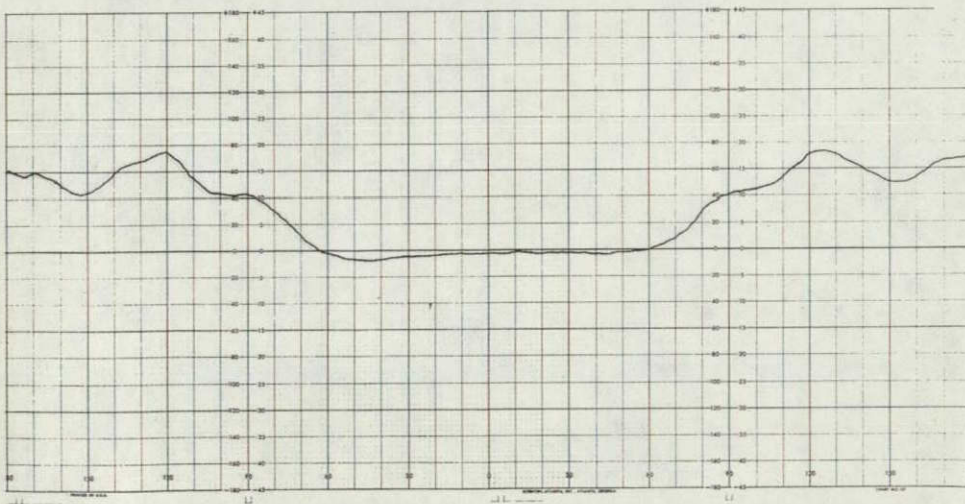
Fig. (5-8c)--Measured far field phase pattern of the 12 GHz multi-
mode waveguide feed.

- 122 -
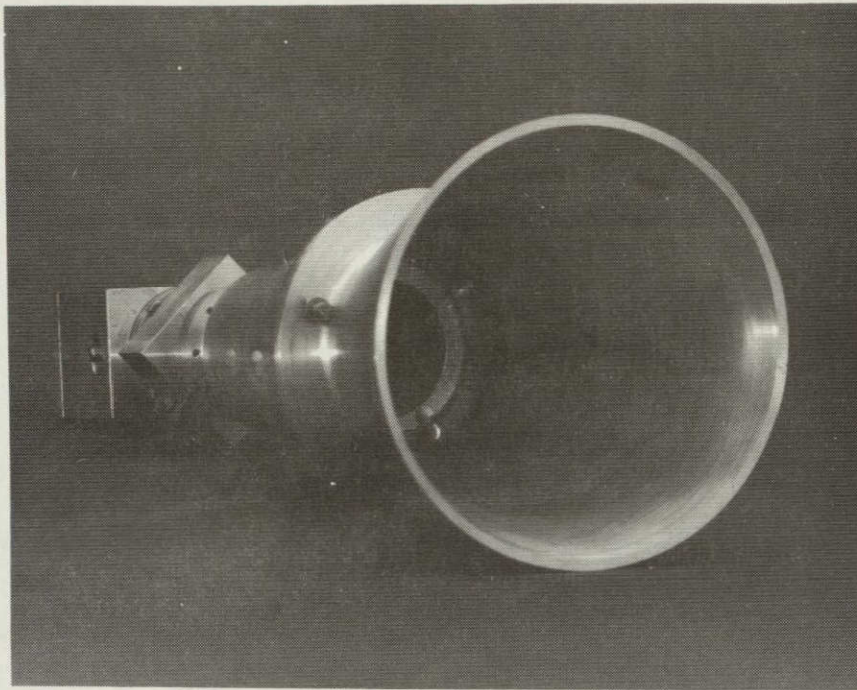
Fig. (5-9a)--Experimental model of the 12 GHz multimode conical horn.
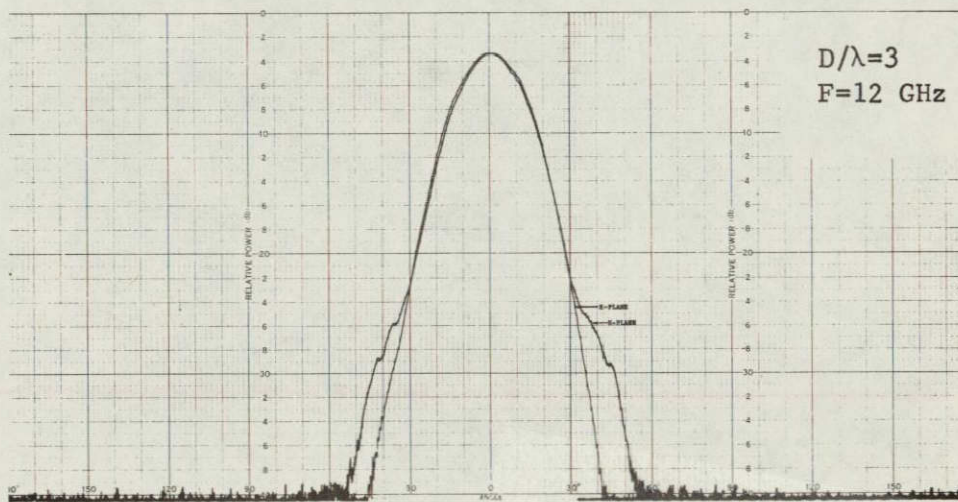
D/λ=3
F=12 GHz

Fig. (5-9b)--E- and H-plane pattern of the 12 GHz multimode conical horn.

in a Cassegrain system. Figure (5-8b) shows the measured E- and H-planes patterns and Fig. (5-8c) shows the far field phase measurement of the guide type horn. As is seen, the radiation pattern of this horn has good circular symmetry and a constant phase extending from -60° to $+60^{\circ}$. The cross polarization component is also small--about 28 dB down from the peak of the principal pattern. The measured E- and H-plane patterns of the horn feed, shown in Fig. (5-9b), are found to be almost identical to -30° off axis. Figure (5-9c) is the axial ratio measurement of this horn. As shown, an axial ratio of less than 1 dB to $\pm 25^{\circ}$ off axis is achieved and a low cross polarization level can be expected.
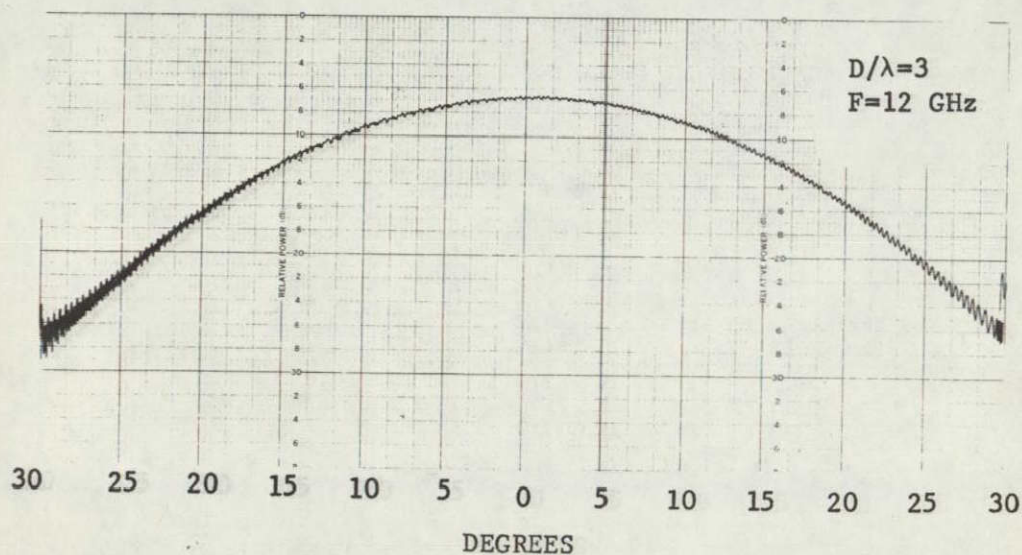
Fig. (5-9c)--Measured axial ratio of the 12 GHz multimode conical horn.

5.3 CIRCULAR WAVEGUIDE POLARIZER

A well-known method of obtaining circular polarization is to produce a 90 degree phase difference between two orthogonal linearly polarized waves of equal amplitude. A circular waveguide periodically loaded with pins may be used as a polarizer. If an incident linearly polarized wave is inclined 45 degrees (Fig. (5-10)) with respect to the pin axis, its
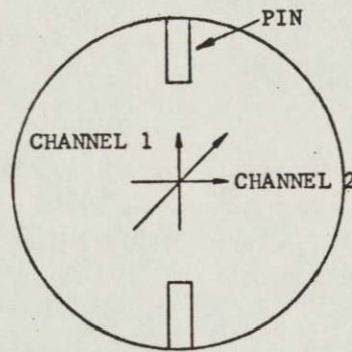
Fig. (5-10)--Orthogonal components of wave in a circular waveguide pin-polarizer.

component parallel to that axis will be advanced in phase (designated here as channel 1) and the orthogonal component (channel 2) will be unaffected. The polarizer loading is so adjusted that the differential phase shift is equal to 90 degrees, thus resulting in circularly polarized wave.

A symmetric pin is used in the polarizer because it reduces the number of higher order modes set up, thus reducing coupling between pins and making the depth of insertion less critical. The inductive type of susceptor is not suitable for use in the 12 GHz band because extremely tiny post is required.

5.3.1 Parameters of a Polarizer

The performance of a polarizer is characterized by the following parameters:

(1) Axial ratio

Axial ratio is defined as the ratio of minor to major axis of the polarization ellipse. Axial ratio is optimized by selecting loading iris or post dimensions so that the differential phase shift is close to 90° across the frequency band.

(2) Cross coupling

Cross coupling is defind as the ratio of the power of the reflected wave in the plane perpendicular to the plane of the incident wave to power of the incident wave. If the cross coupling is high, then the reflected wave in the plane perpendicular to the plane of the incident wave will generate opposite sense of CP wave and therefore the axial ratio of the desired sense of CP wave will be severely degraded. The cross coupling is minimized by minimizing reflection coefficients in both channel 1 and 2.

(3) Input VSWR

Input VSWR is a measure of reflection looking into the input port.

5.3.2 General Analysis

The axial ratio in dB is given by the following equation[53]

$$A.R. \; = \; 20 \, \log \, \tan(1/2 \, \sin^{-1} \, (\sin 2\gamma \, \sin \phi)) \qquad (5.20)$$

where

γ is the ratio of magnitudes of transmission coefficient in channel 1 to transmission coefficient in channel 2

ϕ is differential phase shift between waves in channel 1 and channel 2

In most polarizers, losses are sufficiently small so that (5.20) reduces to

$$A.R. = 20 \log \left(\tan \frac{\phi}{2} \right) \tag{5.21}$$

VSWR of the polarizer can be computed from the reflection coefficient of the two channels,

$$VSWR = \frac{1 + |\rho|}{1 - |\rho|} \tag{5.22}$$

$$\rho = ((\rho_{1,r} + \rho_{2,r})^2 + (\rho_{1,im} + \rho_{2,im})^2)^{1/2}/2 \tag{5.23}$$

where

ρ - polarizer reflection coefficient

$\rho_{1,r}$, $\rho_{1,im}$ - real and imaginary components of channel 1 reflection coefficient.

$\rho_{2,r}$, $\rho_{2,im}$ - real and imaginary components of channel 2 reflection coefficient.

The cross coupling in dB is also computed from the reflection coefficients of channel 1 and channel 2 as follows:

$$c_x = 20 \log \frac{(\rho_{1,r} - \rho_{2,r})^2 + (\rho_{1,im} - \rho_{2,im})^2}{2} \tag{5.24}$$

where c_x is the cross coupling in dB.

To obtain ρ_1 and ρ_2, we use the generalized network of one of the two channels of a polarizer as represented in Fig. (5-11, which
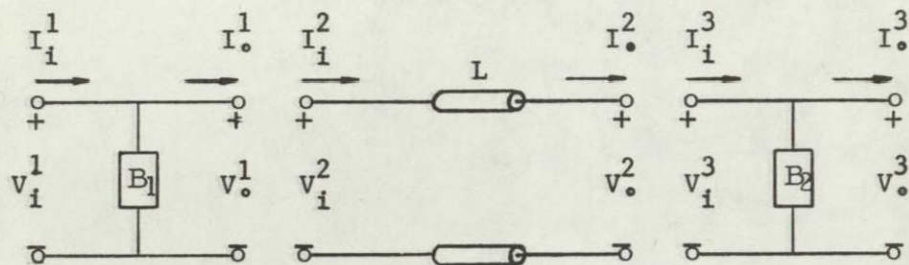
Fig. (5-11)--Generalized network of a polarizer.

consists of susceptance and line length in cascade. The overall transmission matrix is the product of the matrix corresponding to each shunt element and line length.[54,55]

$$\begin{bmatrix} v_i^1 \\ I_i^1 \end{bmatrix} = \begin{bmatrix} A \end{bmatrix}_{total} \begin{bmatrix} v_0^n \\ I_0^n \end{bmatrix} \quad \text{where} \quad \begin{bmatrix} A \end{bmatrix}_{total} = \begin{bmatrix} A_1 \end{bmatrix} \begin{bmatrix} A_2 \end{bmatrix} \cdots \begin{bmatrix} A_n \end{bmatrix}$$

$$(5.25)$$

and

$$\begin{bmatrix} A_n \end{bmatrix} = \begin{bmatrix} \cos\beta\ell & jZ_0\sin\beta\ell \\ jY_0\sin\beta\ell & \cos\beta\ell \end{bmatrix} \quad \begin{array}{l} \text{for uniform transmission} \\ \text{line of length } \ell \end{array}$$

$$\begin{bmatrix} A_n \end{bmatrix} = \begin{bmatrix} 1 & 0 \\ jB & 1 \end{bmatrix} \quad \begin{array}{l} \text{for shunt element of sus-} \\ \text{ceptance } jB \end{array}$$

Reflection coefficients for each channel are obtained using the following

relation:

$$\rho = \frac{B - C}{2A + B + C} \qquad (5.26)$$

Where ρ is the reflection coefficient of channel 1 or channel 2, and

A,B,C,D are the elements of $\begin{bmatrix} A \end{bmatrix}_{total matrix}$. Phase shift of each channel

is obtained from the following relation

$$\tan\theta = \frac{B + C}{A + D} \qquad (5.27)$$

The analysis of a general circular waveguide polarizer may be implemented

by the use of a digital computer.

5.3.3 Experimental Results

The equivalent susceptance, B/Y_o , of a symmetric capacitive post

as a function of depth of insertion into a circular waveguide has been

determined experimentally, using the nodal shift method.[56] The results

of these measurements are shown in Fig. (5-12).

A three-element polarizer design is shown in Fig. (5-13). A

preliminary design was made consisting of a polarizer loaded with equal

susceptances spaced 0.45 in. apart. The susceptances at both ends were

then tapered to improve the VSWR while the total differential phase shift

was still kept close to 90 degrees. Spacing is not critical and by it

can be reduced by repeated computer trials. The final dimensions are

shown in Fig. (5-14). The experimental results are shown in Fig. (5-15).
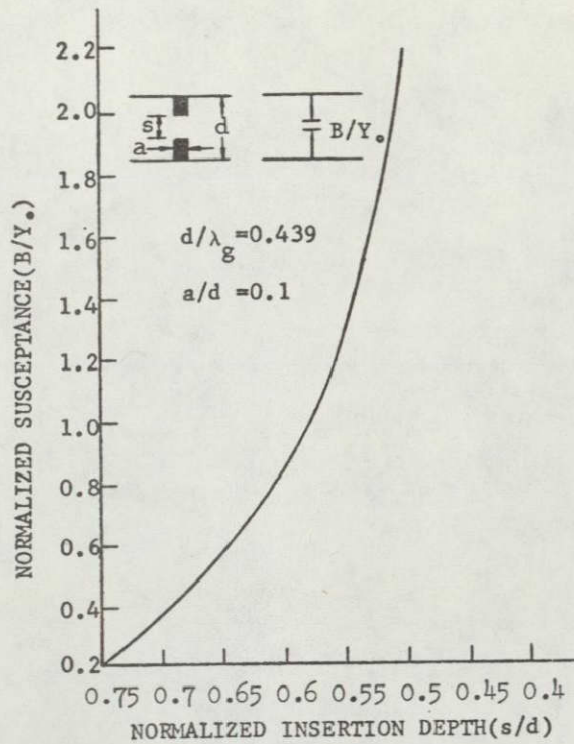
Fig. (5-12)--Measured susceptance of a capacitive post in a circular wave-
guide.
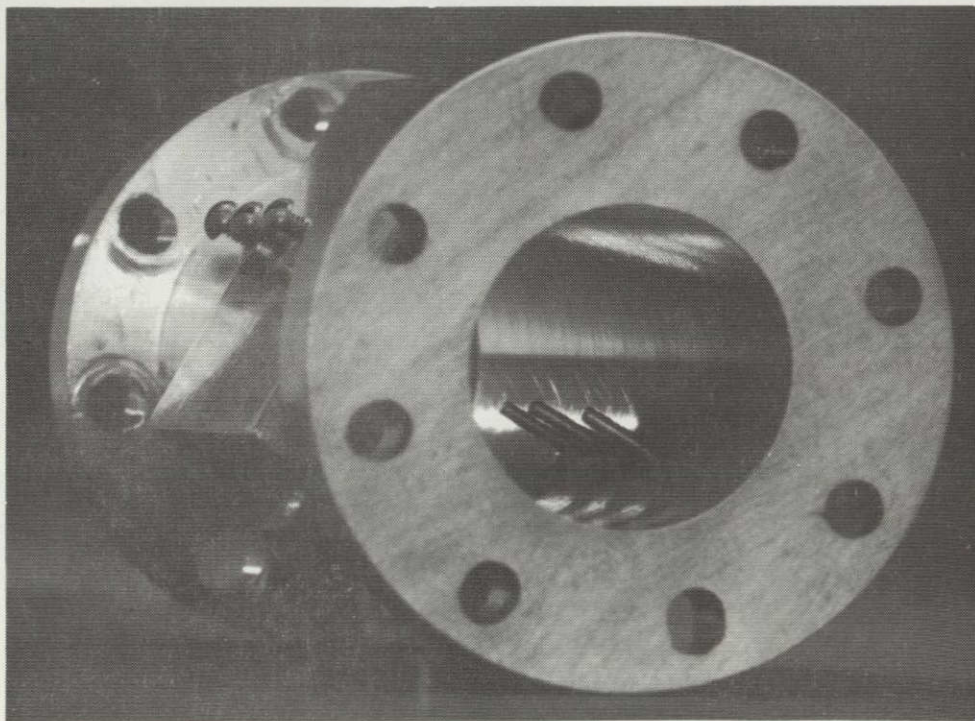
Fig. (5-13)--Experimental model of a 3-pin 12 GHz polarizer.
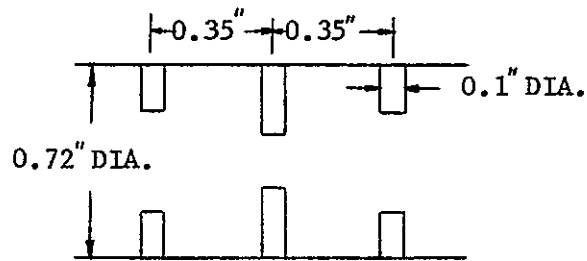
Fig. (5-14)--Dimensions of the experimental polarizer.
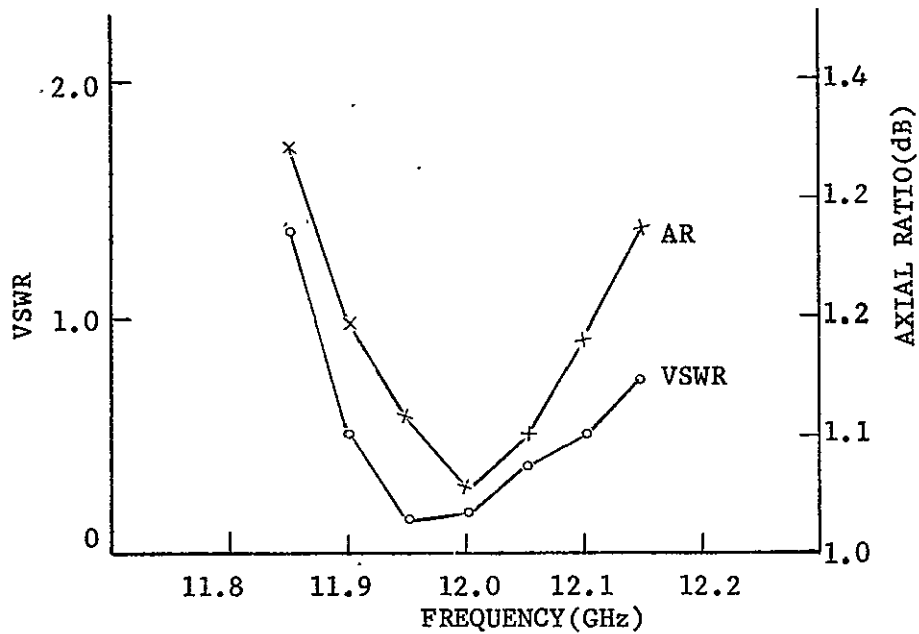
Fig. (5-15)--Measured VSWR and axial ratio of the experimental
polarizer.

5.4 Waveguide High-Pass Filter With Exponential-Raised-To-Cosine Taper

A piece of uniform waveguide is intrinsically a high-pass filter. In general, when a waveguide high-pass filter is used in a waveguide circuit, its dimensions are smaller than those of the adjacent components. The design of a waveguide high-pass filter therefore involves (1) the design of a transition between different sizes of waveguide to attain low passband reflection, and (2) the choice of proper lengths to obtain the required stop band isolation. To match two different sizes of waveguide a tapered transition has been shown[60] superior to quarter-wave or other resonant type transformers from the standpoint of bandwidth and reflection characteristics. The tapered transition has a characteristic impedance that varies continuously in a smooth fashion and can be considered as a nonuniform transmission line. The choice of the type of transition is the most important step in the design.

In studying certain analytic functional variations of characteristic impedance which satisfy the basic properties of a high-pass filter, Tang[57] found that the following function yields a reflection characteristic with the steepest rise near cutoff:

$$Z(X) = (Z_1 Z_2)^{1/2} e^{\ln(Z_1/Z_2)^{1/2} \cos^2(\frac{\pi x}{2L})} \qquad (5.28)$$

where

$Z(X)$ = Characteristic impedance of the filter

Z_1, Z_2 = Impedance at ends of the taper

L = Filter length

The discovery of this function is an important contribution to the design. Unfortunately, Tang's analysis did not show how to take into account the fact that in a waveguide the phase constant, $\beta(x)$, is also a function of the cross-sectional geometry and hence, also a function of position (x) along the taper. His conclusions are valid only for a TEM line, where the phase constant is a constant, and thus have to be modified for the case of a waveguide, especially when the operating frequency is close to the cutoff frequency of the waveguide. A technique is devised here to specify the profile of the high-pass filter whose characteristic impedance is experessed explicitly as a function of $\beta(x)$ and x . The methodology of design is also different between Tang's approach and the approach adopted here. It can be seen that Tang specified the character-istic impedance function of the entire filter at one time while we utilize a separate matched taper transition, followed by a length of uniform waveguide which can be properly adjusted for any desired isolation in the stop band. We will analyze both the reflection characteristics and the transmission characteristics of the composite structure. The manufacturing tolerance can also be investigated using our analysis technique.

5.4.1 Specification Of The Profile Of A Waveguide Taper By The Use Of
       a Numberical Technique

The impedance and reflection coefficient of a nonuniform waveguide is derived in Appendix B. From Eq. (B-15), Appendix B we know that a rigorous exact mathematical solution is possible only when the character-istic impedance of the line, $Z_c(x)$, is specified. For convenience,

Eq. (B-15) is rewritten as follows:

$$\Gamma(0) = \frac{1}{2} \int_0^{\theta_0} e^{-j2\theta} \frac{d(\ln Z_c)}{d\theta} d\theta$$

where

$$\Gamma(0) = \text{input reflection coefficient}$$

$$\theta = \int_0^X \beta(x) dX$$

$$\theta_0 = \int_0^L \beta(x) dX$$

As indicated, Z_c must be specified as a function of θ for the wave-guide taper. Since this may be rather difficult Z_c is usually expressed as a function of x only as an approximation. However, the operating frequency is close to the cutoff frequency of the waveguide, this approximation is no longer valid. Although Tang specified $Z_c(x)$ of the whole filter at one time and this approach is to design the transition section first. The form of his result still can be used. The following characteristic impedance function, which takes into account the fact that the phase constant varies along the taper, is suggested for the tapered transition.

$$Z_c(\theta(x)) = (Z_1 Z_2)^{1/2} e^{\ln(Z_1/Z_2)^{1/2} \cos \frac{\pi\theta}{\beta s}} \qquad (5.29a)$$

where

$$\theta(X) = \int_0^X \beta(X)dX$$

$$\bar{\beta} = \frac{1}{s} \int_0^s \beta(X)dX$$

S = Length of the taper

Z_1, Z_2 = End impedance of the transition

Note that, if $\beta(X)$ is a constant, (5.29a) becomes

$$Z_c(X) = (Z_1 Z_2)^{1/2} e^{\ln(Z_1/Z_2)\cos \pi X/s} \qquad (5.29b)$$

which is the characteristic impedance variation along half the filter as

Tang suggested. It is worth noting that $Z_c(\theta(X))$ in (5.29a) satisfies

the following boundary conditions.

(A) $Z_c(\theta(0)) = Z_1$

(B) $Z_c(\theta(s)) = Z_2$

(C) $\left. \dfrac{dZ_c(\theta(X))}{dX} \right|_{X=0} = \left. \dfrac{dZ_c(\theta(X))}{dX} \right|_{X=s} = 0$

The next question is how to specify the profile of the taper from

Eq. (5.29a). Specifically, how can X be determined for a given

$Z_c(\theta(X))$? A numerical technique will be employed here to deal with the

problem. From Eq. (5-29), the following result is obtained:

$$\frac{\theta(X)}{\bar{\beta}} = \frac{s}{\pi} \cos^{-1} \left(\frac{1}{\ln(Z_1/Z_2)^{1/2}} \ln \frac{Z_c(\theta(X))}{(Z_1 Z_2)^{1/2}} \right) \qquad (5.30)$$

For convenience it is rewritten as

$$\frac{\theta(X)}{\bar{\beta}} = \frac{s}{\pi} \cos^{-1}\left(\frac{1}{-\frac{1}{2}\ln\left(\frac{z_2}{z_1}\right)}\left(\ln\frac{z_c(\theta(X))}{z_1} - \frac{1}{2}\ln\frac{z_2}{z_1}\right)\right)$$

(5.31)

Referring to Fig. (5-16), we see that

$$z_1 \leq z_c(\theta(X)) \leq z_2$$

(5.32)

It follows that

$$0 \leq \ln\frac{z_c(\theta(X))}{z_1} \leq \ln\frac{z_2}{z_1}$$

(5.33)

Now we define the parameter

$$D = \frac{\ln\frac{z_2}{z_1}}{N}, \text{ where N is an integer}$$

(5.34)

Then we partition the space $\theta(X)$ into N section $\theta(X_1)$, $\theta(X_2)$,...$\theta(X_n)$ that $\ln\frac{z_c(\theta(X))}{z_1}$ has equal increments. That is

$$\ln\frac{z_c(\theta(X_i))}{z_1} = iD \text{ where } i = 1, 2, \dots N$$

(5.35)

X_i is the position where (5.35) is satisfied.

In terms of i and D, (5.31) becomes

$$\frac{\theta(X_i)}{\beta} = \frac{s}{\pi} \cos^{-1} \left(\frac{1}{-\frac{1}{2} ND} \left(iD - \frac{1}{2} ND \right) \right)$$

$$\frac{\theta(X_i)}{\beta} = \frac{s}{\pi} \cos^{-1} \left(1 - \frac{2i}{N} \right) \tag{5.36}$$

where

$$\theta(X_i) = \int_0^{X_i} \beta(x) dX$$

Thus, $\theta(x_i)/\bar{\beta}$ can be calculated for a given i, corresponding to value of $Z_c(\theta(X))$ such that

$$\ell n \frac{Z_c(\theta(X))}{Z_1} = i \frac{\ell n \frac{Z_2}{Z_1}}{N} \tag{5.37}$$

Our next step is to find X_i and ΔX_i after $\theta(X_i)/\bar{\beta}$ is obtained from (5.36). For convenience we define

$$\bar{\theta}_i = \frac{\theta(X_i)}{\bar{\beta}} \quad , \ i = 0, 1, 2, \ldots N \tag{5.38}$$

Note that $\bar{\theta}_0 = 0$. It follows directly from the definition

$$\bar{\theta}_1 = \frac{1}{\bar{\beta}} \int_0^{X_1} \beta(X) dX \approx \frac{1}{\bar{\beta}} \beta(X_1) \Delta X_1$$

$$\bar{\theta}_2 = \frac{1}{\bar{\beta}} \int_0^{X_2} \beta(X) dX = \frac{1}{\bar{\beta}} \int_0^{X_1} \beta(X) dX + \frac{1}{\bar{\beta}} \int_{X_1}^{X_2} \beta(X) dX$$

$$\approx \bar{\theta}_1 + \frac{1}{\bar{\beta}} \beta(X_2) \Delta X_2 \tag{5.39}$$

$$\vdots$$

$$\bar{\theta}_i \approx \bar{\theta}_{i-1} + \frac{1}{\bar{\beta}} \beta(X_i) \Delta X_i$$

where

$$\Delta X_i = X_i - X_{i-1} ,$$

The above approximations are a direct result of assuming N is very large so that $\beta(x)$ is constant in each incremental interval of X_i, ΔX_i. We let

$$\Delta \bar{\theta}_i = \bar{\theta}_i - \bar{\theta}_{i-1} , \ i - 1, 2, \dots N \qquad (5.40)$$

It is a simple task to show that

$$\Delta \bar{\theta}_i \approx \frac{1}{\bar{\beta}} \beta(X_1) \Delta X_1$$

$$\Delta \bar{\theta}_2 \approx \frac{1}{\bar{\beta}} \beta(X_2) \Delta X_2$$

$$\vdots$$

$$\Delta \bar{\theta}_i \approx \frac{1}{\bar{\beta}} \beta(X_i) \Delta X_i \qquad (5.41)$$

which may be written as

$$\frac{\Delta \bar{\theta}_1}{\beta(X_1)} \approx \frac{1}{\bar{\beta}} \Delta X_1$$

$$\frac{\Delta \bar{\theta}_2}{\beta(X_2)} \approx \frac{1}{\bar{\beta}} \Delta X_2$$

$$\vdots \qquad\qquad (5.42)$$

$$\frac{\Delta \bar{\theta}_i}{\beta(X_i)} \approx \frac{1}{\bar{\beta}} \Delta X_i$$

Summing both sides, of Eq. (5.42) the following result is obtained

$$\sum_{i=1}^{N} \frac{\Delta\bar{\theta}_N}{\beta(X_i)} = \frac{1}{\bar{\beta}} \sum_{i=1}^{N} \Delta X_i = \frac{1}{\bar{\beta}} S \qquad (5.43)$$

$$\bar{\beta} = \frac{S}{\sum_{i=1}^{N} \frac{\Delta\theta_i}{\beta(X_i)}}$$

The taper length S can be assigned several trial values, $\Delta\theta_i$ can be

obtained from (5.38) and (5.40), and $\beta(X_i)$ can be calculated from

$Z_c(\theta(X_i))$. Thus ΔX_1, ΔX_2, ... ΔX_i can be calculated from Eq. (5.42).

Finally, X_i can be obtained from the relation

$$X_i = \sum_{0}^{i} \Delta X_i \ , \ i - 1, \ 2, \ ..., \ N$$

This procedure can be implemented with the aid of a digital computer.

Although we have only focused on the exponential-raised-to-cosine function,

the above analysis does not lose its generality and can be applied to

design tapers using other functions.
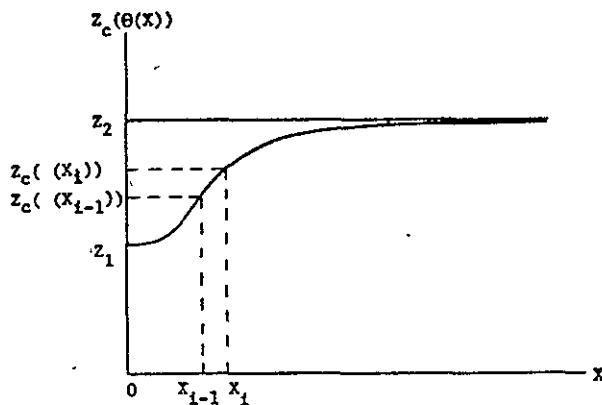
Fig. (5-16)--Typical plot of $Z_c(\theta(X)) = (Z_1 Z_2)^{1/2} \ e^{\ln\left(\frac{Z_1}{Z_2}\right)^{1/2}} \cos \frac{\pi\theta}{\bar{\beta}S}$.

In order to compare designs using Eqs. (5.29a) and (5.29b), the reflection characteristics of two high-pass filters are calculated as shown in Fig. (5-17). These filters consist of two tapered transitions in cascade. Curve A is the design using Eq. (5.29b), which considers the phase constant invariant along the filter. The group of curves labelled B represents the design using Eq. (5.29a). The performance of the design presented in this paper is obviously far superior to that suggested by Tang. The partition number (N) in Eq. (5.34) also affects the performance of the filter, as can be seen from the various curves in Group B of Fig. (5-17), where comparisons have been made for N = 10, 20, 30 and 40. The larger the value of N, the closer the stepped profile will approach the original smooth profile of the filter. In this example the reflection characteristic shows little change for N $\geq$ 30.

5.4.2 Experimental Results

A waveguide high-pass filter of circular cross-section was designed and fabricated for the 12 GHz low-cost Educational Television ground station (see Fig. (5-18)). This filter is designed to have 20 dB isolation at 11.82 GHz and a VSWR less than 1.20 over the frequency band from 11.94 GHz to 12.06 GHz, a separation of 1% between pass band and stop band. The exponential-raised-to-cosine taper has a length of 2.75 inches with its profile specified in the table of Figure (5-19). The detailed dimensions of the whole filter are shown in Fig. 5-19. It can be seen that the tapered transition first transforms a guide of 0.72 inch in diameter to a guide of 0.583 inch in diameter which has a cutoff frequency at 11.866 GHz. The 0.583 inch guide is then extended 0.25 inch
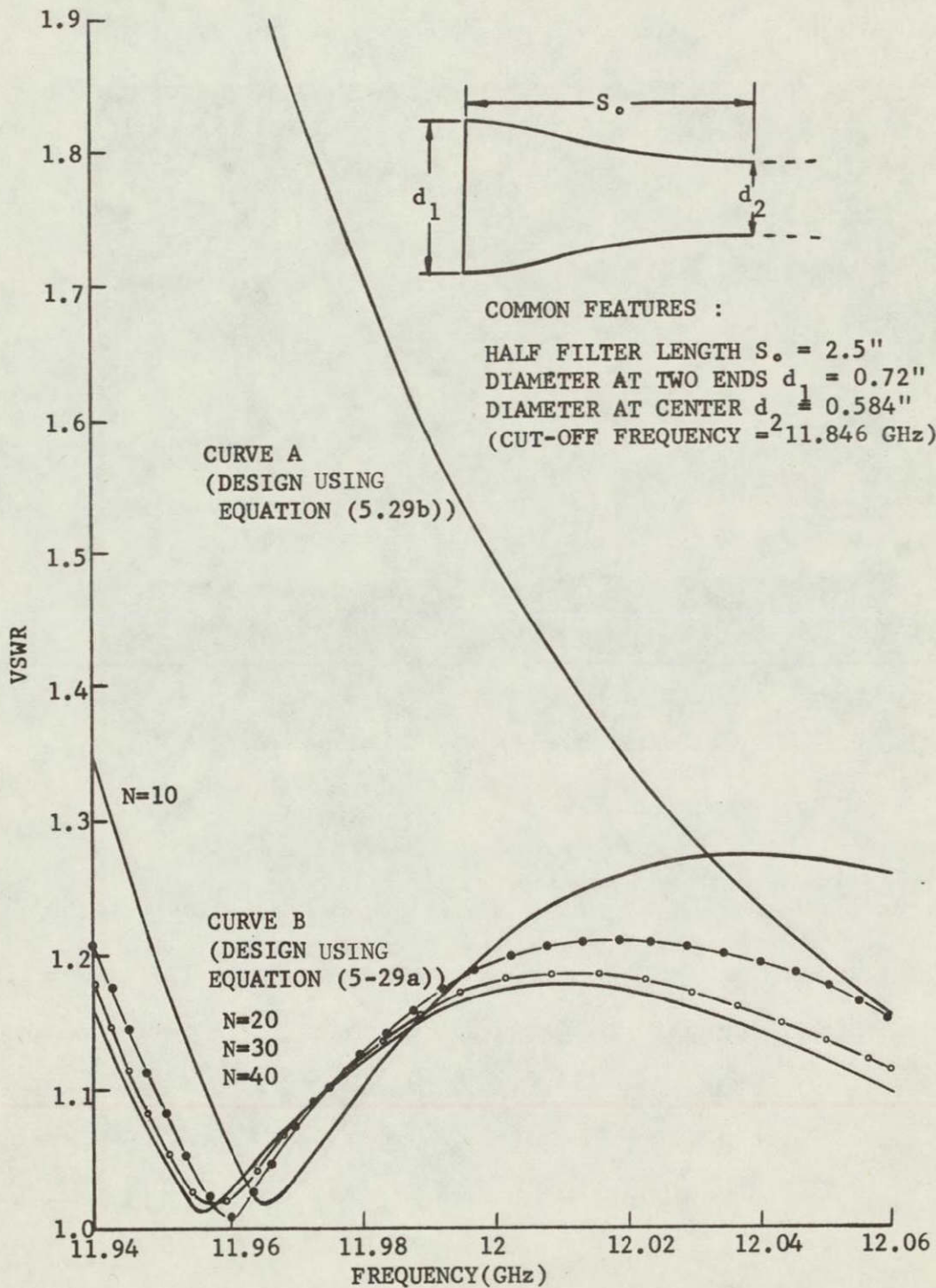
Fig. (5-17)--Comparison of VSWR of different filter designs.

to add more isolation at the stop band. It is then followed by an
identical tapered transition which transforms the 0.583 inch guide back
to the 0.72 inch guide. The whole filter is a symmetric structure.
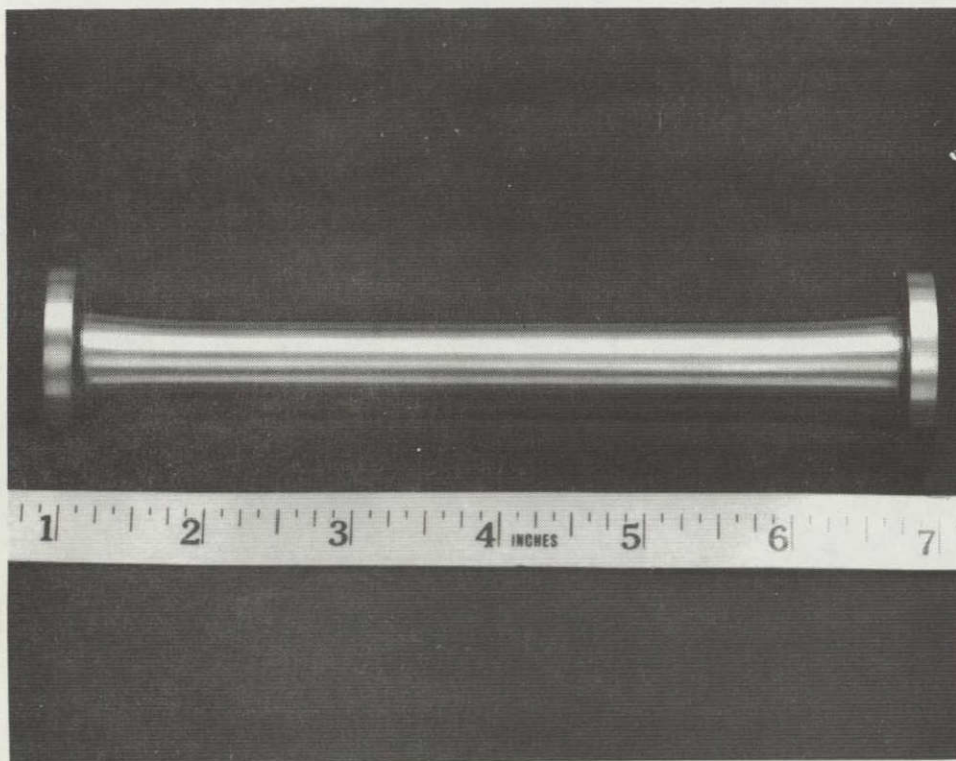
Fig. (5-18)--Experimental model of 12 GHz high-pass filter.

The design is analyzed with a computer program which considers the
filter as a stepped waveguide structure as shown in Fig. (B-1) and the
scattering matrix (S-matrix) is then used to calculate the transmission
loss and the reflection characteristics. The calculated and measured
results are compared in Figs. (5-20) and (5-21). It is worth noting
that a machining error of .002 inches in the cutoff guide section (center
section of the filter) has been made, which causes the measured curves
to shift toward lower frequency. As will be seen that except for this

X	Y
0.00000	0.36000
0.12520	0.35340
0.17980	0.34755
0.22370	0.34235
0.26250	0.33775
0.29850	0.33355
0.33260	0.32985
0.36560	0.32645
0.39780	0.32340
0.42970	0.32060
0.46140	0.31810
0.49320	0.31575
0.52520	0.31365
0.55750	0.31175
0.59030	0.31000
0.62380	0.30835
0.65790	0.30685
0.69290	0.30550
0.72890	0.30425
0.76590	0.30310
0.80420	0.30200
0.84380	0.30100
0.88500	0.30010
0.92780	0.29925
0.97250	0.29850
1.01920	0.29775
1.06830	0.29710
1.11990	0.29645
1.17450	0.29590
1.23230	0.29535
1.29400	0.29485
1.35990	0.29440
1.43100	0.29400
1.50820	0.29360
1.59270	0.29320
1.68650	0.29290
1.79240	0.29255
1.91520	0.29225
2.06390	0.29200
2.26200	0.29175
2.75000	0.29150
2.87500	0.29150

Symmetric With
Respect to X=2.875
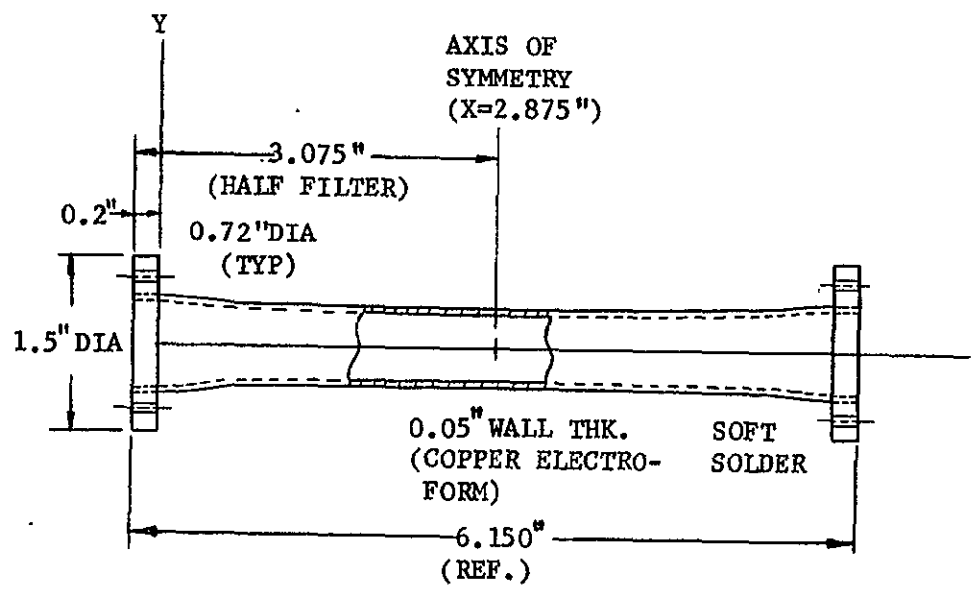
Fig. (5-19)--Dimensions of the experimental circular waveguide high-pass filter.
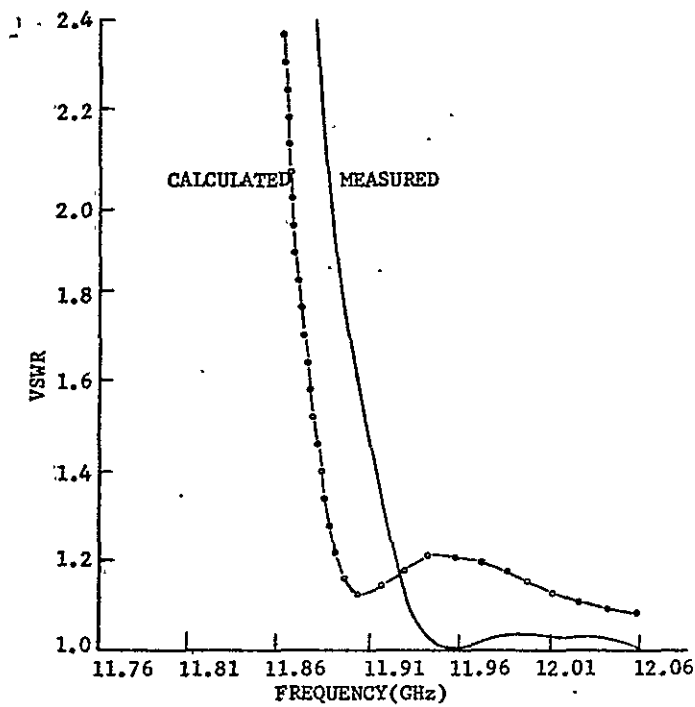
Fig. (5-20)--Calculated and measured VSWR of the 12 GHz filter.
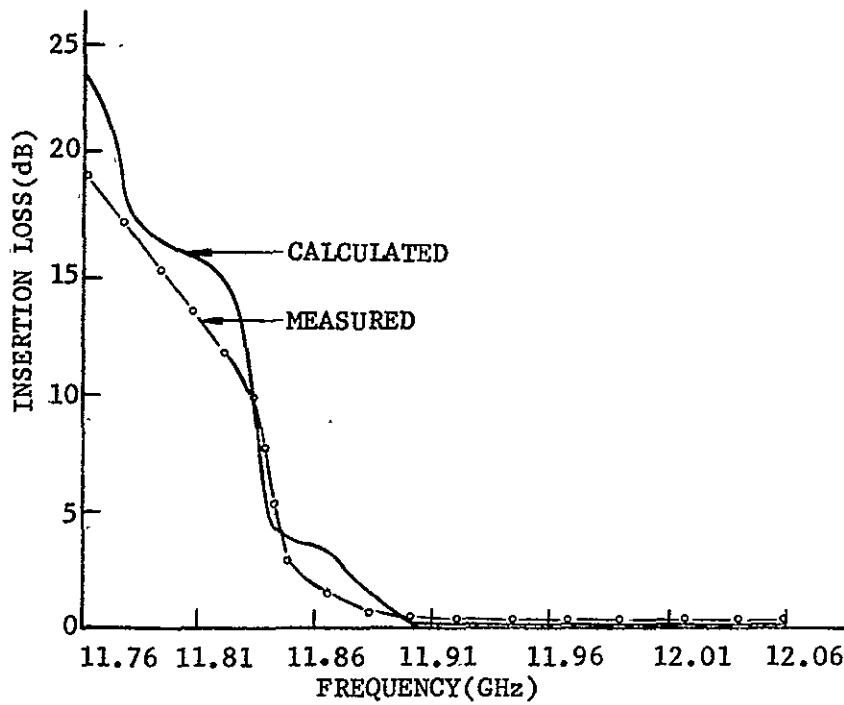
Fig. (5-21)--Calculated and measured insertion loss of the 12 GHz filter.

slight dimensional error the theory gives excellent prediction of the experimental characteristics of the high-pass filter.

5.5 12 GHz ANTENNA SYSTEM PERFORMANCE SUMMARY

To evalute the performance of an antenna system with the feed and microwave components designed in this chaper, a seven-foot prime focus receiving antenna with $F/D = 0.48$ is assumed. The assembled feed system is shown in Fig. (5-1a).

5.5.1 Frequency Range

The system is designed to be operated over the 11.90 GHz to 12.10 GHz band.

5.5.2 Efficiency

The efficiency factors discussed in Chapter 2 are calculated by a computer program using the measured pattern of the multimode waveguide feed. The results are tabulated in Table 5-1. The blockage loss is calculated based on the feed support structure proposed in Fig. (5-23). The rms surface randomness is assumed to be 0.04".
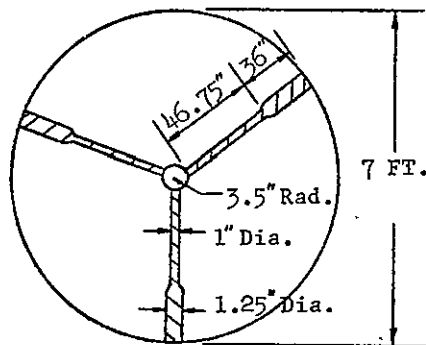
Fig. (5-22)--Proposed feed-support configuration for blockage calculation.

Table 5-1.

EFFICIENCY SUMMARY (12 GHz)

Spillover	0.964
Aperture	0.731
Phase	1.000
Cross Polarization	0.997
Blockage	0.916
Surface	0.997
Total	64%
RF Loss	1.92 dB

5.5.3 Feed System Insertion Loss and Gain Computation

Feed system losses consisting of the dissipative and the reflective portions are shown in Table 5-2.

Table 5-2.

FEED SYSTEM INSERTION LOSS

Item	Loss (dB)
Horn	0.05
Polarizer	0.10
High-Pass Filter	0.25
Waveguide-to-coax Adaptor	0.05
Total	0.45

The losses shown in Table 5-2 are representative of actual values measured. The combination of RF scattering and dissipation produce a gain value of 46.20 dB at 12 GHz as shown in Table 5-3.

Table 5-3

GAIN COMPUTATION

Ideal Gain (dB)	48.57
RF Loss	1.92
Feed Loss	0.45
Net Gain	46.20

5.5.4 Noise Temperature and G/Ts

The total noise from RF scattering is summarized in Table 5-4 for antenna elevation angles of 10 and 45 degrees.

Table 5-4

RF SCATTERING NOISE TEMPERATURE

Source	Noise Temperature $^\circ$K	
	10° elevation	45° elevation
Spillover	5.11	3.49
Cross Polarization	0.07	0.02
Blockage	7.56	10.58
Surface	0.48	0.15
Main Beam	20.56	6.70
Total	33.68°K	17.94°K

In addition to noise from the antenna aperture, the feed loss contribution is required to complete antenna system temperature, T_{AS}, calculation. The feed loss of this system is found to be 0.45 dB. From Eq. (2.15)

$$T_{AS} = \frac{T_A}{L} + \left(\frac{L-1}{L}\right)T_0 \quad .$$

we found

$$T_{AS} = 59.08^\circ K \text{ at } 10^\circ \text{ elevation}$$
$$= 44.85^\circ K \text{ at } 45^\circ \text{ elevation}$$

The system noise temperature, T_s, is calculated according to

$$T_S = T_{AS} + T_R$$

For a receiver of 7 dB noise figure, $T_R = 1170^\circ K$.
Thus,

$$T_S = 1229.08^\circ K \text{ at } 10^\circ \text{ elevation}$$
$$= 1214.85^\circ K \text{ at } 45^\circ \text{ elevation}$$

The G/T_s is found to be 15.70 dB/K° for 10° elevation and 15.36 dB/K° for 45° elevation.

- 148 -

CHAPTER 6

COST ANALYSIS OF SATELLITE GROUND STATION

6.1 ECONOMIC PARAMETERS OF A SATELLITE COMMUNICATION GROUND STATION

The economic aspects of a small size (less than 20-foot diameter antenna)
ground station are governed by the sensitivity parameter-figure-of-merit
(or G/Ts) as defined in Chapter 2. The cost of an antenna increases
with increasing antenna diameter, and the cost of a receiver increases
with decreasing noise temperature. It is therefore possible to select
a certain combination of antenna size and receiver noise characteristics
to minimize the cost of a ground station while still meeting a particular
sensitivity requirement.

The cost of receivers operating at 2.6 GHz and 12 GHz has been studied
in Volume I and the results are summarized in Fig. (6-1), where receiver
cost versus noise figure (or type of pre-amplifier) is plotted, using pro-
duction quantity as a parameter. The noise figure investigated ranges from
2 dB to 10 dB. Actually the region comprising both low cost and good signal
quality is from a noise figure of 4 dB to 8 dB. The cost of an antenna is
determined primarily by the following factors:

A. Reflector manufacturing techniques .

B. Type of antenna feed.

C. Installation

D. Tracking requirements

E. Size

Cost savings resulting rom large quantity production is another major

factor under consideration.

---

*The term "receiver" as used throughout the report includes only the
amplification circuit and electronics of the converter but includes the
antenna and feed RF system.
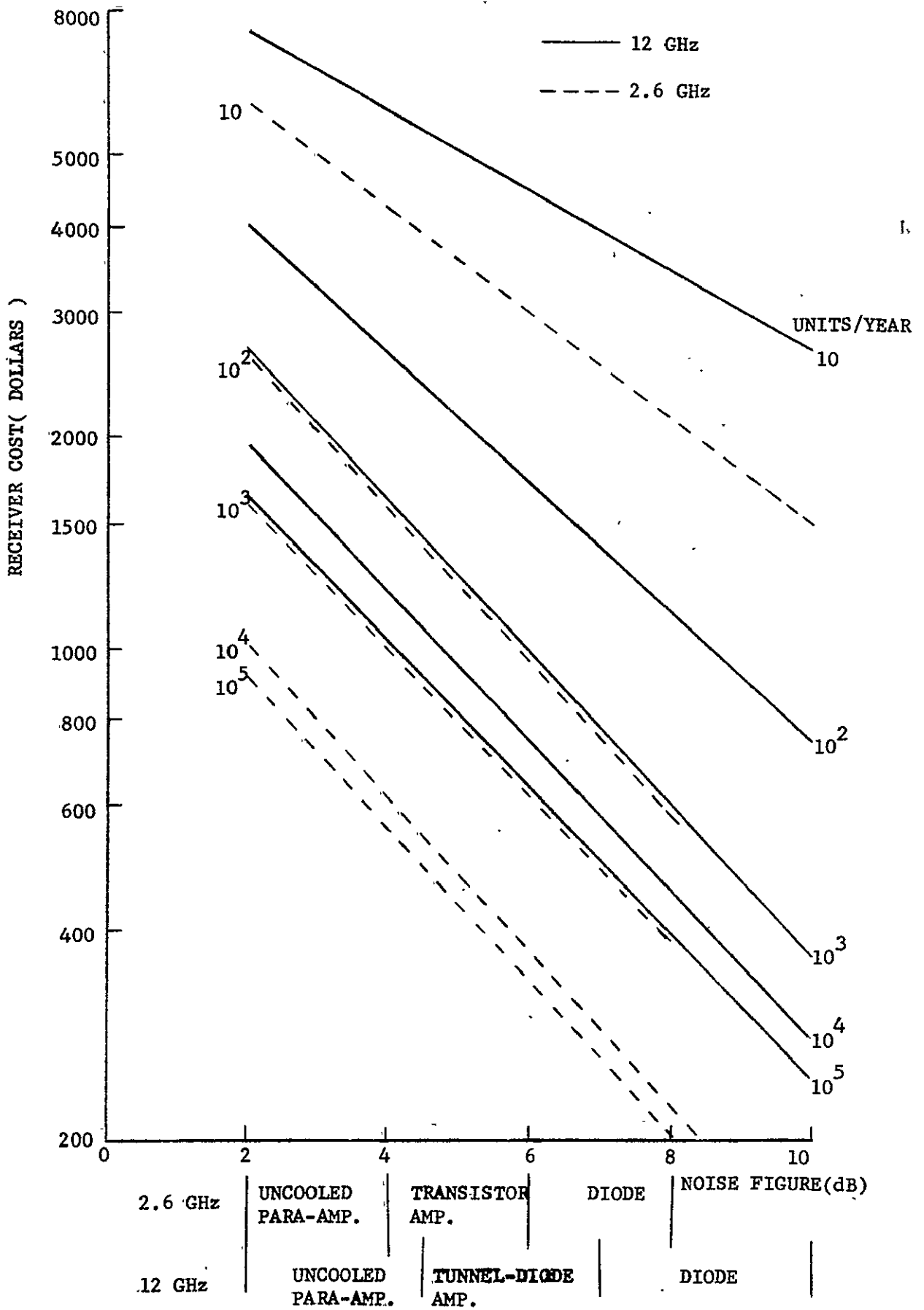
Fig. (6-1)--Receiver cost versus noise figure.

6.2 REFLECTOR COST

Reflector construction types can be categorized as follow:

A. Fiber-glass

B. Chicken wire

C. Flat segmented aluminum

D. Spun aluminum

E. Stamped aluminum

F. Zoned reflector

Some of these techniques have been well developed; and hence reliable estimates in cost can be made through quotes and discussion with manufacturers.. The total cost of a reflector depends not only on the type of construction but also on such important factors as transportation and assembly time. Furthermore, other factors such as gain reduction, surface uniformity, structure rigidity and damage resistance should also be taken into account in the process of making decisions. Comparisons among the above-mentioned techniques are summarized in Table 6-1.

A chicken wire type reflector does not have a strong mechanical structure or good surface uniformity. Further since it cannot be built at low cost it is ruled out for consideration in this study. A flat segmented aluminium reflector has been evaluated by Janky[3] and shown to be a potential candidate for use at 2.6 GHz. However, an inevitable gain reduction (approximately 2 dB for a seven-foot reflector), and a lack of cost advantage over spun aluminum or stamped aluminum for mass production makes this reflector unattractive at 12 GHz..

Table 6-1

COMPARISON OF REFLECTOR MANUFACTURING TECHNIQUES

Manufacturing Techniques	Advantages	Disadvantages
Fiber-Glass	.Uniform Surface .Light Weight	.Know-How Limited To Fabricate Small Reflector (15 FT.)
Chicken Wire	.Low Wind Resistance	.Non-Uniform Surface .Weak Structure .Expensive At 12 GHz
Flat Segmented Aluminum	.Low Cost At 2.6 GHz For Moderate Production Quantity .Easy Shipping	.Gain Reduction .Expensive At 12 GHz
Spun Aluminum	.Uniform Surface	.Expensive For Small Quantity Production
Stamped Aluminum	.Uniform Surface	.Expensive For Small Quantity Production
Zoned Reflector	.Low Cost For Moderate Quantity Production .Strong Mechanical Structure .Easy Mount	.Gain Reduction

Fiber-glass, spun-aluminum and stamped aluminum reflectors are commonly used in small terrestrial communication stations and all are good quality reflectors. Therefore, cost is the dominant factor in determining a choice between them in a low cost system. In general, for reflectors less than seven feet, fiber glass and spun aluminum have lower cost than that estimated for the stamped aluminum reflector, (Table 6-2). The selling price, which includes overhead cost and profit, is obtained by multiplying the factory cost by a factor of 2.5.[58]

Zoned reflectors reduce reflector cost compared to stamped aluminum techniques for low quantity product ion. As shown in Table 6-3 the tooling cost per unit reflector for a production quantity of 100 units is much lower than that of smoothly stamped aluminum. Because all the zones are designed to lie on the same plane, the zoned petals can be assembled easily on inexpensive straight metal mounting strips. The assembly cost is also reduced substantially. Mechanically, this reflector is strong and can be fabricated from thinner material. It can also be easily mounted on the wall of a building which results in installation cost reduction. No vendor has been willing to quote on the flat sheet zone reflector. Lack of experience is cited as a major reason. However, they do agree that as contour in the radial direction is straight line instead of a parabola, it would be easier and cheaper to build the straight contour using sheet metal than to build a parabolic contour fixture to hold parabolic shaped metal panels, as is conventionally used for reflectors of diameter greater than 15 feet.

Table 6-2

COST OF STAMPED ALUMINUM REFLECTOR (8 PANELS, 7-FOOT)

.Item	Production Quantity		
	10	10^2	10^3
tooling	$ 850.00	$ 85.00	$ 8.50
aluminum sheet	45.00	32.00	23.00
assembly parts	60.00	40.00	22.00
feed support	75.00	50.00	33.50
test	30.00	20.00	10.00
Total factory cost	1060.00	227.00	96.50
Selling price (x2.5)	2650.00	567.50	241.25

Table 6-3

COMPARISON OF STAMPED SEGMENT ALUMI-
NUM SMOOTH REFLECTOR AND ZONED REFLECTOR
(Each reflector consists of 8 panels,
and only tooling costs are compared)

Reflector	Production Quantity		
	10	10^2	10^3
smooth reflec-tor	$ 850.00	$ 85.00	$ 8.50
zoned reflec-tor	$ 590.00	$ 59.00	$ 5.90

6.3 INSTALLATION COST

To obtain an idea of how this factor contributes to the cost of
an antenna, a curve showing installation cost versus antenna diameter
is given in Fig. (6-2); this information is the result of a study
conducted by General Electric Co..[2] For a fixed size antenna, the
higher the frequency the narrower the beam. Therefore the antenna mount
strength specification is more severe for 12 GHz than for 2.6 GHz.
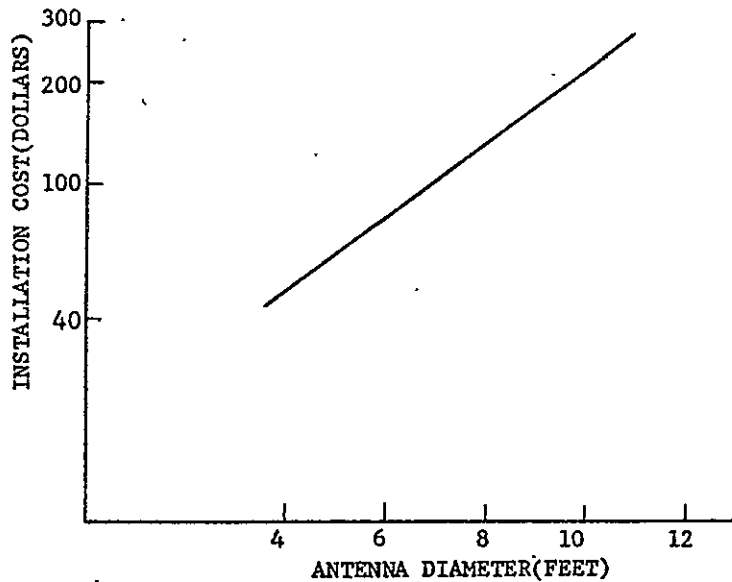
Fig. (6-2)--Small antenna installation cost.

6.4 COST OF ANTENNA FEED SYSTEM

In the proposed low cost Educational Television ground station only
circular polarization reception is required. Three potential configurations
of an antenna feed system which satisfy the requirement are presented

for cost estimation:

A. Waveguide system: consisting of a horn radiator, a waveguide polarizer and a high pass filter (or Band Pass Filter).

B. Helicon system: consisting of a helicone and a strip line bandpass filter

C. Archimedean system: consisting of an Archimedean spiral radiator and a strip line bandpass filter.

Table 6-4 to Table 6-6 show the cost of these alternatives.

Note that all three components of a waveguide system are diecast as an integrated unit.

6.5 COST OF TRACKING SYSTEM

It has been found that an earth station with automatic tracking capability costs twice as much as one without tracking. This finding is not surprising, because a conventional monopulse tracking system, with either conical scan or multimode tracking, requires a tracking receiver, a complicated tracking feed network, and a steering mechanism. A mass-producible auto-track system-the so called step-track system-was proposed in Chapter 2. Table 6-7 shows the estimated cost of such a system, for which a block diagram is shown in Fig. (6-3). It is assumed that the feed (instead of the reflector) is instructed to move within five beamwidths of the boresight axis to seek maximum signal strength. A small stepper motor is sufficient, because only the feed is moved.

Table 6-4

COST OF WAVEGUIDE SYSTEM

Item	Quantity of parts	Production Quantity (Units/Year)				
		10	10^2	10^3	10^4	10^5
die cast aluminum	2	380	40	6.6	3.4	3.4
testing		43	4.5.	0.8	0.4	0.3
Total Factory Cost		$423	$44.5	$7.4	$3.8	$3.3

Table 6-5

COST OF HELICONE SYSTEM

Item	Quantity of parts	Production Quantity (Units/Year)				
		10	10^2	10^3	10^4	10^5
cone(die cast alumi.)	2	50	12	1.0	0.7	0.6
helix	1	20	3	0.5	0.4	0.4
strip line bandpass filter	1	100	75	50	37.5	35
testing		50	10	5	5	5
Total Factory Cost		$220	$100	$56.5	43.6	41.0

Table 6-6

COST OF ARCHIMEDEAN SYSTEM

Item	Quantity of parts	Production Quantity (Units/Year)				
		10	10^2	10^3	10^4	10^5
cavity (sheet metal)	1	5	1.5	1	1	1
duroid	2"x2"	5.2	1.5	1	0.95	0.9
mask	1	5	0.5	0	0	0
photoetching	1	5.7	2	1.5	1.1	0.9
Robert's balun	1	5	2.5	1.5	1	1
bandpass filter	1	100	75	50	37.5	35
testing		55	12	7	7	7
Total Factory Cost		$180.9	$84.0	$62.0	$48.55	$45.8

Fig. (6-3)--Proposed Block diagram of a step-track system.

Table 6-7

COST OF A STEP-TRACK SYSTEM

Item	Quantity	Production Quantity		
		10	10^2	10^3
operational amplifier (LM 208)	1	$ 30.00	24.00	20.00
AGC meter	1	5.00	4.00	2.50
operational amplifier (LM 308)	1	15.00	12.00	10.00
capacitor	1	2.64	2.10	1.80
resistors	10	2.10	1.60	1.40
dump	1	1.80	1.40	1.10
voltage comparator (LM311)	3	14.55	11.70	9.75
flip flop (SN7474N)	3	6.60	6.0	3.30
one shot (SN74121)	2	8.68	6.92	5.90
NAND gate (SN7400N)	14	13.72	6.58	4.20
hex inverter (SN7404N)	11	12.98	6.27	6.00
D/A converter	1	50.00	31.00	20.00
up/down synchronous binary counter	1	12.70	9.00	7.50
stepper motor	2	160.00	100.00	60.00
miscellaneous(sockets , pins, test point, wire, etc.)		5.00	3.00	1.50
Total		340.77	225.57	154.95
assembly and test		160.00	100.00	50.00
Total Factory Cost		500.77	325.57	204.95
Selling Price (x2.5)		1251.93	814.93	512.38

6.6 ANTENNA COST

The cost of an antenna including reflector, feed and installation, is summarized in Fig. (6-4), where antenna cost versus diameter is shown, using production quantity as a parameter. This data came from rough estimates by manufacturers. Manufacturing techniques are specified in the figure. It is worth noting that the manufacturing technique associated with different sizes of antennas does not necessarily represent a unique technique. For example, for high quantity production and small size antennas both fiberglass and stamped aluminum techniques yield low cost reflectors.

The additional cost of a step-track system is also shown in the figure; this cost is essentially independent of the antenna diameter because only the feed needs to be moved.

6.7 COST OPTIMIZATION OF A GROUND STATION

This section summarizes the cost optimization result as cited in reference [8]. As noted in section 6-1 the cost of an antenna increases with increasing diameter (or gain), and the cost of a receiver increases with decreasing noise temperature. By the use of Figs. (6-1) and (6-4) the cost of a receiving station can be optimized for a given G/Ts. The receiver noise temperature T_R can be found as follows:

$$T_R = T_s - 50^{\circ}K \quad \text{at 2.6 GHz}$$
$$= T_s - 100^{\circ}K \quad \text{at 12 GHz}$$

where an antenna noise temperature of $50^{\circ}K$ at 2.6 GHz and $100^{\circ}K$ at 12 GHz is assumed. By varying the gain and receiver noise temperature (or noise
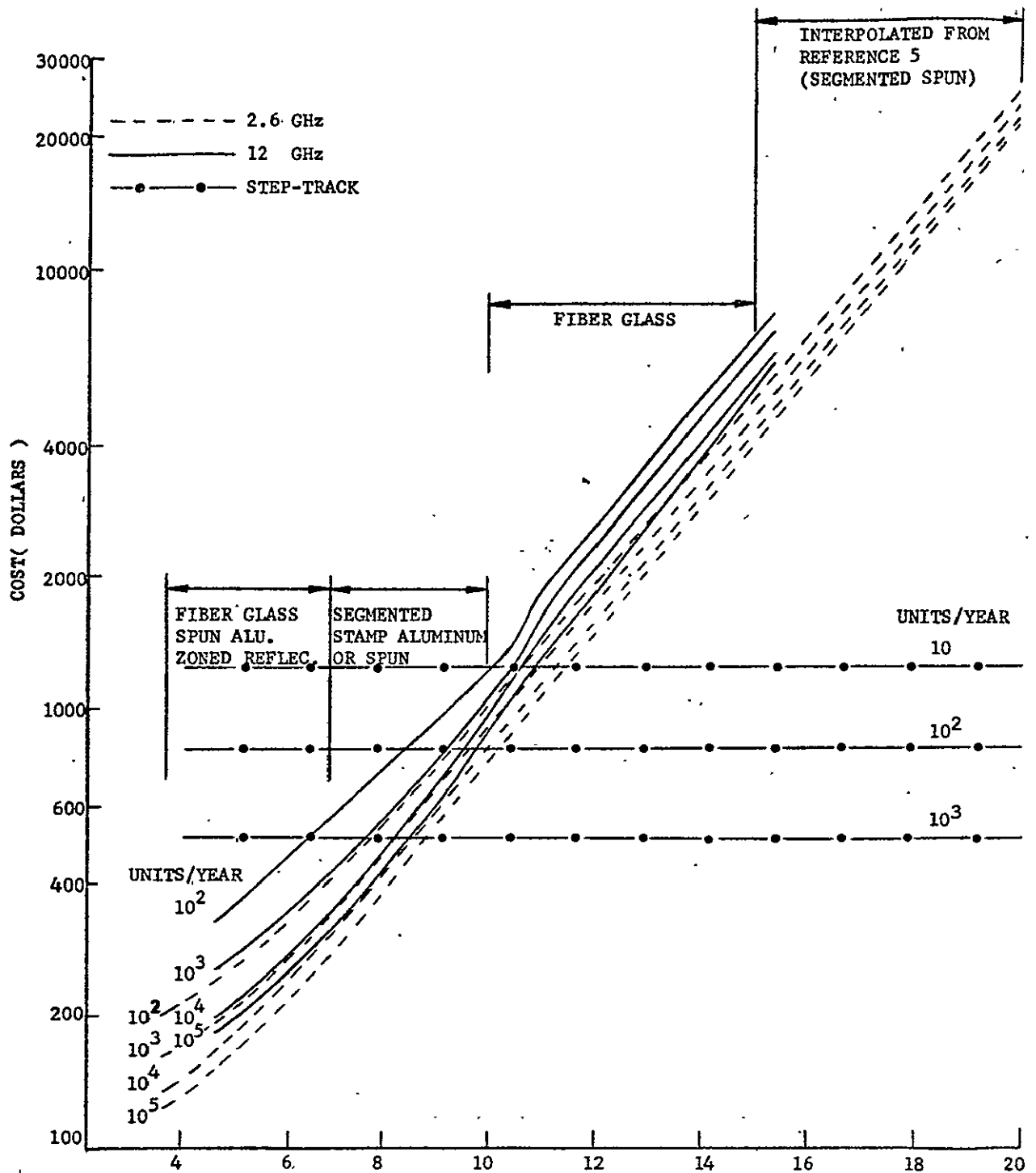
Fig. (6-4)--Small antenna cost.

figure) but keeping the ratio G/Ts constant we obtain a number of com-

binations of antenna diameter and receiver noise figures. We then evaluate

the cost of each combination and select the combination which yields the

minimum cost. The results are shown in Fig. (6-5) for both 2.6 GHz and

12 GHz. As shown, these curves have very steep slope which implies that

the use of low noise receiver but small antenna is more economical than

the use of higher noise receiver but larger antenna, particularly with

high production quantity. Figure (6-6) shows the cost of the most econo-

mical G/Ts.
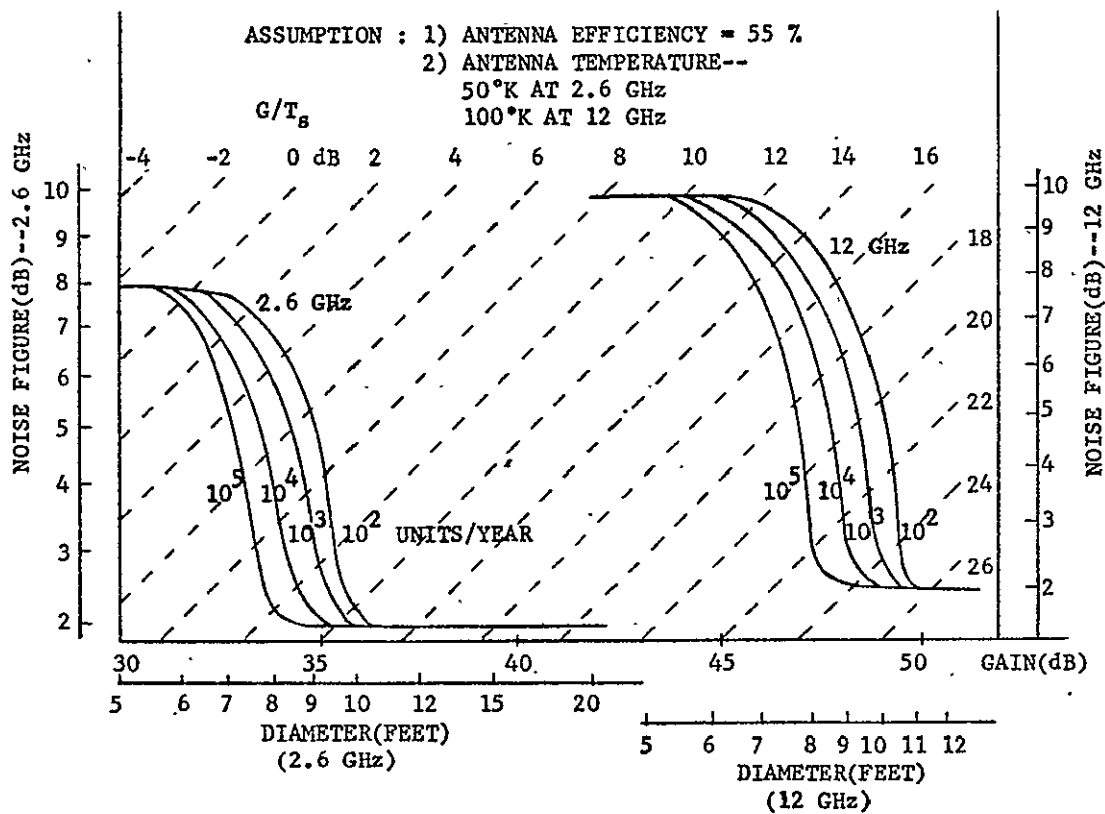
Fig. (6-5)--Optimum ground-station -- for 2.6 GHz and 12 GHz band.
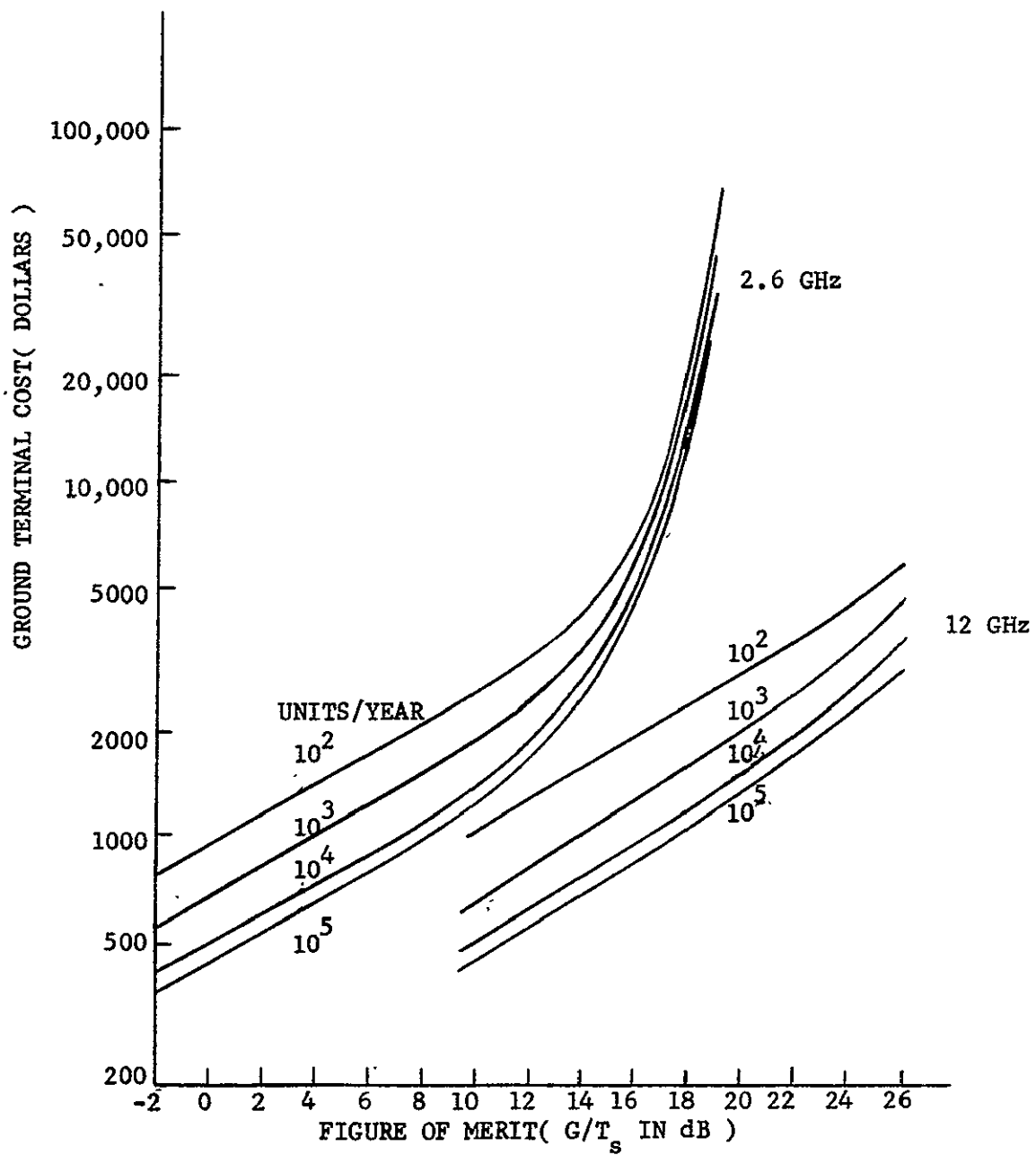
Fig. (6-6)--Optimized ground station cost.

CHAPTER 7

CONCLUSIONS

Economic studies on satellite systems (Ref. 1 to 6) show that the
regional point-to-point communication satellite system and the direct-
broadcast satellite system have cost advantages over other systems to
serve, for example, geographically dispersed populations, only if low-
cost smaller ground stations (less than 20-foot antennas) are used. This report
completed the analysis of antenna characteristics of low cost earth ter-
minals. It discussed the influence of these characteristics on such
important system parameters as interference and cost. It also indicated
the limitations they impose on hardware design alternatives and on antenna
system configurations. A working model of a 12 GHz antenna feed sub-
system was built and tested and found to have an insertion loss of only
0.5 dB and a 15 dB rejection of the image noise located within 1% of
the operating frequencies. Most important of all, this feed can be
fabricated as an integrated part using die casting techniques, resulting
in cost savings under mass production. For example it would cost only
$3.80 for a production quantity of 10,000 units per year.

Specifically, the accomplishments and findings resulting from this
research can be summarized, according to the component and system aspects,
as follows:

Components:

A. A low-cost antenna feed with low sidelobes and a circularly symmetric
beam has been designed using both TE_{11} and TM_{11} circular modes;

- 165 -

the latter is excited by a step discontinuity. Should a horn-type

feed of this kind be needed, the length of the horn can be minimized

by choosing a length which yields a differential phase shift of

180° between TE_{11} and TM_{11} modes instead of 360°.

B. The capacitive pin-type polarizer has been optimized in the sense

of minimum length and broadest band by the use of a general analysis

program and precisely measured equivalent circuit parameters of the

pins.

C. A unique design (done with numerical Hermitian techniques) of a non-

uniform waveguide high-pass filter with the steepest cut-off charac-

teristics ever reported was presented. The success of the design

of this filter is vital for the 12 GHz band low-cost system, because

an IF as low as 120 MHz can be used .

D. Designs and evalutions of zoned reflectors have been completed.

These reflectors have a flat base, small depth and a strong mechanical

structure.

E. A low-cost auto-track system has been proposed, using stepping feed

techniques.

F. Sidelobe suppression in reflector-type antennas using a two absorber

array technique has been experimentally evaluated and found to reduce

only the first sidelobe.

Systems:

A. The off-axis gain of non-auto-tracking stations has been optimized

by establishing a special illumination function at the reflector

aperture. For example, the off-axis gain of a 7-foot prime focus

antenna is maximized using an illumination taper of 14 dB instead of the conventionally used 10-dB taper.

B. A prime' focus antenna was found to be sufficient for a low-cost but not a low noise system. For the antenna feed, waveguide systems are the favored choice for the 12 GHz band, while printed-element systems are recommended for the 2.6 GHz band.

C. Protection ratios of FM television and telephone systems have been analyzed and standard antenna radiation pattern models have been established. It was found that even standard antenna pattern models yield about 35% better orbit frequency space utilization than that of CCIR models, which were never meant to apply to small antennas.

D. Costs of reflectors, antenna feeds and step-track systems have been estimated. It was found the cost of step-track systems is not sensitive to antenna size if only the antenna feed is moved.

The following subjects are recommended for future study:

A. An integrated waveguide feed system at 12 GHz should be built by die casting to evaluate the effects of environment changes, such as temperature, on performance and to obtain accurate cost information.

B. A step-track system should be built and tested, since it is the most promising auto-track scheme to be used in a low-cost receiving system for tracking synchronous satellites.

C. Study should be continued on the best low-cost, mass producible antenna design operated for both transmitting and receiving.

D. A band-pass filter with a very steep cut-off at 2.6 GHz should be studied because the normal type of waveguide high-pass filter at

this frequency is very bulky.

E. To obtain more reliable cost information on zoned reflectors efforts should be continued to convince manufacturers of the potential of these reflectors in a low-cost system.

F. From our preliminary work and a recent JPL study cited in reference 33 in which 180 degree out-of-phase rings are used in a reflector to reduce near-in sidelobes, zoned reflectors can become a low sidelobe antennas if the zone positions are properly selected. Studies on this should be continued.

G. It is thought that absorber arrays with more than two elements could yield more effective reduction of sidelobe levels, since parameters can be adjusted to match practical sidelobe structures in which a null does not necessarily occur between radiation pattern lobes as discussed in Chapter 3. Tests using circularly polarized waves are also recommended.

H. Antenna patterns showing cross polarization components (both linear polarization and circular polarization) should be solicited from industry in order to establish a universal cross polarization pattern model for polarization isolation calculations.

I. Interference in an inhomogeneous satellite system, in which satellites have different EIRP, should be investigated.

APPENDIX B

MODE CONVERSION IN A CIRCULAR WAVEGUIDE BY A STEP DISCONTINUITY

The conversion of a portion of the TE_{11} mode energy to the TM_{11} mode
in a circular waveguide can be achieved by introducing a symmetric dis-
continuity in an oversized section of guide. This oversized circular
guide must be capable of propagating the TM_{11} mode, but cutting off
other unwanted higher order modes. Modes between the TE_{11} and TM_{11},
that is, TM_{01} and TE_{21}, will not be excited because of the symmetry
of the discontinuity. For the purpose of propagating a circularly
polarized wave, the discontinuity should have circumferential symmetry.
The step discontinuity shown in Fig. (5-6) is considered favorable in
many applications because it can force the TM_{11} mode to propagate
in the forward direction. Some assumptions are necessary to simplify
the complexity of the boundary condition.

It has been shown that, if the tangential electric field is specified
over a closed boundary, the electromagnetic field inside the boundary
can be determined uniquely. For a first order approximation we may
assume that the TE_{11} electric field has a perfect match at the junction
and let the transverse field at the discontinuity plane $(Z = 0)$ be the
same as the TE_{11} incident field;[59] i.e.

(transverse field):

$\vec{E}_t$ (transverse field):

$$E_\rho = j\eta \frac{\lambda_{cTE_{11}}}{\lambda} E_0 \frac{J_1(k_c\rho)}{k_c\rho} \sin\phi \qquad \text{for } \rho \leq a \qquad (B.1)$$

$$= 0 \qquad\qquad a \leq \rho \leq b$$

$$E_\phi = j\eta \, \frac{\lambda_{cTE_{11}}}{\lambda} \, E_0 J_1'(k_c \rho)\cos\phi \qquad \text{for } \rho \leq a$$

$$= 0 \qquad\qquad\qquad a \leq \rho \leq b$$

$$J_1'(k_c a) = 0 \text{ (or } k_c a = 1.841)$$

The transverse electric field of the TM_{11} mode in the oversized guide is given

$$\vec{E_t}^{TM_{11}} \ (TM_{11} \text{ mode transverse field}) \text{ where}$$

$$E_\rho^{TM_{11}} = -j \, \frac{\lambda_{cTM_{11}}}{\lambda_{g_{TM_{11}}}} \, A \, J'(\chi\rho)\sin\phi$$

$$E_\phi^{TM_{11}} = -j \, \frac{\lambda_{cTM_{11}}}{\lambda_{g_{TM_{11}}}} \, A \, \frac{J_1(\chi\rho)}{\chi\rho} \cos\phi \qquad (B.2)$$

$$J_1(\chi b) = 0 \ (\chi b = 3.832)$$

At the left side of the junction in Fig. (5-6), only the TE_{11} mode can propagate; but at the junction plane an infinite number of modes are excited to match the boundary condition, such that

$$\vec{E_t} = \vec{E_t}^{TE_{11}} + \vec{E_t}^{TM_{11}} + \text{ other modes.} \qquad (B.3)$$

From the mode orthogonality property:[55]

$$\iint_\Sigma \vec{E_t}^{TE_{mn}} \cdot \vec{E_t}^{TE_{pq}} \, dS = 0$$

$$\iint_\Sigma \vec{E_t}^{TM_{mn}} \cdot \vec{E_t}^{TM_{pq}} \, dS = 0 \qquad\qquad \text{if } m \neq p \text{ or } n \neq q$$

$$\qquad\qquad\qquad\qquad\qquad\qquad\qquad\qquad\qquad (B.4)$$

$$\iint_\Sigma \vec{E_t}^{TE_{mn}} \cdot \vec{E_t}^{TM_{pq}} \, dS = 0$$

Therefore, we obtain (at $Z = 0$)

$$\int_0^b \int_0^{2\pi} \vec{E}_t \cdot \vec{E}_t^{TM_{11}} \rho d\rho d\phi = \int_0^b \int_0^{2\pi} \vec{E}_t^{TM_{11}} \cdot \vec{E}_t^{TM_{11}} \qquad (B.5)$$

From the recurrence relations

$$J_1'(Z) = J_0(Z) - \frac{J_1(Z)}{Z} \qquad (B.6)$$

$$(J_1'(Z))^2 + (J_1(Z)/2)^2 = (J_0(Z))^2 - \frac{2J_1'(Z)J_1(Z)}{Z} \qquad (B.7)$$

$$\int_0^b \int_0^{2\pi} \vec{E}_t^{TM_{11}} \cdot \vec{E}_t^{TM_{11}} \rho d\rho d\phi$$

$$= -\pi A^2 \left(\frac{\lambda_{cTM_{11}}}{\lambda_{gTM_{11}}}\right)^2 \int_0^b ((J_1'(\chi\rho))^2 + (J_1(\chi\rho)/\chi\rho)^2 \rho d\rho \qquad (B.8)$$

$$= -\pi A^2 \left(\frac{\lambda_{cTM_{11}}}{\lambda_{gTM_{11}}}\right)^2 \frac{b^2}{2} J_0^2 (\chi b)$$

Next,

$$\int_0^b \int_0^{2\pi} \vec{E}_t \cdot \vec{E}_t^{TM_{11}} \rho d\rho d\phi$$

$$= \pi\eta \frac{\lambda_{cTE_{11}} \lambda_{cTM_{11}}}{\lambda \lambda_{gTM_{11}}} E_0 A \int_0^a \frac{J_1(k_c\rho)}{k_c\rho} J_1'(\chi\rho) + J_1'(k_c\rho) \frac{J_1(\chi\rho)}{\chi\rho} \rho d\rho$$

$$(B.9)$$

$$= \Gamma\eta \frac{\lambda_{cTE_{11}} \lambda_{cTM_{11}}}{\lambda \lambda_{gTM_{11}}} \frac{E_0 A}{k_c \chi} J_1(k_c a) J_1(\chi a)$$

- 171 -

From (B.8) = (B.9) we can solve for A

$$A = -\eta E_0 \frac{\lambda_{cTE_{11}} \lambda_{gTM_{11}}}{\lambda \lambda_{cTM_{11}}} \frac{2J_1(k_c a)J_1(Xa)}{k_c Xb^2 J_0^2 (Xb)} \qquad (B.10)$$

At this point we define a conversion factor C_s as

$$C_s = \frac{|E_\rho^{TM_{11}}|}{|E_\rho^{TE_{11}}|} \quad \text{at} \quad \rho = b, \ \phi = 90^\circ \qquad (B.11)$$

By direct substitution from (B.1) and (B.2) we obtain

$$C_s = 0.754 \frac{J_1(3.832 \frac{a}{b})}{J_1(1.841 \frac{a}{b})} \qquad (B.12)$$

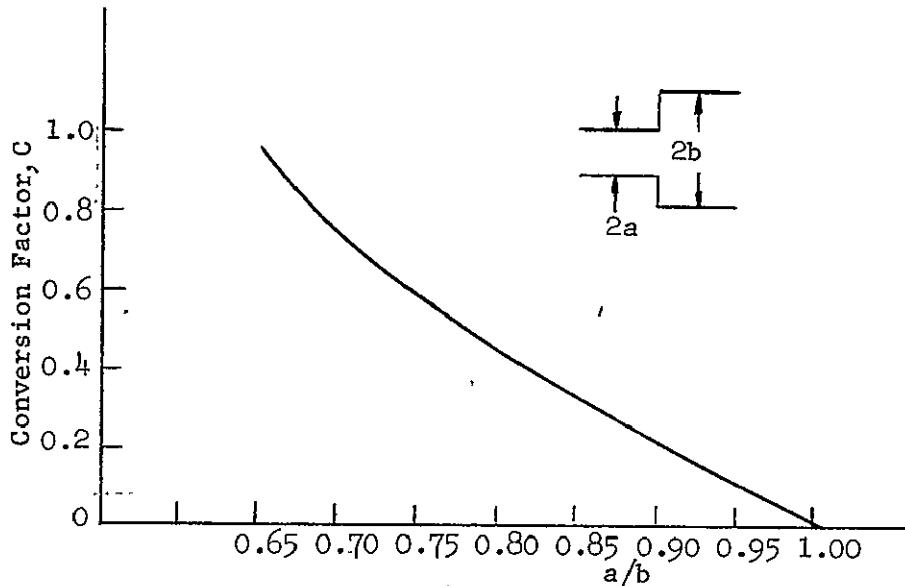The conversion factor C is plotted in Fig. (-1) as a function of a/b.

Fig. (B-1)--TM_{11}/TE_{11} mode conversion factor.

APPENDIX C

IMPEDANCE AND REFLECTION COEFFICIENT OF A NONUNIFORM WAVEGUIDE

The tapered high-pass waveguide filter can be considered as a non-uniform transmission line and the differential equations satisfied by the voltage, $(V(X))$, and current $(I(X))$ at any point (X) along the line (see Fig. (C-1)), are as follows:[59,60]

$$\frac{dV}{dX} = -Z(X) I(X) \qquad\qquad (C.1)$$

$$\frac{dI}{dX} = -Y(X) V(X) \qquad\qquad (C.2)$$

Where $Z(X)$ and $Y(X)$ are the series impedance and shunt admittance per unit length of the line, both are a continuous function of X. To find the differential equation for the reflection coefficient, Γ, we first approximate the continuous taper by considering it to be made up of a number of sections of line of differential length ΔX. Let Z_{in} be the input impedance at X and $Z_{in} + \Delta Z_{in}$ be the input impedance at $X + \Delta X$. If we assume that the line is lossless, then the nominal characteristic impedance, Z_c, will be real and the propagation constant, $\gamma(X)$, will be purely imaginary $(\gamma(X) = j\beta(X))$. According to transmission line theory, the following relations hold (see Fig. (B-1)).

$$Z_{in} = Z_c \frac{(Z_{in} + \Delta Z_{in}) + jZ_c \tan(\beta(X)\Delta X)}{Z_c + j(Z_{in} + \Delta Z_{in})\tan(\beta(X)\Delta X)}$$

$$\approx Z_c \frac{Z_{in} + \Delta Z_{in} + jZ_c \beta(X)\Delta X}{Z_c + j(Z_{in} + \Delta Z_{in})\beta(X)\Delta X}$$

$$= \frac{Z_{in} + \Delta Z_{in} + jZ_c\beta(X)\Delta X}{1 + \dfrac{j(Z_{in} + \Delta Z_{in})\beta(X)\Delta X}{Z_c}}$$

$$\approx (Z_{in} + \Delta Z_{in} + jZ_c\beta(X)\Delta X)(1 - j\frac{Z_{in}}{Z_c}\beta(X)\Delta X)$$

$$= Z_{in} + \Delta Z_{in} + j\beta(X)Z_c\Delta X - j\frac{Z_{in}^2}{Z_c}\beta(X)\Delta X$$

$$+ \text{ higher order terms in } \Delta Z_{in}\,\Delta X \text{ and } \Delta X^2$$

This gives the result

$$\frac{\Delta Z_{in}}{\Delta X} = j\frac{Z_{in}^2}{Z_c}\beta(X) - j\beta(X)Z_c + \text{ higher order terms}$$

$$\frac{dZ_{in}}{dX} = \lim_{\Delta X \to 0} \frac{\Delta Z_{in}}{\Delta X} = j\frac{Z_{in}^2}{Z_c}\beta(X) - j\beta(X)Z_c , \qquad (C.3)$$

Now we also have

$$Z_{in} = \frac{1 + \Gamma}{1 - \Gamma} \qquad (C.4)$$

Differentiating (C.4) with respect to X we obtain

$$\frac{dZ_{in}}{dX} = \frac{1 + \Gamma}{1 - \Gamma}\frac{dZ_c}{dX} + \frac{2Z_c}{(1 - \Gamma^2)}\frac{d\Gamma}{dX} . \qquad (C.5)$$

Combining (C.3), (C.4) and (C.5) we obtain

$$\frac{d\Gamma}{dX} = 2j\beta(X)\Gamma - \frac{1 - \Gamma^2}{2} \cdot \frac{d(\ell n Z_c)}{dX} \qquad (C.6)$$

- 174 -

This equation also can be obtained by defining the nominal characteristic impedance, propagation constant, and the voltage reflection coefficient by the following:

$$Z_c = \left(\frac{Z(X)}{Y(X)}\right)^{1/2}$$

$$j\beta = (Z(X)Y(X))^{1/2}$$

$$\Gamma = \frac{Z_{in} - Z_c}{Z_{in} + Z_c}$$

and making use of (C.1) and (C.2). If $|\Gamma^2| \ll |$ everywhere along the line as would be expected within the pass band, then (C.6) can be approximated as follows:

$$\frac{d\Gamma}{dX} = 2j\beta(X)\Gamma - \frac{1}{2}\frac{d(\ell n Z_c)}{dX} \qquad (C.7)$$

In the case of a waveguide taper, β and Z_c are functions of the cross-section geometry and hence, a function of X along the taper. In order to integrate Eq. (C.7), an auxiliary variable θ is introduced as follows:

$$\theta = \int_0^X \beta(X)dX \ , \ d\theta = \beta(X)dX \qquad (C.8)$$

We also have

$$\frac{d\Gamma}{dX} = \frac{d\Gamma}{d\theta} \cdot \frac{d\theta}{dX} = \beta(X)\frac{d\Gamma}{d\theta}$$

$$\frac{d(\ell n Z_c)}{dX} = \frac{d(\ell n Z_c)}{d\theta}\frac{d\theta}{dX} = \beta(X)\frac{d(\ell n(Z_c))}{d\theta} \qquad (C.10)$$

Substituting (C.8), (C.9) and (C.10) in (C.7) we obtain

$$\frac{d\Gamma}{d\theta} - 2j\Gamma = -\frac{1}{2}\frac{d(\ell n Z_c)}{d\theta} \qquad (C.11)$$

Since

$$\frac{d(\Gamma e^{-j2\theta})}{d\theta} = e^{-j2\theta}\left(\frac{d\Gamma}{d\theta} - 2j\Gamma\right) \tag{C.12}$$

(C.11) can be transformed to:

$$\frac{d(\Gamma e^{-j2\theta})}{d\theta} = -\frac{1}{2}e^{-j2\theta}\frac{d(\ln Z_c)}{d\theta} \tag{C.13}$$

$$\Gamma e^{-j2\theta}\Big|_0^{\theta_0} = -\frac{1}{2}\int_0^{\theta_0} e^{-j2\theta}\left(\frac{d(\ln Z_c)}{d\theta}\right)d\theta \tag{C.14}$$

where

$$\theta_0 = \int_0^L \beta(X)dX$$

L = length of the non-uniform waveguide

Because the waveguide is matched at the end of the taper, $\Gamma(\theta_0) = 0$

Thus

$$\Gamma(0) = \frac{1}{2}\int_0^{\theta_0} e^{-j2\theta}\frac{d(\ln Z_c)}{d\theta}d\theta \tag{C.15}$$

where $\Gamma(0)$ is the input reflection coefficient. For a TEM line β is constant and (C.15) reduces to

$$\Gamma(0) = \frac{1}{2}\int_0^L e^{-j2\beta X}\frac{d(\ln Z_c)}{dX}dX \tag{C.16}$$
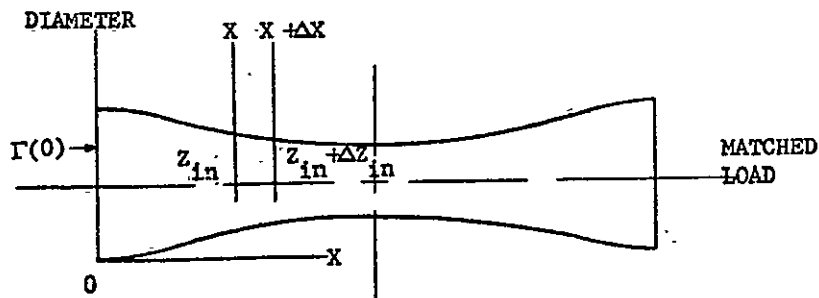

Fig. (C-1)--Tapered circular waveguide high-pass filter.

- 176 -

REFERENCES

1. Stanford University of Engineering, "Advanced System for Communication and Education in National Development", Stanford University, June 1967.

2. General Electric Co., "Ground Signal Processing System Summary Report on Analysis, Design and Cost Estimating", Contract NAS-3-11520, NASA CR72709, June 1970.

3. Janky, J.M., "Optimization in the Design of a Mass-Producible Microwave Receiver Suitable for Direct Reception from Satellite" PH.D. Dissertation, Stanford University, March 1971.

4. Potter, J.G., "Minimum Cost Satellite Teleconferencing Networks", PH.D. Dissertation, Stanford University, 1972.

5. Stanford University, "Teleconferencing Cost Optimization of Satellite and Ground System for Continuing Professional Education and Medical Services", Institute for Public Policy Analysis, Stanford University, May 1972.

6. Hult, J.L., et al., "The Technology Potentials for Satellite Spacing and Frequency Sharing", The Rand Co., Santa Monica, Calif. N68-37837, October 1968.

7. CCIR "Decisions of the World Administrative Radio Conference for Space Communications Regarding Frequency Allocation to the Broadcasting Satellite Service", Geneva, 1971.

8. Ohkubo, K., "Ground-Terminal Optimization and System Cost/Performance Analysis for Broadcasting Satellites", SEL Report (in press), Stanford University, 1972.

9. Philco-Ford Co., "Domestic Satellite System-Earth Terminals", Technical Report, 1971.

10. Ducan, J.W., "Off-axis gain of Pencil Beams", Proceedings of IEEE, January 1970.

11. Silver, S., "Microwave Antenna Theory and Design", McGraw-Hill, 1949, p.194.

12. Hogg. D.C., "Effective Antenna Temperature Due to Oxygen and Water Vapor in the Atmosphere", Journal of Applied Physics, September 1959.

13. Chen, S.N.C. and Peak, W.H.,"Apparent Temperature of Smooth and Rough Terrain", IRE Transactions on Antennas and Propagation, November 1961.

14. Williams, W.F., "High Efficiency Antenna Reflector", Microwave Journal, July 1965, p.79.

15. Potter, P.D., "Suppressed Sidelobe Horn Antenna", Invention Report No. 30-133, JPL, Pasadena.

16. Hughes Aircraft Company, "Low Noise High Efficiency Cassegrain Antenna Studies", Multimode Feeds, NASA Contract No. NAS5-3282, December 1963, p.71-80.

17. Carver, K.R., "A Comparison of the Helicone and Conical Horn Antennas", AIAA National Meeting on Space Technology and Earth Problems, October 1969.

18. Wolfe, J.J. and Bawer, R., "Designing Printed-Circuit Spiral Antenna", Electronics, April 28, 1961.

19. Patterson, W.F., "An Investigation into Problems Related to Spiral Antennas and Antenna Arrays", North American Aviation Inc., Report No. NA64H-1019.

20. Kaiser, J.A., "The Archimedean Two-Wire Spiral Antenna", IRE
    Transactions on Antennas and Propagation, May 1960, p.312.

21. Roberts, W.K., "A New Wide-Band Balum", Proc. IRE, December 1957,
    Volume 45, p.1628.

22. Mathaei, Young and Jones, "Microwave Filters, Impedance-Matching
    Networks and Coupling Structures", McGraw-Hill, 1964.

23. Silver, S., "Microwave Antenna Theory and Design", McGraw-Hill,
    1949, p.488.

24. Tom. N.N. and Heckert, G.P., "Step Track-A Simple Autotracking
    Scheme for Satellite Communication Terminals", AIAA 3rd Communication
    System Conference, Los Angeles, April 1970.

25. Stacey, B.A. and Prime, H.A., "The Application of Search Techniques
    to Autotracking", IEE Conference on Earth Station Technology,
    October 1970, London.

26. Smith, H., Philco-Ford Co., Private Communication.

27. Jowett, J.K.S. and Jefferis, A.K., "Ultimate Communications Capacity
    of the Geostationary Satellite Orbit", Proc. IEEE, August 1969,
    Volume 116, No. 8, p.1307.

28. Fuenzalida, J.C., "A Comparative Study of the Utilization Capacity
    of the Geostationary Orbit", INTELSAT/IEE Conference on Digital
    Satellite Communications, London, November 1969, p.213.

29. Tillotson, L.C., "A Model of a Domestic Satellite Communication
    System", BSTJ, December 1968, P.2114-2122.

30. CCIR Doc M/1059-E, 2 March 1971, Chapter 3, P.1, On Satellite
    Broadcasting.

31. Johns, P.B.,"Graphical Method for the Determination of Interference
    Transfer Factors Between Interfering Frequency-Modulated Multichannel
    Telephony Systems", Electronics Letter, 1966, No.2, p.84-86.

32. Goebels, Jr. F.J. etc., "Analytical and Experimental Investigation of Sidelobe Suppression Techniques for Reflector Type Spacecraft Antenna", NASA Report, NASA CR-72462, 1969.

33. Williams, W.F., "Reduction of Near-In Sidelobes Using Phase Reversal Aperture Rings", JPL Quarterly Technical Review, January 1972, Volume 1, No.4, p.34.

34. Silver, S., "Microwave Antennas", McGraw-Hill, New York, 1950, p.173.

35. Albernaz, J., PH.D. Thesis, Stanford University, 1972.

36. Hult, J.L., et al., "The Technology Potentials for Satellite Spacing and Frequency Sharing", The Rand Co., Santa Monica, California, N68-37837, October 1968.

37. Duncan, J.W., "Antenna Beam Isolation Investigation", Report No. 17565, TRW System Group, Redondo Beach.

38. Rusch, W.V.T. and Potter, P.D., "Analysis of Reflector Antennas", Academic Press, 1970, p.29-30.

39. COMSAT FILING on FCC Domestic Communications Satellite System, March 1, 1971, Volume 2, II-98.

40. CCIR XIIth Plenary Assembly, New Delhi, 1970, Volume IV, Part 2, Report 391-1, p.183.

41. COMSAT and AT & T Joint Filing on Domestic Communication Satellite System, October 19,1970, Appendix II.

42. Rumsey, V.H., Deschamps, G.A. Kales, M.L. and Bohnert, J.I., "Techniques for Handling Elliptically Polarized Waves with Special Reference to Antennas", Proc. IRE, May 1961, p.533-552.

43. COMSAT Report, "COMSAT as Manager for INTELSAT", October 18,1968, P.A12-A12 (Contract No. CSC-SA-19).

44. Private Communication with TRW System, Redondo Beach, California.

45. Teggart, Jr. R.B., "Instructional Television via Satellite-
The Design of a Low-Cost Antenna for Direct Reception", 1970,
Engineer thesis, Stanford University.

46. Han, C.C. and D.F. Ford, "Multifunction C-Band Antenna Feed for
ATS F and G Satellites", 21st Annual Air Force Antenna Research
Symposium, December 1971.

47. Potter, P.D., "A New Horn Antenna with Suppressed Sidelobes and
Equal Beamwidth", Microwave Journal, June 1963, p.71.

48. Han, C.C., "A Multimode,Circularly Polarized, Elliptical Beam
Rectangular Aperture Antenna for Spacecraft Applications".
Submitted for publication to IEEE Transaction on Antenna and
Propagation.

49. Silver, S. "Microwave Antenna Theory and Design", McGraw-Hill,
1949, p.337-338.

50. Piefko, G., "Reflection at Incidence of an Hmn-Wave at Junction
of Circular Waveguide and Conical Horn", in Electromagnetic Theory
and Antennas, Volume 6, Pt. 1, Jordon, E.C. Ed., New York, Pergamon,
1963, p.209-234.

51. Tomiyasu, K., "Conversion of TE_{11} Mode by a Large Diameter Conical
Junction", MTT Transaction, May 1969, p.277.

52. Cohn, S.B., "Flare-Angle Changes in a Horn as a Means of Pattern
Control", Microwave Journal, October 1970, p.41.

53. "Reference Data for Radio Engineers" 4th edition, ITT, New, York,
p. 666-670.

54. Ragan, G.L., "Microwave Transmission Circuits", Boston Technical

Publishers, Inc., Lexinton, Mass., 1964, p.547.

55. Altman, G.L., "Microwave Circuits", D. Van Rostrand, New York, 1964,

p.399-406.

56. Han, C.C., and A.E. Smoll, "Computer-Aided Determination of

Equivalent Circuits for Waveguide Discontinuities" , IEEE -

MTT International Microwave Symposium, April 1971.

57. Tang, C.C.H., "Nonuniform Waveguide High-Pass Filter with

Extremely Steep Cut-off", IEEE Transactions, MTT-12, May 1964,

p..300.

58. Private Communication with Hewlett Packard Company,

59. Ramo, Whinnery and Van Duzer, "Fields and Waves in Communication

Electronics", Wiley, J., 1965, p.430.

60. Ghose, R.N., "Microwave Circuit Theory and Analysis", McGraw-Hill

1963, p.69.

THE FOLLOWING PAGES ARE DUPLICATES OF

ILLUSTRATIONS APPEARING ELSEWHERE IN THIS

REPORT. THEY HAVE BEEN REPRODUCED HERE BY

A DIFFERENT METHOD TO PROVIDE BETTER DETAIL